Influence of lightning on electron density variation in the ionosphere using WWLLN lightning data and GPS data

Prepared by: Mahmud Mohammed Amin

Supervisors: Prof. Michael Inggs

and

Prof. Pierre Cilliers

May 2015

Dissertation presented for the degree of

MPhil in Engineering

Department of Electrical Engineering

University of Cape Town

I declare that this dissertation is my own work and that apart from the normal guidance of my supervisors, I have received no assistance apart from that which has been stated.

Signed:

Mahmud Mohammed Amin
Department of Electrical Engineering
University of Cape Town
South Africa

Abstract

In this study we have demonstrated that a seasonal and diurnal correlation exists between occurrence frequencies of wave-like structures in the form of Traveling Ionospheric Disturbances (TID) in the ionosphere and tropospheric lightning in the mid-latitude region over South Africa. Lightning induced changes in total electron content (TEC) are strongest between September and March, with the more-pronounced effects occurring 12:00 – 22:00 UT, but from April through August there is a low probability of having significant lightning-induced TID occurrence. The strongest oscillations in the total electron content of the ionosphere have dominant periods of range 0.6 to 0.8 and 1.2 to 2.5 hours, typical periods for medium scale TIDs and large scale TIDs respectively. Since ionospheric scintillation is caused by irregularities in electron density which act as wave scatterers, it is feasible that lightning-induced TIDs may provide the mechanism for causing the concomitant and co-located changes in ionospheric total electron content that was observed. Both the lightning and the ionospheric irregularity have spatial dependence over South Africa dominating around Bloemfontein. We have also found a strong seasonal and diurnal correlation between occurrence frequencies of the high rate of change of TEC index (ROTI $\geq$ 0.8 TECU/min) as a proxy for amplitude scintillation S_4 index and lighting stroke rate. The correlation coefficient linking diurnal lightning stroke rate and high ROTI is found to be about 86%. While the seasonal correlation between the monthly average ROTI and average stroke rate is about 70%, the seasonal average ROTI and average stroke rate correlation is found to be about 84% . This therefore implies that the presence of lightning is a likely cause of the generation of TIDs and subsequent irregularities in the ionosphere.

Acknowledgements

I would like to extend my sincere gratitude to my two able supervisors Prof. Michael Inggs and Prof. Pierre J. Cilliers for their guidance and support during this study. Thanks to the South African National Space Agency (SANSA) Space Science management and staff for their financial assistance, hospitality and encouragement during my study. Special thanks goes to the National Astrophysics and Space Science Programme (NASSP) administration of University of Cape Town who sponsored this study and University of Cape Town for enrolling me for this study.

A vote of thanks goes to Dr. Gopi Krishna Seemala who developed the GPS_TEC software used in this study for the processing of the GPS data. We would also like to thank WWLLN and Trignet networks for proving us with the lightning and GPS data respectively. The assistance of Dr. John Bosco Habarulema, Emirant Bertillas Amabayo, Stefan Lotz, Vumile Tyalimpi and many others is highly appreciated. Thanks to all my friends and colleagues at the office who assisted me in many different ways. My sincere thanks goes to my Father and the entire family and to Swabira Bashiru for their well wishes and prayers during the period of this study.

Contents

List of Figures

List of Tables

Abbreviations

AE	**A**urora **E**lectrojet
AGW	**A**tmospheric **G**ravity **W**ave
ASHA	Adjusted Spherical Harmonic Analysis
CC	cloud-to-cloud
CG	cloud-to-ground
DCB	**D**ifferential **C**ode **B**ias
Dst	**D**isturbance storm time
EIWG	Earth-ionosphere waveguide
ELF	**E**xtremely **L**ow **F**requency
EMP	**E**lectro **M**agnetic **P**ulse
ESKOM	Electricity Supply Commission
Es	**S**poradic E layer
foEs	**T**he critical frequency of Es
GB	**G**iga Byte
GISTM	**G**PS **I**onospheric **S**cintillation and **T**EC **M**onitor
GNSS	**G**lobal **N**avigation **S**atellite **S**ystem
GPS	**G**lobal **P**ositioning **S**ystem
GRT	**G**eneralized **R**eileigh **T**aylor
HartRAO	Hartebeesthoek Radio Astronomy Observatory
HF	**H**igh **F**requency
IIE	**I**onospheric **I**rregularity **E**vent
IGS	International GPS service
IPP	**I**onospheric **P**ierce **P**oint
ISR	**I**ncoherent **S**catter **R**adar
LEO	**L**ow **E**arth **Or**bit

LSTID	**L**arge **S**cale **T**ID
LT	**L**ocal **T**ime
MF	**M**edium **F**requency
MSTID	**M**edium **S**cale **T**ID
PLL	**P**hase **L**ock **L**oop
PPS	**P**ulse **P**er **S**econd
QE	**Q**uasi **E**lectrostatic
RAM	**R**andom **A**ccess **M**emory
RINEX	Receiver Independent Exchange
ROT	**R**ate **O**f **T**EC
ROTI	**R**ate **O**f **T**EC **I**ndex
SAMA	**S**outh **A**tlantic **M**agnetic **A**nomaly
SAST	**S**outh **A**frican **S**tandard **T**ime
SNR	**S**ignal-to-**N**oise **R**atio
STEC	**S**lant **T**EC
TEC	**T**otal **E**lectron **C**ontent
TLE	**T**ransient **L**uminous **E**vent
TID	**T**raveling **I**onospheric **D**isturbance
TOGA	**T**ime **O**f **G**roup **A**rrival
UT	**U**niversal **T**ime
UV	**U**ltraviolet
VLF	**V**ery **L**ow **F**requency
VTEC	**V**ertical **T**EC
WBMOD	**W**ideBand MODel
WWLLN	**W**orld **W**ide **L**ightning **L**ocation **N**etwork

Chapter 1

Introduction

The aim of this study is the identification and characterization of the link between lightning and ionospheric irregularities in the mid-latitude region over South Africa. TIDs are wave-like structures manifesting themselves as ionospheric electron content variations [Davies, 1990; Wanninger, 1993].

The effects that an ionospheric medium induces on the radio signal passing through it have been under continuous investigation. The main area of concern to the ionospheric community is the disturbances that the ionosphere causes to radio signals propagating through it. These disturbances can be described in terms of total electron content (TEC) variability. The F region plasma density contributes significantly to the diurnal TEC variability. Characterization of the ionosphere is done by monitoring the variation of TEC along a ray path through the ionosphere from the bottomside (i.e., D-region) to the topside (i.e., F region) of the ionosphere. Recent studies [e.g., Amabayo et al., 2014; Deng et al., 2013; Dujanga et al., 2013; Oron et al., 2013] show that TEC enhancement or depletion are well correlated with scintillations in the F region. Small-scale irregularities often associated with TEC depletions are responsible for the strong scintillations observed. Wautelet et al. [2010] conducted a climatological study of ionospheric small-scale irregularities based on long-term GPS measurements at Brussels over the mid-latitude region in the northern hemisphere. These authors show that the major part of the ionospheric irregularities is not due to geomagnetic phenomena and hence these irregularities are the most frequent sources of disturbances detected by GPS. Their results show that the irregularities have diurnal dependence with a principal maximum

around 10:00 LT and and a secondary maximum of occurrence during nighttime. Their results also revealed that the irregularities are numerous during local Autumn and Winter months, even during low solar activity periods.

From the temporal and spatial distribution of ionospheric irregularities, it is well known that the strength and the frequency of the scintillation or irregularities reach their peak in the ionospheric equatorial anomaly region and quickly decrease outside the crest latitudes. A study of mid-latitude ionospheric scintillation by Radicella and Ezquer [2002] reveals that scintillation activity level is low in the mid-latitude regions. The results of a similar mid-latitude ionospheric scintillation study by Hajkowicz and Minakoshi [2003] conducted over Kokobunji (35.7°N, 139.5°E) in the East Asia show strong evidence of enhanced scintillation activity during Summer nighttime. Another ionospheric scintillation study conducted by Hajkowicz and Dearden [1988] using data from Brisbane (geographic latitude 27.5°S and longitude 152.5°E) reported that the magnitude and occurrence of scintillation activity strongly depended on the time of the day, season and solar cycle. Seasonal dependence of southern hemisphere mid-latitude ionospheric scintillation was investigated by Hajkowicz [1989] and this author identified a consistent principal maximum during Summer solstice.

A number of physical processes have been suggested as being the cause of spatial and temporal variations of the ionosphere. Aurora and solar events cause variations in time scales of seconds to hours. More recently, the ionospheric community has begun to realize that the small scale ionospheric electron content variability cannot be merely explained by latitudinal and seasonal factors or by geomagnetic activity and that there exists some influence of processes in the lower atmosphere (below ∼12 km) that could have a significant effect on ionospheric electron distribution [e.g., Immel et al., 2009; Vadas and Fritts, 2004]. Modeling of atmospheric gravity waves (AGWs), originating from thunderstorms, has predicted variations in total electron content (TEC) of ±7% [Vadas and Liu, 2009]. Typhoons, hurricanes, tornadoes and even seismological events may also have observable consequences in the ionosphere [Kazimirovsky et al., 2003]. Lightning couple energy directly to the mesosphere and the lower ionosphere through quasi-electrostatic (QE) and electromagnetic pulsed (EMP) fields [Pasko et al., 1997; Taranenko et al., 1993]. The fields heat the partly ionized atmosphere and cause additional ionization thereby changing the atmospheric conductivity. Electromagnetic waves from lightning discharges may also have an indirect effect on the lower ionosphere via

reflection effects or interactions with radiation belt electrons that can be precipitated from the mesosphere into the upper atmosphere. The most spectacular examples of upward directed lightning effects on the middle and upper atmosphere are the emission of optical phenomena such as Red Sprites, Blue Jets, and Elves [Sentman et al., 1995], but other fascinating observations have occurred as well. These include explosive spread F, particle precipitation, ionospheric plasma instability generation, D region heating, and ionization [Kelley, 1997].

Studies on the impact of lightning on the occurrence of ionospheric irregularities have been conducted mainly in the American [e.g., Kelley, 1997; Lay et al., 2013], European [Davis and Johnson, 2005; Davis and Lo, 2008; Johnson and Davis, 2006] and Australian [Kumar et al., 2009] sectors of the mid-latitude region. In the current study, we studied the influence of lightning activity on the occurrence of ionospheric irregularities such as TIDs and ionospheric scintillation at mid-latitude stations in the southern Africa sector by using GPS data from the Trignet network and lightning measurements from the World-Wide-Lightning-Location-Network (WWLLN). We have also performed a statistical study of ionospheric irregularity event (IIE) occurrence over southern Africa in the mid-latitude region. The IIE in this context is defined as the ROTI being above a threshold value of 0.8 TECU/min. The method of calculating ROTI has been described in Chapter 4 and more information about ROTI can be obtained from [Wautelet et al., 2010, and the references there in]. About 9,537 occurrences of IIE were found by using GPS measurements made at six GPS receiver stations within South Africa over the period of 282 geomagnetically quiet days in 2012. We count the number of IIE within different timescales: daily sums and hourly sums to describe temporal behavior of the IIE.

1.1 Objective of the Study

The objective of this work is to investigate influence of lightning on the formation of ionospheric irregularities at mid-latitude stations located in South Africa. This objective is approached through an investigation of the correlation between the frequency of occurrence of ionospheric irregularities and lightning strikes over a number of locations in South Africa where there are GPS dual frequency receivers from which the local variations in the ionospheric TEC can be determined. Lightning data from World Wide

Lightning Location Network (WWLLN) were used to identify periods and regions of intense disturbances in the atmosphere. The observations of the ionosphere were conducted by analyzing TEC measurements obtained from trans-ionospheric GPS signals. Due to its wide coverage GPS-derived TEC is widely used as a tool for the study of ionospheric irregularities, and their effect on the radio waves propagating through the ionosphere [Kelley et al., 1996].

1.2 Project Motivation

The most useful feature of the ionosphere in terms of radio communications is its ability to reflect and refract radio waves. The electrons in the ionosphere create a medium through which the signals are refracted and diffracted as they traverse the ionosphere [Davies, 1990]. However, ionospheric irregularities cause degradation of both HF radio communication through rapid fading and to transionospheric radio communication through random fluctuations in signal amplitude and phase, termed as amplitude and phase scintillations respectively.

The impact of ionospheric scintillation on GPS signals have raised concerns and identified the need to investigate the causes and the nature of these irregularities responsible for scintillation in the mid-latitude regions. The presence of TIDs in the ionosphere has consequences on the performance of precise navigation systems. For example, according to Hernández-Pajares et al. [2006], the presence of TIDs in the ionosphere can introduce a significant error during the ionospheric interpolation process within the networks with baselines from tens to hundreds of kilometers. This is because the slant differential ionospheric delays need to be interpolated with high precision in order to navigate with a few centimeters of error by fixing the carrier phase ambiguities in real time. The frequency of occurrence of southern hemisphere ionospheric scintillation and TIDs at mid-latitudes and the mechanisms responsible for their formation are not yet well understood.

Investigations of ionospheric irregularities of are of great importance to the ionospheric community due to their detrimental effects on the performance of precise navigation systems. The Regional Space Weather Center for Africa of the International Space Environment Center, based at the South African National Space Agency (SANSA) Space Science (located at Hermanus (34.42°S, 19.22°E)) in South Africa launched a campaign

in December 2006 to study ionospheric scintillation over southern Africa and the South Atlantic by means of signals from GPS satellites.

There are sufficient motivations and resources at this point in time to explore the potential link between lighting activity and the ionosphere over South Africa. The South African National Space Agency (SANSA) is well-endowed with means and data to study lightning and the ionosphere. The automatic lightning detector at SANSA Space Science in Hermanus, and several other such detectors in South Africa, form part of the World Wide Lightning Location Network (WWLLN) which logs the incidences of lightning strikes all over the world (http://webflash.ess.washington.edu/).

SANSA Space Science manages four ionosonde stations in South Africa which uses radar signals in the HF-band to characterize the bottom side ionosphere. Ionosonde data can provide evidence of the existence of the sporadic E-layer, and track changes in the sporadic E-layer electron density, which may be linked to lightning. Ionosonde recordings are typically done at 15 minute intervals.

SANSA Space Science also has access to GPS data in the L-band from about 60 dual frequency reference receivers of the Trignet network in South Africa, managed by Directorate of the National Geospatial Information (http://www.trignet.co.za/). Trignet GPS data can be used to determine the total electron content of the ionosphere at 1 second intervals, and also provide evidence of rapid changes in the total electron content which can reduce the accuracy of GPS navigation.

1.3 Relevance of the Study

Irregularities in the ionosphere disturb and distort trans-ionospheric signals. Models such as WBMOD (WideBand MODel) and the ionospheric scintillation model of North West Research Associates have been used to model observations in the northern hemisphere [Secan et al., 1997]. However, currently no proven model exists for predicting ionospheric scintillation over the mid-latitude regions of the southern hemisphere. As a result, there is an incomplete understanding of ionospheric scintillation over mid-latitude regions compared to high and low latitudes, particularly in the southern Africa. Therefore investigating the sources and impacts of ionospheric irregularities over southern Africa will provide a basis for developing a prediction model which can be used to

advise users of the Earth-space environment, such as radio astronomers and HF communications during seasons of intense lightning activities.

1.4 Dissertation Layout

This dissertation is composed of six Chapters including this one. Chapter 2 gives the background on the ionosphere, its variability and brief theoretical introduction to types of lightning and techniques (Time of Group Arrival (TOGA)) used for measuring lightning. Chapter 3 provides background information on Total Electron Content (TEC), its variability and irregularity (TIDs), ionospheric scintillation and some basic parameters used to characterize this phenomenon. Chapter 4 provides a description of the data source, types of data used and the procedure of analysis. Chapter 5 presents the results and the observations i.e., correlation between lightning and ionospheric irregularities as well as the influence of lightning on AGWs/TIDs. Chapter 6 offers a discussion, conclusion and recommendation for future work.

Chapter 2

Ionosphere, Lightning and Radio Wave Propagation

This chapter reviews the literature on the morphology of the ionosphere and its effects. It provides essential background on various ionospheric layers, variability and radio waves propagation. Part of this chapter is devoted to some ground- and space-based instruments used to routinely sound the ionosphere; these are powerful tools to access the different scales of the dynamics of the ionosphere. Some sections of this chapter also provide literature on lightning phenomena, types of lightning and measurement techniques as well as the effect of lightning on the upper atmosphere.

2.1 The ionosphere

The ionosphere is formed primarily as a result of the ionization of the neutral atoms and molecules in the upper atmosphere by ultraviolet (UV) radiation from the Sun. A significant quantity of electrons and ions are created during the ionization and are removed by a recombination of electrons and positive ions which takes place continuously. The ionosphere is an electrically balanced medium. The ionosphere is divided into the D, E and F regions each characterized by its altitude range, composition and plasma density. The F region splits into the F1 and F2 layers during the day [McNamara, 1991; Moldwin, 2008]. The state of ionization and dynamics of the ionosphere is mainly influenced by the Sun. At night there is no supply of ionizing radiation from the Sun

to produce ions and electrons, however, recombination continues to take place and so the density of electrons in the D, E and F1 layers gradually diminish. Although the F2 layer continues to exist after sunset its plasma density slowly decreases throughout the night. A representative plasma density altitude profile of the ionosphere is shown in Figure 2.1. The degree of ionization is determined by the flux of ionizing radiation together with the temperature and chemical composition of the upper atmosphere and plasma transport. The ionization process is greatly affected by time of the day, season and geographical location (polar, auroral zones, mid-latitudes, and equatorial regions). The local winter hemisphere is away from the Sun and as a result the received radiation is spread out over a larger area in the winter hemisphere, thus receiving less solar flux than during the summer.

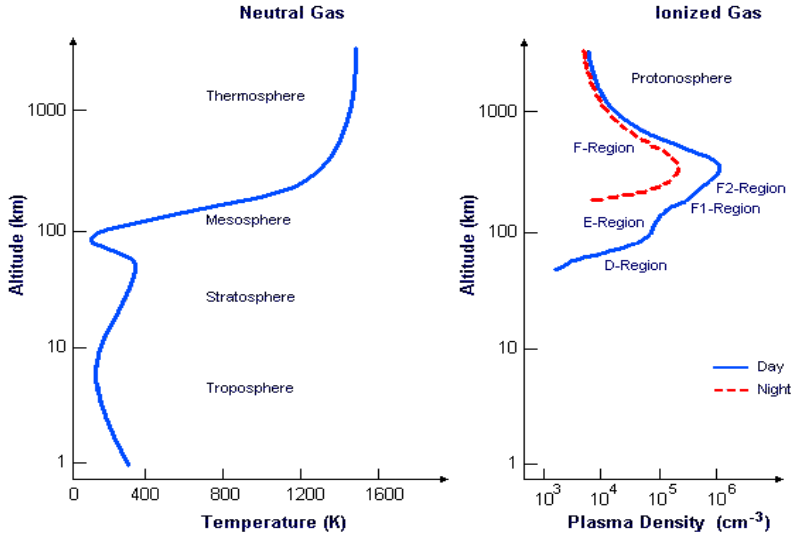

FIGURE 2.1: Typical profile of temperature in the atmosphere and plasma density in the ionosphere. credit: http://www.astrosurf.com/luxorion/Radio/atmosphere-ionosphere.gif

2.1.1 Properties of the Ionosphere

The ionosphere has different properties according to the geographical latitudes. At the low latitudes (i.e., regions within 30° on either side of the magnetic equator) the magnetic field lines run nearly horizontal over the magnetic equator hence the ionosphere is strongly influenced by electromagnetic forces that occur. The primary consequence of this effect is that the electrical conductivity of the ionosphere becomes abnormally large over the equator hence provides a conducive environment for the generation of

irregularities through the generalized Reileigh-Taylor (R-T) instability mechanism. This mechanism occurs very frequently in the post-sunset equatorial ionosphere, resulting in the explosive release of the stored gravitational energy in the ionosphere.

In the high latitudes, the geomagnetic field-lines connect the ionosphere to the outer part of the magnetosphere which is driven by the solar wind. The polar region magnetic field is coupled to the magnetosphere and interstellar medium, thus allowing energy to flow directly into the ionosphere. This coupling may result in the formation of aurora, and can create great turbulence, leading to intense scintillation on trans-ionospheric radio signals.

In the middle latitude the ionosphere is connected to the inner magnetosphere and co-rotates with the Earth therefore is less sensitive to external influence. The mid-latitude ionosphere also acts as a source for plasmaspheric plasma [Kelley, 2009]. The first step in this process is that heavy ions, such as O^+ are produced by photoionization on the dayside. Next, light ions that can escape Earths gravity, such as H^+, are produced through charge exchange reactions at high ($\sim$ 500 km) altitudes. The H^+ ions then are moved up the magnetic field lines by a parallel electric field, into the inner magnetosphere. This parallel electric field is produced by electrons which can diffuse much easier than ions down a pressure gradient, causing charge separation. Then, on the night side, plasmaspheric plasma can flow back down into the ionosphere, maintaining the plasma density in the topside ionosphere. With reference to the Figure 2.1, the effects of this process can be seen in the plasma density in the Protonosphere, which has very little difference between day and night.

2.1.2 Effect of the Ionosphere on Radio Propagation

The most important feature of the ionosphere in terms of radio communications is its ability to reflect and refract radio waves. The effect of the ionosphere on radio waves is frequency dependent and relates to the electron concentration in the ionosphere [McNamara, 1991]. Trans-ionospheric radio signals from GNSS (Global Navigation Satellite Systems) like the Global Positioning System (GPS) have been used to obtain information about the Earth's ionosphere simultaneously from a global network of stations [Hofmann-Wellenhof et al., 1997; Kintner et al., 2007; Wanninger, 1993; Yizengaw et al., 2007].

The ionosphere is a highly dynamic medium whose structure is characterized by electron density irregularities, and is also a highly dispersive medium at L-band GPS frequencies. The presence of electrons in the ionosphere makes it practically important in radio communication; it transmits, reflects and refracts radio waves as they traverse the ionosphere. Small scale irregular structures in the electron density of the ionosphere scatter radio signals that pass through them. The scattering of these signals produces fluctuations in the phase and amplitude of the radio signals usually termed as ionospheric scintillations [Forte and Radicella, 2005].

Ionospheric scintillation is defined as a rapid fluctuation in the amplitude and phase of trans-ionospheric signals induced by small scale structures of increased or decreased electron density in the ionosphere. Generation of small scale structures in the ionosphere is usually attributed to the R-T gravitational instability processes which operate on the steep upward gradient of the bottomside of the F region [Hoang et al., 2010; Huang et al., 2002]. However, in recent years, the ionospheric community has begun to realize that tropospheric weather (below ∼12 km) could have significant effect on ionospheric electron distribution [e.g., Immel et al., 2009; Vadas and Fritts, 2004]. For example, modeling of atmospheric gravity waves (AGWs), originating from thunderstorms, has predicted variations in TEC associated with these AGWs of ±7% [Vadas and Liu, 2009].

2.1.3 E layer radio wave propagation

The E layer is the layer of the ionosphere that lies between 90 km and 120 km above the Earth's surface. The ionization is produced daily by soft x-ray (1-10 nm) and far ultraviolet (UV) solar radiation of molecular oxygen, but is greatly enhanced at high latitudes on the nightside by the energetic particle precipitation that causes the aurora [Kelley, 2009]. The dominant ions in this region are NO^+ and O_2^+. The prevalence of specific ions and neutrals at about 90 km altitude can be seen in Figure 2.2, which depicts ion and neutral density profiles versus altitude.

The E layer can reflect radio waves with frequencies below ∼ 10 MHz at oblique incident angles, but absorbs radio waves above this frequency. After sunset an increase in the maximum height of the E layer increases the frequency at which radio waves can travel a given distance by reflection. Besides the regular structure of the E layer, there are occasional irregular layers that affect the propagation of radio waves. The most significant of

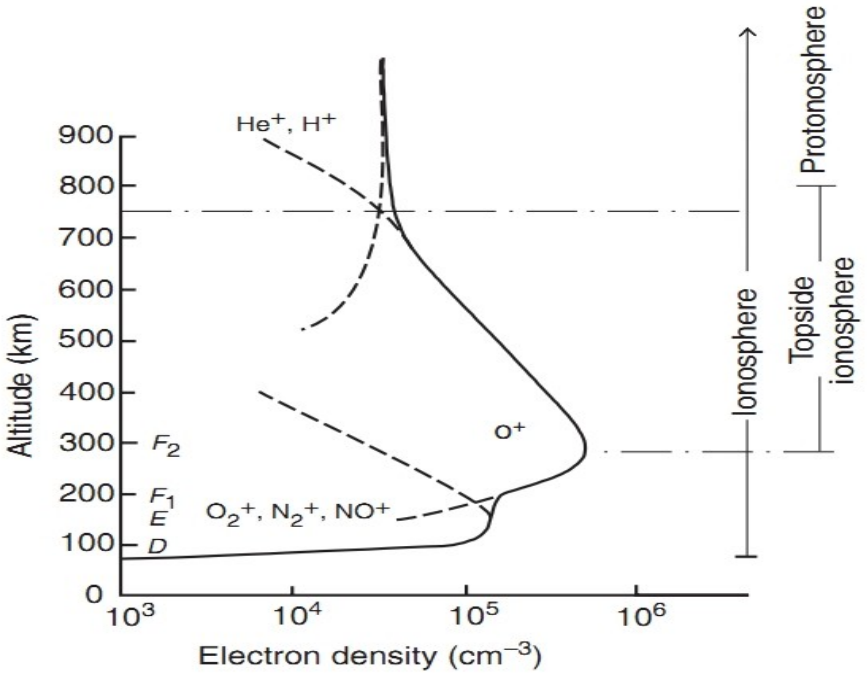

FIGURE 2.2: Ionospheric ion compositions at different altitudes. Banks et al. [1976]

these is the sporadic E layer often denoted as Es [Davies, 1990]. The occurrence the Es layer is dependent upon the geomagnetic latitude and its formation has been explained using wind shear theory [e.g., Bencze et al., 2004; McNamara, 1991]. The wind shear theory associates the formation of the Es layer to the vertical shear of the horizontal wind which changes the vertical ion (and electron) distribution due to the interaction between the wind and geomagnetic field (i.e. by U × B drift). The main source for mid-latitude Es clouds is wind shear produced by internal buoyancy or gravity waves, that create TIDs. According to Amabayo [2011] most of these TIDs are produced by severe thunderstorm cell complexes with overshooting tops that penetrate the stratosphere.

According to Bencze et al. [2004], the Es layer can reflect radio waves up to 225 MHz during intense Es events which often last from a few minutes to several hours. The Es layer is characterized by small, thin clouds of intense ionization. The frequency of Es propagation is high when high signal levels are attained and this is generally common during the summer months. The Es phenomenon is commonly experienced on the 10-m band, especially from May to August, although it may appear at any time. The critical frequency (foEs) of this transient layer varies with time and space, and is less at the mid-latitudes than elsewhere. The Es layer is known to be more persistent during local summer and daytime than during winter and nighttime [Davies, 1990].

2.1.4 F layer radio wave propagation

The F region extends from $\sim$ 200 km to $\sim$ 600 km above the Earth's surface. The F region is divided into sub-layers F1 and F2. The F1 is well approximated as a Chapman layer while in the F2 layer, because recombination is not the only important process, it is not well approximated as a Chapman layer. In the most dense regions of the F layer an increase in the density of mobile electrons increases the refractive index of the layer. Thus radio signals in the HF band are refracted permitting radio communication over long distances. Radio waves in the HF band (3-30 MHz) become useful for terrestrial communication only when they are refracted enough to bring them back to the Earth. The F2 layer supports the sky wave propagation of radio waves, thus facilitating HF radio communications over long distances [Davies, 1990].

2.1.5 Ionospheric Variations

The amount of energy from the Sun reaching the Earth's atmosphere varies with the time of the day, season, geographic location (polar, auroral zones, mid-latitudes, and equatorial regions) and also varies periodically in an 11 year cycle (solar cycle). Therefore the main source of ionization (i.e., solar UV and X-ray) in the ionosphere is determined by the position of the Sun in the sky at a particular location on Earth and solar cycle. Hence the structure of the ionosphere varies in systematic ways.

2.1.5.1 Diurnal Variations

Diurnal variation is the change in ionospheric electron concentration from day to night brought about by the daily rotation of the Earth. During the day when the Sun is directly overhead, the intensity of sunlight reaching the upper atmosphere is greatest and the level of ionization is maximized. At nightside of the Earth, the amount of sunlight reaching the atmosphere is zero and production due to photoionization is reduced to the lowest level. At the dayside of the Earth, the high plasma conductivity of the E region will suppress any electric field inhibiting the development of the plasma instability [Wernik et al., 2004]. However, after sunset, the E region conductivity drops considerably and the electric fields generated within the bottomside of the F region can develop plasma instabilities. The rapid post-sunset uplifting of the F region supports the onset

of ionospheric plasma irregularities. Fluctuations in the ion drift velocity or plasma density, caused by GWs or other large scale structures, can initiate the generation of the initial perturbation [Davies, 1990]. The rotation of Earth therefore gives rise to diurnal variation in the ionospheric electron density.

2.1.5.2 Seasonal Variations

The seasonal variation of the ionosphere is caused partly by the maximum elevation of the Sun above the Earth as well as changes in the neutral atmosphere from which the ions are produced. In addition to its daily rotation, the Earth revolves in a complete orbit around the Sun once each year. Since the axis of the Earth tilts to the plane of orbit, the angle of incident solar radiation varies seasonally between hemispheres. During the local winter, the hemisphere is further away from the Sun and as a result the amount of radiation emanating from the Sun is spread over a larger area on the hemisphere, thus less solar flux is received than during the summer.

2.1.5.3 Geographic Variations

The shape of the Earth causes a geographical variation in the angle of incident solar radiation. Since the Earth is essentially spherical, the Sun is more nearly overhead in equatorial regions than at higher latitudes. Equatorial regions, therefore, receive the most Solar UV and X-ray. As the observer moves from the equator towards the pole or from the day side towards the night side, the intensity of the Solar UV and X-ray reaching the atmosphere decreases because the angle the Sun makes with the upper atmosphere is more oblique. The curvature of Earth therefore give rise to geographic variation in the ionospheric electron concentration.

2.1.5.4 Variations due to Solar Cycle

The Sun's output of energy is not constant in time but changes over a period of ~ 11 years cycle, which is measured in terms of the number of sunspot visible on the disk. During solar maximum, the rate at which flares occur or the intensity of the 10-cm radio flux reaching the Earth's atmosphere increases. Associated with this increased energy input is enhancement of the the plasma density in the ionosphere. This is caused by

the variation of the intensity of the ionizing radiations in the X-rays and UV radiation. The temperature of the upper atmosphere also varies approximately by a factor of two between sunspot minimum and maximum and consequently the density of gas at a given altitude varies by a large factor [Hunsucker and Hargreaves, 2002]. These give rise to a solar cycle variation in the intensity of ionization of the ionosphere.

2.1.5.5 Variations due to geomagnetic storms

Impacts of coronal mass ejections on the Earth and consequent disturbances of the Earth magnetic field [Akasofu, 1983; Joselyn and McIntosh, 1981] may result in disturbances of the ionosphere due to electromagnetic coupling between the ionosphere, magnetosphere, and solar wind which leads to geomagnetic storms [Danilov and Lastovicka, 2001; Fuller-Rowell et al., 1996; Habarulema et al., 2013; Lyon, 2000; Zhang et al., 2004]. During geomagnetic storms, the ionospheric structure can be drastically modified by energy input from the Sun. The electron density variations may be positive (increase) or negative (decrease), which may constitute the formation of ionospheric irregularities. According to Buresova [2005], the storm effects in the F2 region ionosphere are predominantly attributed to the ionospheric response to geomagnetic storm effects in the thermosphere. The effects in the lower ionosphere are predominantly caused by the storm-associated precipitating energetic particles. Therefore, during geomagnetic storms the ionosphere becomes most disturbed and the most intense space weather impacts are noted.

2.1.6 Ionospheric measurements

It is important to recognize that different regions of the ionosphere interact with radio waves differently and therefore different sounding techniques have been employed to arrive at our current understanding of the ionosphere. Although Incoherent Scatter Radars (ISR), or instruments on rockets and balloons can be used to measure the ionospheric density up to 90 km, but it is the only ISR that can also measure the topside density and composition of the ionosphere.

Ground-based ionosondes are used for measuring ionospheric behavior in the bottomside ionosphere (i.e., between about 90 km and 350 km), and satellite-based ionosondes are used for measuring the topside (i.e., above $\sim$ 350 km). In situ electron density

measurements at various fixed altitudes in the range 250 km to 800 km are conducted by means of low Earth orbit (LEO) satellites. In addition, recent research has shown that the electron density distribution with latitude, longitude, altitude and time, can be inferred from TEC by means of ionospheric tomography[Fremouw et al., 1992; Yizengaw et al., 2007].

2.1.7 Rockets and satellites

Several space-based techniques have been widely used to study the electron density structure of the ionosphere. These techniques conducted by means of low Earth orbit satellites or instrumented-rockets allow in situ measurements of vertical and horizontal irregularities (e.g. Sporadic E) that are difficult to interpret from ionograms. Although these measurements are precise, the rocket techniques are local, episodic and restricted by economical factors. Other space-based techniques including radio beacons for total electron content (TEC), radio beacons for scintillation, and topside sounders [Hunsucker and Hargreaves, 2002] are always used to measure high altitude ionosphere. The Global Positioning System (GPS) system consists of a constellation of satellites orbiting at 55° inclination, evenly distributed in six different orbital planes around the globe at 20,200 km altitude. The GPS satellites orbit around the globe with a period of 11 hours 56 minutes. GPS was not originally designed for ionospheric research. Nevertheless, GPS satellites transmit modulated signals on dual carrier frequencies (f1= 1575.42 MHz and f2 =1227.60 MHz) in the L-band. The dual frequency signals provide an excellent tool for continuous monitoring of the generation and evolution of irregularities and determining the total electron content in the ionosphere. The primary information that can be obtained from GPS data include receiver-to-satellite carrier phase, pseudorange, and signal-to-noise ratio (SNR) of the dual frequency signals. The TEC along the signal path (slant path) between the receiver on the ground and each GPS satellite can be estimated due to the dispersive delay of trans-ionospheric signals. Currently, South Africa operates four ionosonde stations, about 60 dual frequency GPS receivers and about 10 GPS ionospheric scintillation and total electron content monitors (GISTM) receivers. Figure 2.3 shows the geographical locations of the ionosonde and GPS receiver stations.

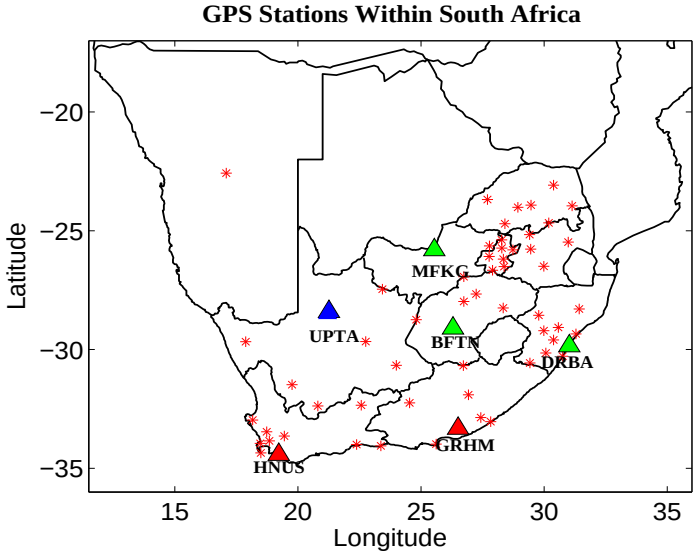

FIGURE 2.3: The red stars indicate geographic location of the dual frequency GPS receivers.The triangles mark the locations of the six GPS receiver of which the data was selected for this study. The red triangles indicate the locations of GPS receivers co-located with ionosondes, the blue triangle indicates the location of a GPS receiver very close to an ionosonde and the green triangle indicates the location of a GPS receivers neither close nor co-located with ionosondes.

2.2 Lightning and Atmospheric Measurements

This section describes briefly lightning discharge processes and types of lightning discharge, effects of lightning energy in the ionosphere and atmospherics (sferics). It also gives essential background of World-Wide-Lightning-Location-Network (WWLLN).

2.2.1 Lightning discharge

Lightning is a transient, high-current electric discharge that occurs in a thunderstorm as a result of localized charge build up sufficient to cause electrical breakdown of the atmosphere. Lightning discharge has a typical conductive path or channel length of 1 to ∼10 km which often comprise intricate multiple branches that extend to several kilometers in the vertical and horizontal directions. Lightning discharge occurs within a cloud, between two clouds, or between clouds and the ground [Uman, 1984]. Lightning discharges that occur within a cloud (i.e., intracloud) or between two clouds (i.e., intercloud) are generally called cloud-to-cloud (CC), and lightning between clouds and the ground are called cloud-to-ground (CG). Each stroke in a cloud-to-ground lightning

discharge begins with a weakly luminous predischarges, called a leader process, which propagates from cloud to ground and which is followed immediately by a very luminous return stroke as the leader approaches the ground [Uman, 1984]. The return stroke usually propagates in opposite direction to the leader (i.e., from ground to cloud in the case of CG discharge). The leader process is usually termed stepped leader because it appear to move towards the ground in a luminous steps of typically 50-meter length with a time delay between steps of approximately 50 μs. Once the stepped leader comes very close to the ground, the resulting high electric field is sufficient to cause an upward directed discharge from the ground to the tip of the leader. The return stroke begins once the connection is established. The return stroke current typically reaches its peak value in about 2 μs and decays to half peak in about 40 μs [Uman, 1984]. Currents of the order of hundreds of amperes may continue to flow for several hundred microseconds.

It is thought that intracloud discharge that occurs between the upper positive and lower negative charge centers with the same cloud is very similar to the cloud-to-ground discharge in that a propagating leader bridges the gap between the charge centers followed by a high intensity return stroke. The total charge neutralized in an intracloud discharge is of the same order of magnitude as the charge transferred in a cloud-to-ground discharge.

2.2.2 Types of lightning discharge

Each group of lightning discharge may involve transport of positive or negative charge; negative cloud-to-ground ($-$CG), the initial process begins in the negative charge center of cloud and develops in the downward direction and effectively transport negative charge to the ground and positive cloud-to-ground (+CG) transport positive charge to the ground, negative cloud-to-cloud ($-$CC) and positive cloud-to-cloud (+CC) also transfer negative and positive charges respectively. For a detailed description of the lightning discharges and physical processes see [Rakov and Uman, 2003].

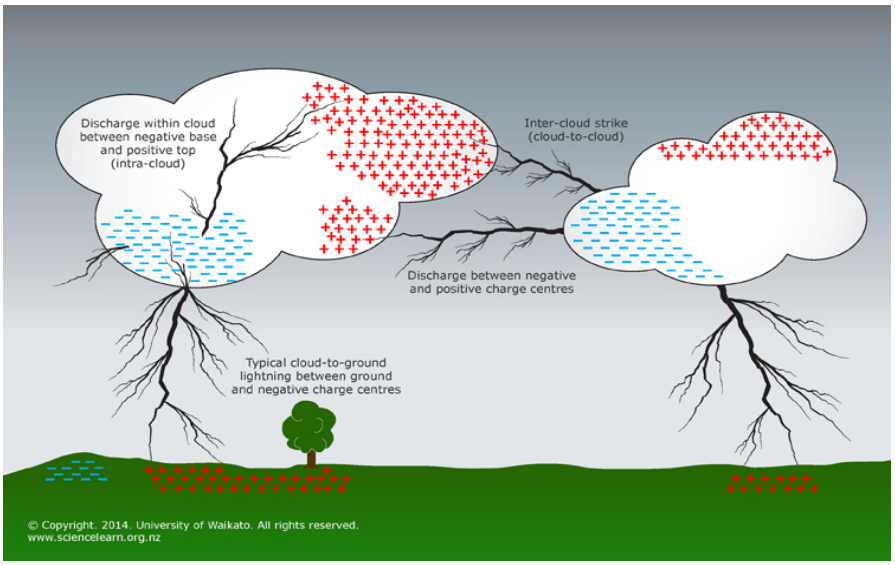

FIGURE 2.4: A cartoon showing the path of lightning discharges. credit: http://sciencelearn.org.nz/Contexts/Gases-and-Plasmas/Sci-Media/Images/

Relevant characteristics of individual lightning involves flash duration, number of return strokes per flash, charge quantity per flash and per stroke, duration and intensity of continuing current, time to peak and return stroke current, etc. Typically, −CG discharges are multi-stroke flashes with an average of 4 subsequent strokes per flash and transfer a total electric charge of 25 C with a peak current of $\sim$ 30 kA, releasing about 500×10^6 J of energy. Usually +CG discharges are single stroke flashes with large peak currents ($\sim$50 kA) due to larger amounts of charge they transfer :the positive charge center in the cloud is typically at higher altitude than the negative charge center and the current flows for a longer amount of time in the stroke channel (median 230 μs) [Rakov and Uman, 2003]. Generation of elves are associated with +CGs lightning [Barrington-Leigh and Inan, 1999]. The CC discharge on average is about 3 times as frequent as CG lightning [Rakov and Uman, 2003] and occurs in the higher altitude than CG discharge. However, it is relatively weaker than CG lightning: it has lower peak currents due to the smaller amounts of charge it transports over shorter distances.

2.2.3 Lightning activity

The most intense thunderstorms on the Earth occur in the tropics and the areas of lowest lightning discharge are at high northern and southern latitudes($> 55°$) [Hunsucker and Hargreaves, 2002]. Lightning occurs mostly over land, in the equatorial regions,

and follows a regular seasonal pattern alternating between the southern and northern hemispheres. The diurnal heating of surface air regulates the convection level and hence the production of thunderstorm. Surface air temperature depends on the length of the day and the maximum elevation of the Sun which varies with season, implying that spring and summer are most conducive to thunderstorm activity [Christian et al., 2003]. At any given time there are up to ∼2000 thunderstorms which are active globally [Stolzenburg and Marshall, 2008] and individual thunderstorms can deliver up to about 6000 strokes per hour [e.g. Rakov and Uman, 2003; Schumann and Huntrieser, 2007]. The average global lightning rate is about 44±5 s^{-1}, however the annual flash density of lightning is not uniform across the globe and can reach a maximum of about 82.7 km^{-2} y^{-1} close to the equator within southern Africa. Also significant level of flash density (i.e., 23.0 km^{-2} y^{-1}) is maintained around Bloemfontein, South Africa [Christian et al., 2003]. Lightning plays multiple roles in wave propagation because not only generates electromagnetic waves but induces modification of the properties of the medium through local ionization.

2.2.4 Electromagnetic radiation from lightning

A lightning discharge or simply called flash may be comprised of one or more component strokes [Malan, 1963]. A flash transforms electrostatic potential energy into electromagnetic energy (radio and light waves), heat, and acoustic energy (thunder). The current flowing along the channel during the return stroke process causes a short pulse of ∼100 μs electromagnetic energy over an extremely wide bandwidth, from a few hertz [Burke and Jones, 1992] to many tens of megahertz [Weidman and Krider, 1986] to be radiated. This implies that each stroke in a lightning discharge is independently a source of electromagnetic energy. However, most of the energy is radiated in the very low frequency (VLF, 3–30 kHz) and extremely low frequency (ELF 3–3000 Hz) band often termed "sferics" [Pierce, 1977]. Sferics energy radiated near the ground propagates in a guided fashion by reflecting between the conducting ground and the lower boundary of the ionosphere, which form what is known as the Earth-ionosphere waveguide (EIWG). Sferics that escape the EIWG suffers small frequency dispersion when traveling through the ionosphere possibly along ducts producing a "tweek" [Yamashita, 1978]. Sferics traveling further along geomagnetic field lines bouncing between two hemispheres through the plasmasphere in the right-handed mode, experience larger frequency dispersion and are

detected in the conjugate hemisphere as whistlers due to their typical whistling tones [Barkhausen, 1930; Helliwell, 1965; Storey, 1953]. Several studies [e.g. Hayakawa et al., 1994; Horner and Clarke, 1955; Jean et al., 1960; Taylor, 1960] have been conducted in order to obtain better understanding of sferics, their variability and applications.

2.2.5 Elves and sprites

Transient luminous events (TLEs) are the most spectacular examples of upward directed lightning effects [Sentman et al., 1995] providing evidence of lightning energy coupling to the atmosphere and lower ionosphere. Sprites are optical phenomena associated with lightning discharge that occur between 40 to 90 km altitude and last for tens of milliseconds [Boeck et al., 1995; Sentman et al., 1995]. Sprites are associated with large electrostatic fields caused by lightning strokes that transfer a large amount of charge to the ground from a given altitude (more than ∼350-600 C-km) [Cummer and Lyons, 2005]. The majority of observed sprites have occurred in association with positive cloud-to-ground strokes, but also have been observed rarely in association with negative CGs [Barrington-Leigh and Inan, 1999; Taylor et al., 2008]. The large altitude extent of the sprite (50-80 km) indicates that changes in conductivity and electron density could arise over a large altitude range. This could be significant in cloud-to-ionosphere charge movement as well as in lightning energy propagation in the Earth-ionosphere waveguide.

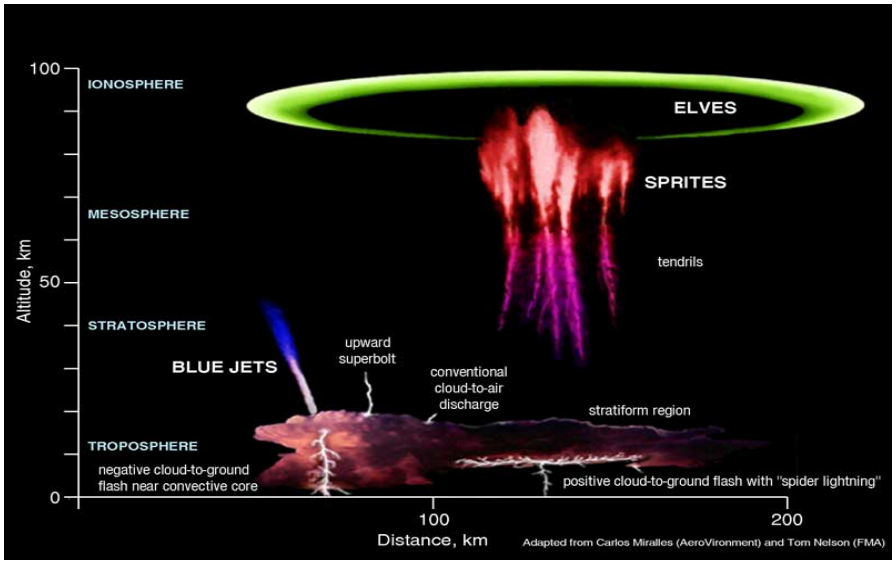

FIGURE 2.5: Sprites and Elves caused by positive CG lightning discharge. credit: http://www.stormscapesdarwin.net/page2.htm

Elves are another type of TLE, but are caused by the lightning electromagnetic pulse (EMP) instead of a quasi-electrostatic field. The lightning EMP expands outward from a high peak current (>50 kA) cloud-to-ground stroke and can interact with a region of the lower ionosphere up to 700 km in diameter [Barrington-Leigh and Inan, 1999]. When it reaches an altitude of 85-95 km after ∼1 ms, its electric field can interact with the ionospheric plasma, causing optical excitation and secondary ionization [Barrington-Leigh and Inan, 1999]. The elves themselves are the optical emissions, which expand in a ring shape and last 1 to 3 ms. The first images of elves were published in the work of Fukunishi et al. [1996]. Mende et al. [2005] reported enhanced electron density in the same region as a detected optical emission from an elve.

2.3 Lighting location systems

Lightning flashes are powerful sources of electromagnetic energy over a wide range of frequencies [Magono, 1980], with the larger fraction of the energy dissipated in the VLF band (i.e., frequencies <30 kHz) bands [Pierce, 1977]. Lightning location techniques rely upon the energy dissipated by lightning discharge, their acoustic signatures (thunder), their optical signatures (lightning), and their signatures in the radio frequency spectrum [Uman, 1987]. In general any observable signal from a lightning flash can be used to determine the location of the lightning source.

The electromagnetic radiations radiated by lightning flashes especially in the Medium Frequency (MF) and Very Low Frequency (VLF) bands can be detected by a single radio receiver or a network of spatially separated radio receiver stations positioned on the surface of the Earth and therefore providing real time observations. Single-site lightning location systems usually combine a direction finder with a technique to estimate the distance of the source. In multi-station lightning location systems the information from individual receiver is, on its own, insufficient but when the information from a number of receivers is combined together at a central site, the location of the lightning discharge can be determined. In general single-station techniques are cheaper to operate but relatively less accurate, while multi-station networks are relatively expensive but tend to offer higher location accuracy and detection efficiency.

2.3.1 World Wide Lightning Location Network

Lightning flashes produce very low frequency (VLF; 3-30 kHz) radiation termed sferics. The lower boundary of the ionosphere and the conducting Earth surface form an electromagnetic waveguide through which the sferic efficiently propagates with little attenuation (a few decibels per 1000 km [Taylor, 1960]). It is this mechanism that makes long-range remote sensing of the sferics, and hence, the WWLLN, possible.

The WWLLN is the only lightning location network with the capability to continuously monitor the location of lightning strokes around the entire world. Regardless the type lightning, the WWLLN employs the Time of Group Arrival (TOGA) described by Dowden et al. [2002] and detects lightning strokes that have peak currents with magnitudes above ∼40 kA [Jacobson et al., 2006]. Dowden et al. [2002] suggested that "a global service of lightning location could be provided with only about 10 well-placed TOGA stations" However, a lightning stroke which is surrounded by VLF receiver stations is much more accurately located than one which is not hence, WWLLN currently has over 50 VLF receiver stations distributed across the globe including two in South Africa (Durban and Hermanus). The WWLLN has been providing continuous accurate locations and times for lightning strokes globally since August 2003 [Jacobson et al., 2006; Lay et al., 2004; Rodger and R. L. Dowden, 2005].

2.3.2 WWLLN configuration

A description of the WWLLN VLF receiver stations is given by Dowden et al. [2002]. Each VLF receiver station consists of a short (1.5m) whip antenna, a VLF receiver,a preamplifier, a processing computer with Internet connection, a Service Unit (containing timing and VLF processing electronics) and a nearby GPS receiver. WWLLN VLF receivers have relatively low noise-free receiver location requirement compared to other long-range lightning location techniques [e.g. Füllekrug and Constable, 2000] partly because, the vertical electric field from strong CG lightning dominates over power-line noise. And more so, the VLF antennas are typically mounted on poor conducting ferroconcrete buildings. These buildings at VLF become adequate conductors and remain at ground potential. This mechanism shields the antenna from local man-made noise. Because of low attenuation and high power spectral density at VLF [Crombie, 1964],

lightning-generated waves in this frequency range can propagate several thousands of kilometers in the Earth-ionosphere waveguide. Since the radio wave pulses (sferics) wavelength near the upper frequency is 15 km, such a whip antenna is purely capacitive (∼15 pF) and so wide band [Dowden et al., 2002]. In a typical VLF detection system, the VLF (1-24 kHz) signals radiated by lightning discharges are detected by the anntena, amplified and then digitized at a sampling rate of ∼48kHz using a 16 bit sound-card in a personal computer (PC). The PC time is synchronized with the Pulse Per Second (PPS) signal of a GPS receiver. The PPS timing accuracy is better than 1 μs, which is smaller than the data sampling period (∼ 2 μs). The GPS receiver also provides an NMEA signal giving the exact location of the station, that is input to the computer via a serial port connection. Each station's computer requires: Linux operating system, a sound card and serial port, a sufficient amount of RAM (248 or 512 MB), 20- 40 GB of hard-disk space and continuous internet connection.

2.3.3 Time of group arrival (TOGA)

Lightning strokes are automatically identified in the incoming data stream. The electric field component of the VLF is sampled at ∼48kHz and the magnitude of the difference between consecutive samples,(i.e., i and i+1) are monitored. When this exceeds a given threshold value, the time of the second sample (i.e., i+1) is recorded as the "trigger time"[Dowden et al., 2002]. A 64-sample waveform consisting of 16 pre-trigger data points and 48 post-trigger points is saved to short-term memory to be analyzed. However, lightning radiated sferic becomes dispersed during its propagation usually thousands of kilometers in the Earth-ionosphere waveguide. If severely dispersed the arrival of the group energy of the dispersed wave packet occur later than the trigger time. This results in discrepancies in the time measurement. The time of group arrival (TOGA) technique was developed to take care of this discrepancy. The TOGA is determined using software developed by Dr. James Brundell. When a sferic waveform is captured, the software determines the time of group arrival (TOGA) of the group energy for that sferic.

The TOGA is arrived as follows: The group velocity of the wave in a waveguide is given by

$$v_g(\omega) = \frac{d\omega}{dk} \tag{2.1}$$

where k is the frequency dependent wave vector. At range r from the lightning stroke and at time t, the electric field of the wave can be expressed as a sum of Fourier components of the frequency, ω:

$$E(r,t,\omega) = \sum A(\omega)cos(\phi(\omega)), \tag{2.2}$$

where

$$\phi(\omega) = \omega t - k(\omega)r + \phi_o \tag{2.3}$$

and ϕ_o is not frequency dependent.

Differentiating Equation 2.3 with respect to frequency (ω) at any time, t, and range, r, gives the slope of the phase $\phi(\omega)$ as,

$$\frac{d\phi}{d\omega} = t - r\frac{dk}{d\omega} = t - \frac{r}{v_g(\omega)} \tag{2.4}$$

where $v_g(\omega)$ from Equation 2.4 is the frequency-dependent group velocity and $t_g(\omega) = r/v_g(\omega)$ is the time taken by the wave group to travel from the lightning source (the return stroke) to the receiver at range r. From Equation 2.4 it is clear that the $d\phi/d\omega$ equals zero when $t = t_g(\omega)$. The frequency range considered is from 6 to 23 kHz, because most of the lightning energy is dissipated over this range, and WWLLN receivers are sensitive over this band. An average $d\phi/d\omega$ is determined over the frequency range. Hence that instant when the regression line of $d\phi/d\omega$ has zero slope when averaged over the frequency range from 6 to 22 kHz defines the TOGA [Dowden et al., 2002]. At each station the software determines the TOGA and reports that time to the central processing computer where it is used in lightning location calculation. The TOGA from an individual station by itself cannot determine the location of the lightning stroke. If five or more stations detect a lightning event, the location and time of the stroke is determined by using the downhill simplex method to minimize the difference in location and time given by the five or more stations. Each lightning stroke location requires the TOGA from at least five stations with time residual of less than 30 microseconds [Rodger et al., 2004; Rodger and R. L. Dowden, 2005]. While detection of an event by four stations would be enough to produce a location estimate, the fifth station allows error analysis.

At each station the software also computes an uncalibrated integrated energy flux density, Y, in the electric field waveform as follows:

$$Y = \sum_{samples} \frac{(E')^2}{c\mu_o} \Delta t \tag{2.5}$$

where E' is the uncalibrated electric field, c is the speed of light, $\mu_o = 4\pi \times 10^{-7}$ W/(Am), and Δt=1/(sampling frequency). The integrated energy, the TOGA, and the station identification number are sent to the central processing station.

2.4 Summary

The background information on the formation of the ionosphere, including factors which cause its variability have been discussed in this Chapter. The interaction of radio waves with different layers of the ionosphere as well as ionospheric measurements were also discussed. We have also discussed lightning phenomena, WWLLN configuration and TOGA technique employed by WWLLN in the measurement of lightning stroke.

Chapter 3

Ionospheric variability and irregularity

3.1 Scope

This Chapter reviews, in the context of the research presented in this work, the literature on TEC measurement and variability, ionospheric scintillation, and the nature of irregularities that cause ionospheric scintillation in the L-band. The influence of the R-T instability mechanism and the solar terminator on the growth of ionospheric irregularities (e.g., AGWs/TIDs) has also been explored.

3.2 Total Electron Content (TEC)

Total electron content is a parameter widely used to characterize the ionosphere hence provides information concerning the state of the ionosphere. The TEC over a specific region of the Earth does not remain constant throughout the year, month, day and even hour. Observations of the ionosphere at smaller time scales reveal the transient variations of TEC. Variation in ionospheric plasma which constitute the TEC has traditionally been attributed to changes in solar radiation and geomagnetic activity, which represent the key drivers in most empirical and assimilative models [e.g., Bilitza et al., 2011; Hajj et al.]. However, atmospheric temperature and pressure changes are apparent in the TEC variations since the ionosphere is coupled with the lower atmosphere. Variations

of the magnetic, (during magnetic storms and sub-storms) and electric fields induce variations in TEC that characterizes the state of the ionosphere. Therefore, accurate monitoring of fast changes will depend on the type of ionospheric measurements, i.e. its ability to resolve smaller time scale changes in TEC.

3.2.1 TEC Variability and irregularity

The nature of the ionosphere is well understood. A number of empirical [e.g., Brunner, 1991; Klobuchar, 2001] and physical models [e.g., Bilitza, 2003] for ionospheric characterization have been suggested. However, TEC is a difficult quantity to model since its variability is complex due to factors such as sunspot activity (∼11 year cycle), seasonal and diurnal variations, the line of sight (elevation and azimuth) of the satellite and position of the observer [Hofmann-Wellenhof et al., 1997]. For instance, the ionospheric wind dynamo generates electric fields which cause plasma drifts which are known to cause the equatorial electron density anomaly [Richmond, 1995]. The atmospheric gravity waves and the strong electric fields give rise to plasma density gradients which in turn cause electron density instabilities manifested in the form of TEC variations. Fluctuations in the ion drift velocity or plasma density, caused by AGWs or other large scale structures, can initiate the generation of the initial perturbation [Davies, 1990].

The ionospheric electron density exhibits regular variations, with a peak during the day to a minimum during the night. The F layer densities over South Africa peak at about 14:00, South African Standard Time, (SAST). SAST = universal time (UT) + 02:00. During early morning (04:00 to 07:00 SAST) and night (18:00 to 20:00 SAST), the ionospheric densities can drop by two orders of magnitude. There are localized enhancements of these variations at late afternoon/evening. These temporal variabilities of TEC do however vary with latitude. The shape of the Earth causes a geographical variation in the angle of incident solar radiation. Since the Earth is essentially spherical, the Sun is more frequently overhead at the low latitude region than at higher latitudes. Therefore, low latitude regions receive more Solar radiation than mid- and high latitudes and hence higher ionization occurs at low latitude regions than at mid-latitude and high latitude regions. The curvature of Earth therefore gives rise to latitudinal TEC variation.

3.2.2 Methods of estimating TEC variability

GPS satellites operate on two different frequencies f_1 and f_2, which are derived from the fundamental frequency (f_o) of 10.23 MHz: $f_1 = 154.f_o = 1575.42$ MHz and $f_2 = 120.f_o = 1227.60$ MHz. The observables from GPS satellites at these two frequencies f_1 and f_2 usually show a differential bias due to different hardware paths inside the transmitter. According to Wanninger [1993], the phases also experience offsets as a result of unknown carrier phase ambiguities and differential equipment phase delays. Satellites are mostly observed along oblique signal paths which pierce the ionosphere at an assumed ionospheric thin shell height. The point of intersection of the ray path with the ionosphere is usually called the ionospheric pierce point (IPP). The IPP corresponds to the height typically associated with the peak electron density in the ionosphere ($\sim$ 350 km for this study). According to Davies and Hartmann [1997] the choice of a particular height of the thin shell only becomes critical under a few conditions; (1) in the evening near the magnetic equator where vertical drift raises the peak of the F2-layer to heights of the order of 600 km and (2) in winter nights in middle and low latitudes when the F2-layer decays and the protonosphere content above about 2000 km is comparable with the ionospheric content. The TEC along the signal path (slant path) between the receiver and the GPS satellite, commonly referred to as slant TEC (STEC), is defined as

$$STEC = \int_R^S N ds \tag{3.1}$$

where TEC is measured in TEC Units (TECU) with 1 TECU = 10^{16} electrons per m^2, N is the electron density, R and S denote the receiver and satellite positions respectively in km and s is the range from S to R. The line integral is assumed to include all the electrons in a column having a cross-section of 1 m^2 and extending from receiver to satellite.

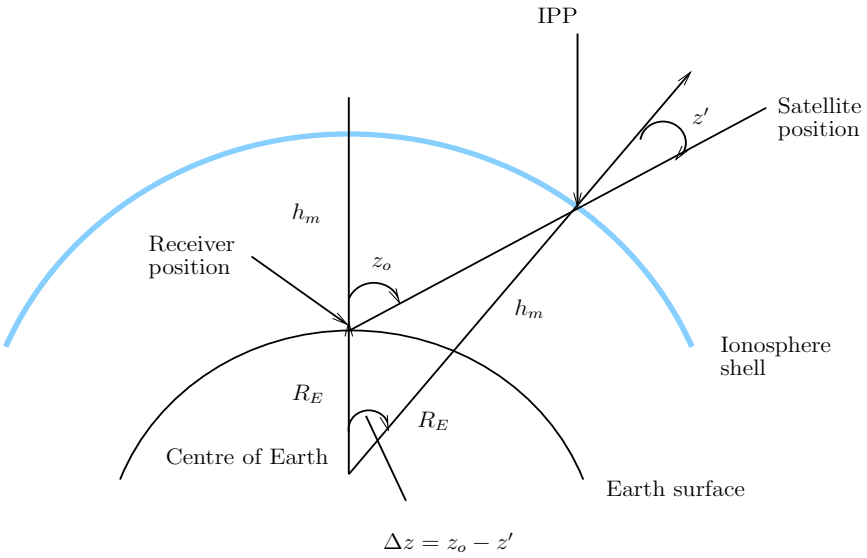

FIGURE 3.1: Geometry used for the calculation of VTEC from STEC.

The vertical TEC (VTEC) is modeled using a mapping function and the geographic position of the IPPs [Hofmann-Wellenhof et al., 1997] as follows

$$VTEC = STEC \times \cos(z') \tag{3.2}$$

where z' is the zenith angle (in degrees) at the ionospheric piecing point (IPP). The zenith angle can also be expressed as

$$\sin(z') = \frac{R_E}{R_E + h_m} \sin(z_o) \tag{3.3}$$

where R_E is the radius of the Earth ($\sim$ 6400 km), h_m is the assumed single layer model of 350 km and z' and z_o is zenith angle of the satellite (in degrees) at the observation site. For a known satellite position, z can then be calculated and the approximate coordinates of the IPP can be determined.

Faraday rotation and group delay

A linearly polarized electromagnetic wave propagating through the ionosphere generally undergoes Faraday rotation of the polarization vector which modifies the polarization and phase characteristics of the electromagnetic signal. This effect is due to the anisotropy of the medium. Faraday rotation is proportional to the square of the wavelength, λ^2 (or $1/f^2$), to TEC, and to the Earth's magnetic field, B [Allnutt, 1989].

Hence, the effect is more effective at the long wavelengths (a few tens of centimeters) than at the shorter wavelengths (a few centimeters). Faraday rotation also varies by one order of magnitude between day and night as solar illumination exerts a major control on the level of ionospheric activity. Finally, Faraday rotation varies with latitude and is larger at the tropics than at the poles. The rotation of a linearly polarized vector about its direction of propagation when passing through the ionosphere is given by

$$\phi = \frac{2.36 \times 10^4}{f^2} \int NB \cos\theta_B \, dl \text{ radians} \tag{3.4}$$

where f is frequency (Hz), N is electron density (electrons/m^3), B the Earth magnetic field (Wb/m^3), θ_B is the angle between the magnetic field and the direction of propagation, dl incremental distance through the plasma. Sometimes $B \cos\theta_B$ is replaced by an average value B_{av}, and the Equation 3.4 can be reduced as

$$\phi = \frac{C}{f^2} \times \text{TEC radians} \tag{3.5}$$

where TEC $= \int N dl$ electrons/m^2 and C is a constant replacing $2.36 \times 10^4 \, B_{av}$. This implies that variation in TEC translates into relative variations in Faraday rotation hence, causing significant disturbances in the amplitude and phase signal.

The phase path length through a medium does not equal the true path length if the refractive index of the medium does not equal unity. Since the phase path length is directly proportional to the refractive index and the refractive index is a function of frequency, a transmitted signal consisting of a bandwidth or spectrum of signals will suffer a group delay. The delay when acting on a single frequency such as a ranging pulse, will cause the signal to arrive later than it would have done if transmitted in vacuo. That is, the inferred range R, will be greater than the true range since the velocity of light in *vacuo* c would have been assumed in calculating the range. The error ΔR will be:

$$\Delta R = \frac{40.3}{f^2} \times \text{TEC meters} \tag{3.6}$$

3.3 Ionospheric irregularity

The ionosphere is the partially ionized region of the upper atmosphere that lies between ~ 50 km and ~ 1000 km above the Earth's surface. The reason for the extreme variability of the thermosphere–ionosphere system is its rapid response to external forcing from various sources, i.e., the solar ionizing flux, energetic charged particles and electric field imposed via the interaction between the solar wind, magnetosphere and ionosphere, as well as coupling from below ("meteorological influences") by upward propagating, broad spectrum, internal atmospheric waves (planetary waves, tides, gravity waves) generated in the stratosphere and troposphere.

R-T instability

R-T instability develops at the interface between two fluids of different densities when the lighter fluid pushes the heavier fluid. Consider a finite plasma in a magnetic field under the influence of gravity, as shown in Figure 3.2. A perturbation of the interface between the fluids causes sinusoidal variations in the plasma density. The gravitational force on the electrons and ions causes them to drift parallel to the boundary. The $E \times B$ drift produced in the opposite direction amplifies the initial perturbation. When such a disturbance moves onto the surface of the interface in the form of a wave, they generate the so-called GWs and these provide a seed mechanism for the R-T instability [Hoang et al., 2010; Huang et al., 2002]. When GWs propagate perpendicularly to the magnetic field, they generate polarized electric fields, and these are amplified non-linearly by the R-T instability [Huang et al., 2002]. The positive electron density gradient region of the rapidly rising F layer bottomside becomes unstable due to density perturbations, leading to the growth of plasma bubble irregularities by the R-T instability mechanism. The plasma bubbles develop as flux tubes aligned vertically. The rising plasma depletions of large scale sizes with secondary irregularities also develop by cascading processes at the steepening density gradients of the bubbles [Abdu, 2001]. The evening F layer height and the vertical plasma drift are due to the pre-reversal electric field enhancement that is controlled by the thermospheric zonal wind (eastward in the evening) and the longitudinal/local time gradient in the integrated E layer conductivity near sunset. According to Abdu [2001], the growth of R-T instability responsible for equatorial ionospheric

irregularities is summarized by the exponential growth profile in Equation 3.7.

$$A = A_o e^{\gamma t} \tag{3.7}$$

where A_o is the initial instability and t is the time of instability growth.

The growth rate γ in Equation 3.7 can be expanded to give a generalised R-T instability growth rate when chemical recombination is neglected as in equation 2.5

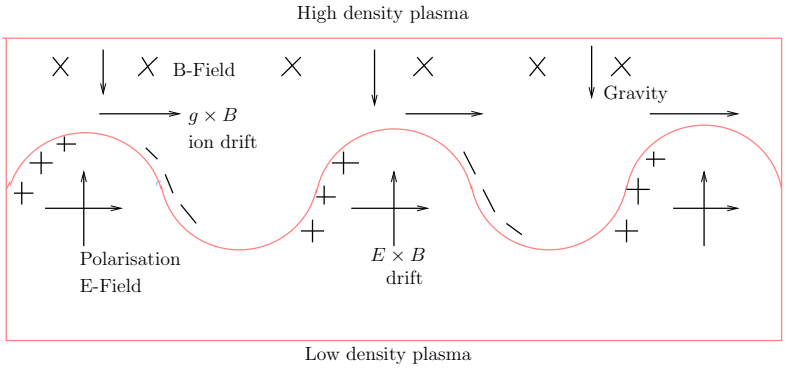

FIGURE 3.2: Illustration of the R-T instability mechanism

$$\gamma \approx \underbrace{\frac{\Sigma_F}{\Sigma_F + \Sigma_F}}_{a} \left[\underbrace{\frac{E \times B}{B^2}}_{b} + \underbrace{U_n}_{c} + \underbrace{\frac{g}{\nu^{eff}}}_{d} \right] \underbrace{\frac{\partial N}{N \partial h}}_{e}, \tag{3.8}$$

Atmospheric gravity waves (AGWs) generation

It is known that atmospheric gravity waves of natural origin can be produced not only by magnetic storms and aurora-related phenomena but also by other natural phenomena, such as, earthquake, weather fronts, tropospheric turbulence, jet flows, Solar terminator, and volcanic eruptions [Hocke and Schlegel, 1996; Oliver et al., 1997]. Atmospheric gravity waves (AGWs) can be generated also by artificial effects, such as, man-made explosions, heating by high power radio radiation, launching of heavy rockets, and chemical discharges from space vehicles. Waves of various time and spatial scales are generated

during terrestrial thunderstorms and active weather systems in the lower atmosphere [Curry M. J. and Murty R. C., 1974; Kelley, 1997]. These waves carry energy upward from the lower atmosphere where they are produced into higher altitudes where the gas density is lower. Since fewer molecules exist at increasing heights, the wave carries its energy onwards by oscillating with increasing amplitude. Thus the wave amplitude grows larger as it rises above the source. According to McNamara [1991], because of the very large change in atmospheric density. AGWs have intrinsic exponential growth of amplitude hence suggests strongly that AGWs may have their origin in very much less obvious waves at lower levels in the atmosphere.

These atmospheric waves, as they propagate to the ionosphere, generate plasma disturbances sufficient to cause plasma instability from which ionospheric heterogeneities of different scales originate. According to Kelley [2009], theoretical and experimental studies have proved that the development of plasma bubbles or regions of low-density plasma can be initiated by long-period internal gravity waves (due to R-T instability in the equatorial ionosphere and Perkins instability in the middle-latitude ionosphere). At the same time, the boundaries of the bubbles, can act as sources producing extremely low- and very low-frequency waves which are recorded by the spacecraft [Larkina et al., 1983]. Later, the development of R-T and Perkins instabilities will cause the neutral component to begin to move upward hence, the formation of plasma depleted regions, and the subsequent heating of the neutrals.

Solar Terminator

The boundary between day and night (i.e., the solar terminator) represents a region of sharp change in the energy input from solar radiation, which consequently leads to strong gradients in the Earth's atmosphere and ionosphere [Hernández-Pajares et al., 2006; Liu et al., 2009]. It is believed that as the Earth rotates, the solar terminator traverses through the atmosphere and such movement may causes the generation of atmospheric waves, turbulence, and instabilities in the ionosphere plasma [Antonova et al., 2006; Beer, 1978; Cot and Teitelbaum, 1980; Somsikov, 1983, 1987; Somsikov and Ganguly, 1995]. Liu et al. [2009] state that the atmospheric irregularities and inhomogeneities are generated as a consequence of the atmospheric gas in the vicinity of the solar terminator attaining a non-equilibrium state. Terminator wave is indiscernible in the dawn side

wind. Most wave structures are observed at night, with some extension to the sunlit region around solstices. The midnight density maximum seems to be closely connected to terminator wave structures, hence indicating a possible role of terminator waves in its formation [Liu et al., 2009].

Traveling ionospheric disturbances (TIDs)

Atmospheric gravity waves (AGWs) manifest themselves in the ionosphere as traveling ionospheric disturbances (TIDs). The occurrence of the TID can be explained as a consequence of the interaction between AGWs in the thermosphere with the ionosphere [Hernández-Pajares et al., 2006]. Among several techniques used to study TIDs include fixed-frequency observations, analysis of ionosonde traces and multi-frequency HF Doppler and incoherent scatter radar [Davies, 1990; Kelley, 2009]. TIDs are usually classified as large- and medium-size disturbances, differing in their horizontal phase velocity which is higher or lower than the sound velocity in the lower thermosphere (roughly 300 m/s) and in their periods of 0.5 to 3 hours and 15 to 60 minutes, respectively[Hines, 1960; Hocke and Schlegel, 1996; Oliver et al., 1997].

LSTIDs are thought to be generated by impulsive heating in the auroral oval and equatorwards propagation as a result of geomagnetic disturbances such as aurora and ionospheric storms. These disturbances produce an energy transfer toward lower latitudes in the form of thermospheric waves that in high altitudes, interact with the ions [Hernández-Pajares et al., 2006]. LSTIDs predominate during the night hours [Hunsucker, 1982]. Medium-scale TIDs are recorded primarily in the day time and are usually associated with AGWs which are generated in the lower atmosphere. According to Hernández-Pajares et al. [2006] AGWs are formed by a combination of the following: temperature-dependent recombination, wind effects like neutral winds or the solar terminator. The presence of TIDs in the ionosphere has consequence on the performance of precise navigation systems. This is because the slant differential ionospheric delays need to be interpolated with high precision in order to navigate with a few centimeters of error by fixing the carrier phase ambiguities in real time. Hernández-Pajares et al. [2006] states that during the ionospheric interpolation process, the TIDs in the path of trans-ionospheric signal can introduce a significant error within the networks with baselines

from tens to hundreds of kilometers, which are significant distances compared to the MSTIDs wavelengths.

3.4 Effects of ionospheric irregularity on radio waves

Ionospheric irregularities are essentially localized variations in electron density which cause small-scale fluctuations in refractive index which causes ionospheric scintillation [Allnutt, 1989]. Irregularities of different scale sizes, ranging from centimeters to kilometers, develop and create an intense scintillation environment, leading to communication and navigation problems [Abdu, 2001]. The presence of ionospheric irregularities such as TIDs has consequence on the performance of precise navigation systems. This is because the slant differential ionospheric delays need to be interpolated with high precision in order to navigate with a few centimeters of error by fixing the carrier phase ambiguities in real time.

Investigations by Forte and Radicella [2005] suggest that the actual effect of ionospheric scintillation on satellite navigation systems cannot be assessed by analyzing experimental data (even if measured by GPS scintillation monitors) in the classical way. These authors pointed out that this method of analysis deals with average scintillation activity which varies with geophysical conditions such as season and solar activity, but does not take into consideration particular navigation characteristics.

3.4.1 Ionospheric scintillation

Ionospheric scintillation in the mid-latitudes is mostly caused by small scale irregularities in electron density ranging from a few meters to kilometers. Scintillation in the ionosphere is a function of solar activity, geomagnetic activity, time of the year, local time, and geographic location. Ionospheric scintillation in the equatorial latitudes is attributed mainly to the ionospheric equatorial anomaly, which is associated with the sharp gradients in the electron density within this region. According to [Kintner et al., 2007], ionospheric scintillation occurs mostly at the high and low latitudes with a much lower incidence in mid-latitudes. High latitude ionospheric irregularities have been associated with energetic particle precipitation, such as in the South Atlantic Magnetic Anomaly (SAMA) region. Mid-latitude scintillation increases during geomagnetically

active periods. Low latitude ionospheric irregularities are attributed to decreased ionospheric conductivities as a result of plasma bubbles, plasma drifts, neutral winds and pre-reversal enhancement of the equatorial eastward electric field [Du et al., 2000].

When an irregularity appears in the ionosphere as evidenced at HF band by a SF occurrence, the calculated TEC derived from GPS observables at the L-band may show a fluctuation. An irregularity seen as SF may also be correlated with a quick variation in the received carrier-to-noise ratio (C/No) on GPS L-band signals. However, scintillation can also be observed in the frequency of cycle slips in the phase of a GPS signal. An increase in data loss and number of cycle slips often occurs when the signals traversing the ionosphere encounter irregularities causing scintillation. These effects become severe during the occurrence of intense ionospheric scintillation events in the equatorial or auroral regions. The presence of reflecting obstacles in the vicinity of the receiving antenna can cause multipath effects that may produce similar effect as scintillation associated with ionospheric irregularities. The ability of a receiver to cope with scintillation depends on the frequency of occurrence of scintillation, as well as on the radio frequency and the position (azimuth, elevation) of the observed satellite [Conker et al., 2000].

Frequent scintillation may not allow enough time for a GPS receiver to recover from a cycle slip or loss of lock and hence may cause the receiver to lose track of the signals from GPS satellites during loss of lock, which may increase navigation errors or even cause navigation failure [Kintner et al., 2007]. Scintillation makes tracking of GPS satellite signals difficult. Radio communication systems are known to be affected significantly by ionospheric irregularities which in turn limit the ability of the receiver system to coherently integrate weak signals [Dierendonck et al., 1993].

The region of the equatorial anomaly lies approximately $\pm$ 10°–20° on either side of the magnetic equator. This region usually experiences enhanced ionization and has been identified as the most likely region for the source of ionospheric scintillation [Dubey et al., 2005]. Based on in situ and ground-based measurements, Wernik et al. [2004] identified that ionospheric irregularities are more dominant near the magnetic equator and are observable during the pre-midnight period. Ionospheric irregularities can also be observed during the nighttime in auroral zones and at all local times in polar regions. According to [Wernik et al., 2004], high latitude irregularity of scale sizes ranging from hundreds of kilometers to a few centimeters.

3.4.2 Methods of estimating ionospheric scintillation

Several airborne, ground- and satellite-based HF techniques have been used to study ionospheric irregularities that cause scintillation. These include coherent backscatter, in situ rocket and satellite measurements and scintillation techniques which measure radio signal perturbations [Radicella and Ezquer, 2002]. Data from the International GPS Service (IGS) network, originally designed for satellite orbit measurement and Earth observation provide an excellent means of measuring scintillation effects (via ionospheric disturbance and TEC measurements). Due to their wide coverage and continuous availability GPS satellites can be used to monitor ionospheric scintillation activity on a global basis. In GPS data, scintillation at L-band frequencies can be inferred from both dedicated scintillation receivers such as the Novatel GSV4004B GPS ionospheric scintillation and TEC monitor (GISTM) or standard dual frequency GPS receivers which sample at 1 second intervals. The two indices widely used to characterize ionospheric scintillations are: the amplitude scintillation index, S_4 and the phase scintillation index, σ_ϕ. However, a high rate of change of TEC (ROT) along a signal path from the GPS satellite to the receiver is widely accepted as a proxy for S_4 and can be used to characterize amplitude scintillation. Furthermore, the derivative of ROT, (DROT) and their respective standard deviations ROTI and DROTI have been used to quantify amplitude scintillation levels [Du et al., 2000].

Amplitude scintillation and measurement

This phenomenon is mainly due to signal fading and enhancement caused by ionospheric small scale irregularities, which can be observed from the rapidly changing signal-to-noise ratio (S/N) time series measured by GPS receivers. Amplitude scintillation is quantified by the S_4 index, which is essentially a normalized standard deviation of the signal intensity measured over a time period [Datta-Barua et al.] and is mathematically expressed as

$$S_4 = \sqrt{\frac{\langle I^2 \rangle - \langle I \rangle^2}{\langle I \rangle^2}} \tag{3.9}$$

where I is the mean incoming signal power in watts (W). Davies [1990]; Radicella and Ezquer [2002] also proposed another index as an approximate measure of amplitude scintillation, which is defined as:

$$SI = \frac{P_{max} - P_{min}}{P_{max} + P_{min}} \tag{3.10}$$

where P is the received signal power in W.

Severe amplitude scintillation reduces the S/N at the GPS receiver and this causes the received signal intensity to drop below the receiver's lock threshold. This forces the receiver to re-acquire the signal and leads to errors in both GPS carrier measurements and GPS code (or loss of code lock). The lock threshold is determined by the bandwidth of the GPS receiver system and depends on the receiver tracking channel. Wanninger [1993] states that a code correlation can withstand lower signal levels than a squaring channel or a cross-correlation channel. The S/N can be mathematically expressed as

$$\frac{S}{N} = \frac{P_{signal}}{P_{noise}} = \left(\frac{A_{signal}}{A_{noise}}\right)^2 \tag{3.11}$$

where P is the average power in W and A is the root mean square amplitude in volts (V). S/N is usually expressed in decibels (dB) as

$$\frac{S}{N}(dB) = 10log_{10}\left(\frac{P_{signal}}{P_{noise}}\right) = 20 \times log_{10}\left(\frac{A_{signal}}{A_{noise}}\right) \tag{3.12}$$

The ratio C/No is the S/N of a modulated signal and the higher this parameter value, the better the quality of reception. It is expressed in dB-Hz and mathematically defined as

$$\frac{C}{No} = \frac{C}{K_B T} \tag{3.13}$$

where C is the received carrier power in W, K_B is the Boltzmann's constant in Joules per Kelvin (JK^{-1}), and T is the receiver system noise temperature in Kelvin (K). According to Dubey et al. [2005], the nominal C/No for the L1 band is ∼45 dB-Hz; below ∼ 24 dB-Hz, tracking of signals gets interrupted. The authors also state that the L2 signal is affected more than L1 by the decrease in the C/No , since its power is less than that of L1 by ∼6 dB.

Phase scintillation and measurement

This type of scintillation is a consequence of sudden changes in ionospheric diffraction and refraction effects. Ionospheric refraction normally induces slow changes in L1 - L2 phase differences while phase scintillation induces rapid changes. These phase changes can be of the order of > 0.5 cycles of L2 which causes L2 channels aided by L1 tracking data to lose lock. Phase scintillation is known to complicate cycle slip detection and measurement since it can reach cycles of L1 or L2 signals between two epochs with a common epoch rate of ≤ 10 seconds [Wanninger, 1993]. Phase variations are often quantified in terms of the σ_ϕ which is defined as the standard deviation of the refractive component of the GPS signal phase deviation induced by irregularities during transit through the ionosphere. It is mathematically expressed as follows

$$\sigma_\phi = \sqrt{\langle \phi^2 \rangle - \langle \phi \rangle^2} \tag{3.14}$$

where ϕ is the signal phase in degrees or radians. Phase scintillation can cause GPS receiver systems to lose lock on the signal due to rapid changes in the signal frequency. The apparent range rate errors can produce a Doppler shift change in GPS signals, and when this shift exceeds the bandwidth of the phase lock loop (PLL), it results in loss of phase lock.

3.5 Summary

The basic theory of the ionospheric scintillation phenomenon, TEC measurement and factors which influence the occurrence of the scintillation phenomenon were explained in this Chapter. The spectral density of both amplitude and phase scintillation, and the effects of the Fresnel filtering factor on the morphology of the irregular plasma structures causing scintillation were explained. Some of the irregularities responsible for ionospheric scintillation (such as TIDs) are presented. Ionospheric scintillation is sometimes attributed to the R-T gravitational instability processes which operate on the steep upward gradient of the bottomside of the F region. The study of the fluctuations in the signal intensity and phase is used to characterize the behavior of the ionosphere.

This knowledge can be used to check for simultaneous occurrences of scintillation and TIDs phenomena.

Chapter 4

Data Source and Method of Analysis

4.1 Scope

This Chapter describes the main data sets and their analysis for the investigation of the mechanisms responsible for the linking lightning to the occurrence of mid-latitude ionospheric irregularities and ionospheric scintillation.

4.1.1 Lightning data

The WWLLN locates lightning by using the time of group arrival (TOGA) of the very low frequency (VLF) radiation (3–30 kHz) from a lightning stroke. At each receiving site the dispersed wave packet is processed and the TOGA is determined from the progression of phase versus frequency using the whole wave train, lasting a millisecond or more [Dowden et al., 2002]. The stable propagation and low attenuation of VLF waves in the Earth–ionosphere waveguide allows a spacing of the receiver sites of thousands of kilometers, but the ionospheric interaction spectrally distorts the received waveform so that it is not straightforward to infer the vertical current magnitude or polarity.

Unlike most ground based lightning detection networks, the WWLLN is generally thought to be equally capable of detecting cloud-to-ground and cloud-to-cloud flashes with similar detection efficiency (DE) as long as they have comparable peak current and

channel length [Jacobson et al., 2006; Lay et al., 2004; Rodger et al., 2006; Rodger and R. L. Dowden, 2005].

The WWLLN data used in this study span the period 1 January to 31 December 2012. Within this time period, the reported flashes from 20°S to 36°S and from 10°E to 36°E are considered. Following the advice of the WWLLN developers, only those lightning locations that triggered at least five sensors and that had residuals ≤30 ms are regarded as good data and are included in this analysis. The processing algorithm to obtain the data of this analysis is the latest released, and it has been estimated that the algorithm generates 63% more lightning locations than the previous algorithms [Rodger et al., 2009].

The format of the WWLLN data files are ASCII text files labeled with the date and time of the data such as the example given in Table 4.1.

TABLE 4.1: Sample data from WWLLN data file showing geographical locations, energy, time and date of individual stroke records

Date	Time	Lon	Lat	Resid	Nsta	Energy	RMS	nstn
2012/4/23,	00:00:00.149517,	26.5463,	135.4961,	13.2,	9,	2741.38,	332.49,	5
2012/4/23,	00:00:00.834707,	10.7970,	125.8763,	06.2,	7,	1744.95,	131.47,	6
2012/4/23,	00:00:00.943868,	19.4564,	-070.9303,	17.2,	6,	298.00,	118.10,	4
2012/4/23,	00:00:00.922768,	14.1879,	-090.7451,	24.0,	16,	507.86,	136.14,	13
2012/4/23,	00:00:00.943845,	19.3481,	-070.9295,	16.4,	5,	212.37,	48.31,	4
2012/4/23,	00:00:01.205949,	14.2636,	-090.4189,	14.0,	11,	140.89,	33.33,	9

where (as above): Date and time are in UTC, Lat, Lon in Fractional Degrees, Resid is the residual fit error in microseconds (always < 30 microseconds), Nsta is the number of WWLLN stations which detected the stroke (always ≥5), Energy (in Joules) of the lightning stroke detected, RMS is the energy uncertainty in Joules, nstn is the number of WWLLN stations participating in the location fit, and Nsta is the number of station within the range 1000 to 8000 km distant from the stroke and used for the power estimate.

4.1.2 Geomagnetic indices

The geomagnetic field provides a useful tool for studying phenomena occurring in the near-Earth space environment. The geomagnetic field controls the motion of plasma around the Earth. Because charged particles cannot cross magnetic field lines, solar wind flowing from the Sun toward the Earth is deflected around the Earth without penetrating directly into the atmosphere. The geomagnetic field is perpetually varying. The geomagnetic field has also periodic variations at some specific periods of 27 days or 11 years. These periodic variations are considered due to respective periods of solar rotation or activities. In addition, the geomagnetic field shows daily variations because of the Earth's (day/night) rotation.

The overall level of geomagnetic disturbance can be measured by a geomagnetic index called planetary 3-hour-range index (Kp). Kp index was first introduced by Bartels and Johnston [1940] and has since been used in many geomagnetic storm studies [e.g., Bartels and Johnston, 1940; Gosling et al., 1991; Loewe and Prölss, 1997; Ngwira et al., 2011]. Kp is an average standardized K-index derived from a network of geomagnetic observatories between northern or southern geomagnetic latitudes. Kp measures the overall variability of Earth's magnetic field observed at mid-latitudes. It is a logarithmic-scale (like the Richter Scale for earthquakes) and goes from 0 (no activity) to 9 (major storm activity). The average, or most probable, Kp level is about 3. The geomagnetic Kp index data used in this study to separate active from inactive geomagnetic conditions is obtained from the NASA's Space Physics Data Facility (SPDF) Coordinated Data Analysis Web (`http://cdaweb.gsfc.nasa.gov/cdaweb/sp_phys/`). The 10.7 cm radio flux (F10.7) and daily sunspot number SSN (Rz) which were used as solar activity indicators, were also obtained from SPDF. Any day with Kp index of maximum value of 4 and above is not considered in our data analysis.

4.1.3 The GPS network and GPS data

A network of dual frequency GPS receivers was established nation wide by various South African agencies, including Trignet, the Hartebeesthoek Radio Astronomy Observatory (HartRAO) and Electricity Supply Commission (ESKOM). The Trignet network comprises of about 60 GPS receivers stations which are distributed all over South Africa.

Most of the Trignet receivers contribute data to the international GPS service (IGS) network.

GPS data used in this study were recorded using the Trignet network with a fairly good nation wide coverage. The data were recorded in universal time system at 1 second sampling rate and stored in a Receiver Independent Exchange (RINEX) format. This format stores the pseudoranges and carrier phases (L1 and L2) for each satellite. The data from ESKOM are not available for scientific research purposes. The dual frequency GPS data sets used in this study are archived at HartRAO and the IGS trignet GPS network and are available via internent download (http://www.trignet.co.za/). The map in Figure 2.3 shows the location of the GPS stations from which data were obtained for this study and Table 4.2 shows the names of the GPS stations and their coordinates.

TABLE 4.2: Trignet GPS Station Names, Geographical and Geomagnetic Locations

		Geographic coordinates		Geomagnetic coordinates	
Station	code	Long (°E)	Lat(°S)	Long (°E)	Lat(°S)
Bloemfontein	BFTN	26.30	29.10	92.90	29.93
Durban	DRBA	31.02	29.85	97.42	31.48
Grahamstown	GRHM	26.51	33.32	92.10	34.09
Hermanus	HNUS	19.22	34.43	84.67	33.90
Mafikeng	MFKG	25.54	25.81	92.87	26.59
Upington	UPTA	21.26	28.41	88.08	28.39

4.2 Method of analysis

This section describes the necessary procedures implemented in processing the data sets in order to arrive at the results. In this study, patterns of events and variability of TEC were looked for with both the WWLLN data sets and GPS data sets and any occurrences observed on both data sets were investigated.

4.2.1 Dual frequency GPS data analysis

This section offers an overview of the data and procedures for investigating the variability of TEC (i.e., ΔTEC for wave-like structures, TIDs investigation) and, the S_4-proxy scintillation index (S_{4p}), and ROTI (i.e., for ionospheric scintillation investigation).

We have used RINEX data from six of the GPS receiver stations belonging to the Trignet (http://www.trignet.co.za/) network to derive the integrated electron density i.e., the total electron content (TEC) along the signal path between the receiver on the ground and the GPS satellite in space, commonly referred to as slant TEC (STEC). In order to process GPS data, a software package called "GPS_TEC" developed at Boston College was used. The GPS_TEC algorithm computes STEC at each ionospheric piecing point (IPP) and converts it to vertical TEC (VTEC) at each IPP, removes the outliers/jumps and then calculates the mean VTEC as a representation of the TEC above the receiver. The mean VTEC is derived by calculating the two-sigma iteration of the TEC values computed every 2 or 5 minutes from all available satellites measurements. The GPS_TEC algorithm uses Kalman filtering to estimate TEC from GPS data. An example of the output of VTEC derived from the GPS_TEC algorithm is shown in Figure 4.1.

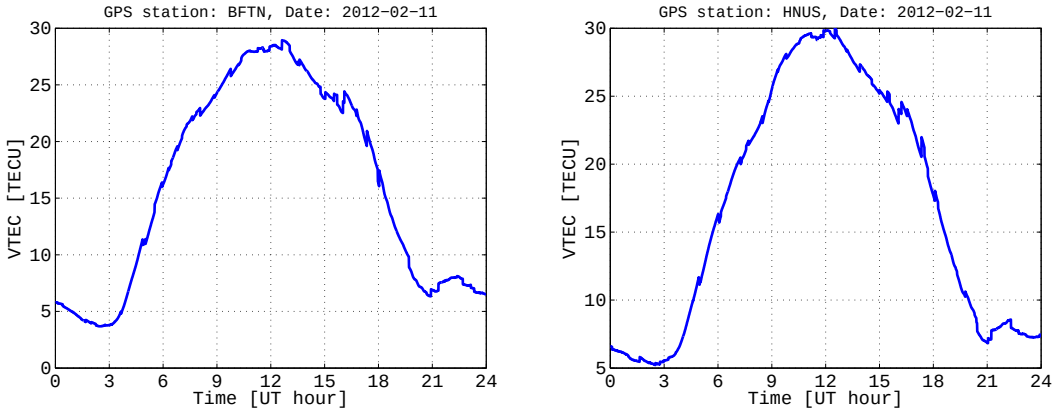

(a) (b)

FIGURE 4.1: VTEC derived using GPS_TEC at (a) BFTN and (b) HNUS for 11 February, 2012.

The GPS_TEC software has been used in many studies [e.g., Amabayo, 2011; Habarulema et al., 2013; Lay et al., 2013; Seemala and Valladares, 2011] to derive information about the ionospheric disturbances. Amabayo [2011] compared the output of GPS_TEC with the output of an independent model called Adjusted Spherical

Harmonic Analysis (ASHA) model developed by Opperman [2007]. The ASHA model uses a spherical harmonics filter to estimate the VTEC above the receiver. Amabayo [2011] found out that the results from both algorithms reflect the nature of the dynamics in the ionosphere, in terms of TEC variability, hence the two algorithms do agree in determining any disturbances in the ionosphere. However, The VTEC calculated using ASHA model is relatively smooth compared to VTEC computed using GPS_TEC algorithm. The smoothness of the TEC derived from the ASHA algorithm is due to its use of a spherical harmonic interpolation algorithm and a 24 hour window of data for deriving the TEC at any given time. The GPS_TEC software derives a TEC value without interpolation other than that which is inherent in the application of a Kalman filter. Therefore the ability of the GPS_TEC algorithm to retain the high frequency fluctuations in the ionospheric data makes it suitable for this study.

4.2.2 The GPS_TEC algorithm

GPS satellites transmit their ephemeris (and other information) on two carrier frequencies (f1= 1575.42 MHz and f2 =1227.60 MHz) on the L-band for research purposes. The time based pseudorange observables associated with f1 and f2 frequencies are denoted by P1 and P2 respectively.

$$(STEC)_{desired} = STEC + B_{Rx} + B_{Rich} + B_{sat} \tag{4.1}$$

where B_{Rx}, B_{Rich} and B_{sat} are the receiver bias, receiver inter-channel bias and satellite biases respectively.

$$VTEC = \frac{STEC}{\left\{1 - \left(\frac{R_E \times cos(\varepsilon}{R_E + h_E}\right)^2\right\}^{-0.5}} \tag{4.2}$$

where R_E is the Earth radius, ε is the elevation angle in radians, and h_E (i.e.,350 km) is the altitude of the thin layer above the surface of the Earth.

The GPS_TEC software calculates TEC with an elevation mask of $\geq 20^{\circ}$, and applies satellite and receiver bias corrections according to Equation 4.1. The software takes RINEX observation files with at least C1 (coarse/acquisition code transmitted on the

f1), L1, L2, P2 observables as inputs. In the presence of signal-to-noise ratio (S/N) observable S1, GPS_TEC derives a proxy for S4 index (S_4p) at ten-minute intervals from 30 second samples of S1 [Amabayo, 2011].

The GPS_TEC algorithm uses the RINEX navigation file of any IGS station available for internet download. It calculates elevation and azimuth angles of the observed satellites which are then used for the VTEC calculation as shown in Equation 4.2. The differential code bias (DCB) files provided by the Center for Orbit Determination in Europe (CODE) are also required. The GPS_TEC algorithm also reads satellite (P1-C1) biases and the (P1-P2) DCB biases, if available. In the absence of biases, it calculates the inter-frequency biases for different satellites visible to the receiver (though this is not very effective as it allows some room for TEC variability). The biases in the observed STEC are accounted for by computation via the Equation 4.1. The receiver biases are estimated by assuming that the nighttime TEC values are fairly constant. Biases are then evaluated by minimizing the root mean square (rms) average error (of TEC values) obtained from different satellites at the same time [Amabayo, 2011].

As is common practice, conversion from bias corrected STEC to bias corrected vertical TEC (VTEC) is performed using a thin shell approach which assumes that the ionospheric plasma is compressed into a thin shell at the peak ionospheric height (h_E). The conversion factor (or mapping function) depends on the elevation angle of the slant path and on h_E as shown in Equation 4.2.

ROTI as S4 amplitude scintillation proxy

The VTEC obtained from the GPS_TEC algorithm is used to derived the rate of change of TEC (ROT) and ROT index (ROTI). These parameters were derived to look for signatures of ionospheric irregularities. The ROT is calculated using Equation 4.4 from 30-second sampled GPS data and the ROTI derived from the ROT, which is defined as the standard deviation over a 5-minute period of ROT [Pi et al., 1997].

The ROT time series contains useful ionospheric information on the variability of dual-frequency phase data. They are especially suitable for the detection of ionospheric disturbances (scintillation, TIDs). A smooth and increasing ROT curve indicates an undisturbed satellite path. Phase scintillations appear as rapid variations due to sudden

changes in ionospheric refraction. Significant remaining errors are multipath, which can reach up to 0.3 TECU/min, and the random observation errors, which usually do not exceed 0.07 TECU/min. This multipath is a site-dependent phenomena whose effect can reach several centimeters on phase measurements and has periods ranging from a few minutes to several hours depending on the separating distance between the reflecting surface and the observing antenna [Warnant and Pottiaux, 2000].

In the absence of measured L-band scintillation values, a phase scintillation index ROTI can be derived from ROT. The ROTI, which can be used as a proxy for the S_4 amplitude scintillation index (S_4p) is defined as the standard deviation over a 5-minute period of ROT calculated from 30-second sampled GPS data [Pi et al., 1997]. Studies [e.g., Basu et al., 1999; Pi et al., 1997] concluded that the ROTI measurements could be used as a proxy for assessing the presence of ionospheric scintillation.

$$\Delta\mathrm{VTEC}(\mathrm{t_k}) = \frac{\mathrm{VTEC}(\mathrm{t_k}) - \mathrm{VTEC}(\mathrm{t_{k-1}})}{\mathrm{t_k} - \mathrm{t_{k-1}}} \tag{4.3}$$

$$\mathrm{ROT} = \frac{\Delta\mathrm{VTEC}(\mathrm{t_k})}{\Delta\mathrm{t}} \tag{4.4}$$

$$\mathrm{ROTI} = \sqrt{\langle \mathrm{ROT}^2 \rangle - \langle \mathrm{ROT} \rangle^2} \tag{4.5}$$

ROTI after Pi et al. [1997] values are for a single satellite while ROTI_{AVE} after Oladipo and Schüler [2013] gives 30 minutes average values for all satellites and the values are valid over a station.

4.2.3 Estimating wave-like structures in the ionospheric data

Equation 4.6 can be used to detect high frequency changes in the TEC due to irregular ionospheric phenomena such as TIDs and scintillation effects. The occurrence of TIDs often cause large gradients in the TEC even on short distances.

$$\Delta VTEC = VTEC - VTEC_{fit} \tag{4.6}$$

The deviation of the ΔVTEC is done by subtracting a modeled data ($VTEC_{fit}$) from the actual VTEC data. The $VTEC_{fit}$ is obtained by using a Matlab third party function called "Savitzky-Golay filtering" (sgolayfilt) with a selected time window of 90 minutes. Then we smooth the ΔVTEC using the sgolayfilt again to remove the noise and the results are shown in Figure 4.2.

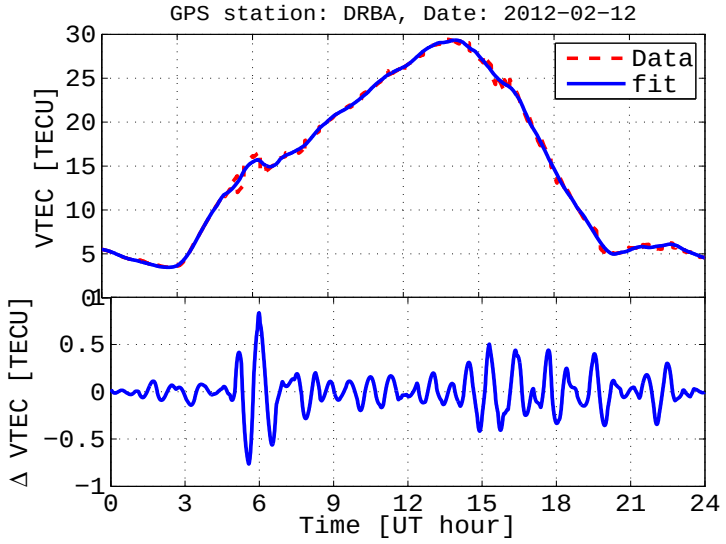

FIGURE 4.2: Example of the VTEC (red dotted curve), $VTEC_{fit}$ (blue solid curve) and ΔVTEC

We used the ΔVTEC as a single valued function of time for individual measuring paths to perform a spectral analysis of the observed waves. We applied a continuous wavelet transform based on the complex Morlet wavelet to get information about the spectral content of the signal and how it changes with time. We studied wave activity in the period range 15 min–3 h. Based on the calculation of the complex Morlet wavelet, we analyzed in more detail wave activity in the period range of 15 min – 1 h (i.e., MSTIDs) and period range of 30 min – 3 h (i.e., LSTIDs). To arrive at our analysis of diurnal and seasonal variation of wave activity in the study region, we determine for each measuring path the maximum power coefficient (MPC) of waves with 95% and above significant level as the arithmetic means of amplitudes of the complex wavelet transform coefficients in the considered period ranges for all time steps. The maximum power of the spectrum (MPS) represent proxies for typical spectral amplitudes for the given measurement path in the individual period ranges. The maxima of daily regional MPS represent the diurnal as well as seasonal variations of wave activity for the individual

period ranges. The results are presented in Figure 5.23 for 282 geomagnetically quiet (i.e., Kp $\leq$ 4) days.

4.3 Summary

The data sources used in this study and the corresponding algorithms used for data analysis are described. The formats of the GPS data and processing techniques used in the analysis are explained. The derivation of the VTEC perturbation as a mechanism of detecting the level of ionospheric disturbance is also explained. The format of the lightning data from WWLLN is also explained. The results and discussion of the processed data are presented in Chapter 5.

Chapter 5

Results and Observation

5.1 Introduction

The cause of mid-latitude ionospheric irregularities (TIDs and scintillation) particularly in the southern hemisphere has not been as effectively established compared to other latitudes. Their appearance in the GPS data have raised concerns and identified the need to investigate them. The results presented in this study are based on the diurnal and seasonal variations of lightning, ionospheric irregularity event (IIE) (i.e., ROTI 0.8 TECU) and vertical TEC (VTEC). The contribution of this study is the understanding the mechanism(s) responsible for the occurrence of the mid-latitude ionospheric irregularities though the analysis of dual frequency GPS data for occurrence frequencies of IIE and their correlation with lightning events.

5.2 Lightning statistics

We have studied 282 days worth of mid-latitude TEC data collected from the six GPS stations and lightning data from WWLLN in 2012 for the study of the plasma irregularities seen at geomagnetically 'quiet' (Kp $\leq$ 4) times. The 282 days comprise 78 Summer days, 66 Autumn days, 68 Winter days and 69 Spring days. About 1,169,569 lightning strokes were recorded by WWLLN in 2012 within the study region (i.e., latitude 20°S to 36°S and longitude 10°E to 36°E). The southern hemisphere local Summer begins from

December to February, Autumn from March to May, Winter from June to August and Spring from October to November.

5.2.1 Seasonal variation

The two ocean current systems, the cold Benguela along the West Coast and the warm Agulhas current along the East Coast influence convection and formation of thunderstorms and hence the lighting activity. The warm Agulhas current which flows down the east coast of Africa from approximately 27° to 40° S coupled with the high pressure systems in the Indian Ocean is conducive for the formation of thunderstorms off the east coast of southern Africa while the cold Benguela which flows northward past the southern tip of Africa inhibits cloud formation off the west cost of southern Africa [Collier et al., 2006]. The effect of these two current systems (Agulhas and Benguela) is apparent in the data hence the high lightning flash density observed off the east coast and low lightning flash density observed off the west coast of the southern Africa. Figure 5.1 reveals that during Spring and Summer the majority of lightning strokes occur over land, whereas during Autumn and Winter relatively greater lightning activity is found over the ocean, in excellent agreement with [Collier et al., 2006].

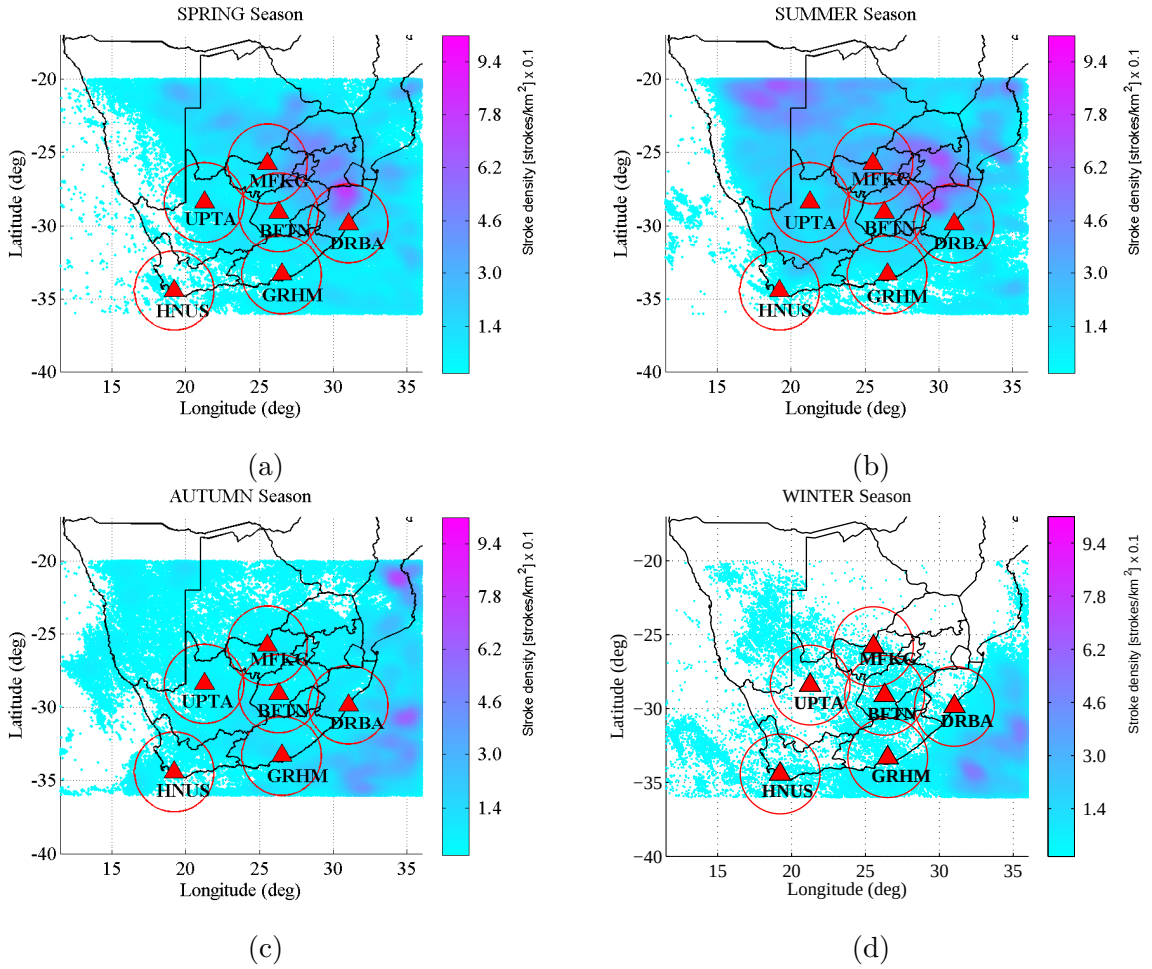

FIGURE 5.1: Stroke density of lightning events per square kilometer as a function of season; (a) Spring, (b) Summer , (c) Autumn and (d) Winter. The stroke density values obtained have been verified by using simulated data with a known stroke density.

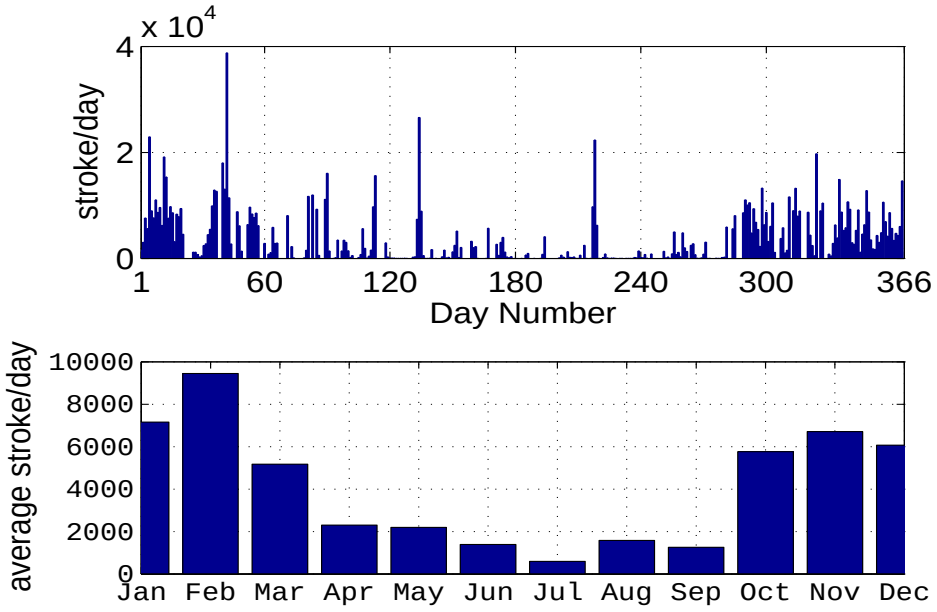

FIGURE 5.2: Seasonal variation of lightning activity over southern Africa (i.e., 20°S to 36°S and 10°E to 36°E) in 2012. The highest stroke rate occurred on 2012-02-11.

The effect of solar heating on the lightning distribution is also observed. The Earth receives heat during the day by solar radiation but continually loses heat by terrestrial radiation. During the day especially in Summer, solar radiation exceeds terrestrial radiation and the surface becomes warmer. This condition results in temperature gradient over land and causes local departure of warm surface air against gravity to higher altitude where they condense to form clouds. and hence the rate of convection, above the land would be maximized during local Summer and Spring when the air temperature relatively higher.

The top panel of Figure 5.2 presents the daily lightning rates in 2012 as measured by the WWLLN over South Africa. Only days which are geomagnetically inactive are considered for this analysis. Since the meteorological conditions necessary to produce lightning are not always present, the day to day variability of lightning are dominated by days for which there was little or no lightning especially during Autumn and Winter seasons. Using the monthly average stroke per day, the seasonal variation lightning is well represented in the bottom panel of Figure 5.2. The Summer lightning activity is dominated by the contribution in the month of February with an average stroke rate of 9.5×10^3 per day and a maximum stroke rate of about 38781 per day on 2012-02-11. This average stroke rate drops to about 596 stroke per day in the month of July during

Winter. This is not unreasonable since it is just recognition of the fact that convective instability which must be present for lightning to occur is limited during Autumn and Winter seasons.

5.2.2 Diurnal variation of lightning stroke density

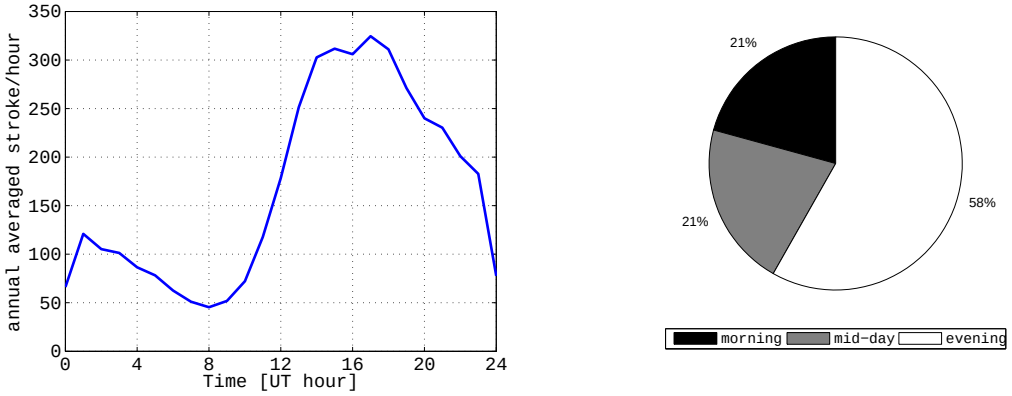

(a) (b)

FIGURE 5.3: (a) Diurnal variation of lightning activity (b) percentage contribution of lightning activity over South Africa during geomagnetically quiet days in 2012.

The association between heating of the air close to the Earth's surface and convection implies a diurnal variation in lightning activity, where the peak should lag some time behind the Sun passing through the meridian [Collier et al., 2006]. Concentrating now on the study region, the diurnal variation of lightning activity as a function of universal time (UT) is plotted in Figure 5.3(a). The effects of diurnal heating are most apparent in the data, where a pronounced peak occurs in the late afternoon, in excellent agreement with [Eriksson, 1976], who found the peak flash rate to occur at around 17:00 SAST, while a low level of activity is maintained consistently at other times. The peak is broad, starts rising at noon and subsides around midnight.

In Figure 5.3(b), the diurnal activity of lightning occurrence is also divided into three South African Standard Time (SAST) periods: morning (00:00–08:00 SAST), midday (08:00–16:00 SAST) and evening (16:00–24:00 SAST); SAST = UT+2 hr. More than half the lightning strokes occur within the latter portion of the day, consistent with the development of storms over South Africa in the late afternoon and early evening [Preston-Whyte and Tyson, 1988].

The annualized diurnal variation in lightning activity plotted in Figure 5.3(a) is dominated by the contributions from Summer and Spring, and hence reflects an activity maximum in the late afternoon and a minimum during the morning hours. Williams and Heckman [1993], considering data for Summer in Darwin, Australia, found a peak in the lightning flash rate between 16:00 and 17:00 local time (LT), with a half-width of around 6 h, consistent with what we observed in the Summer data. In Winter with cool and dry conditions, the level of activity is consistently low throughout the day during Winter. In Autumn a minor increase is evident in the afternoon.

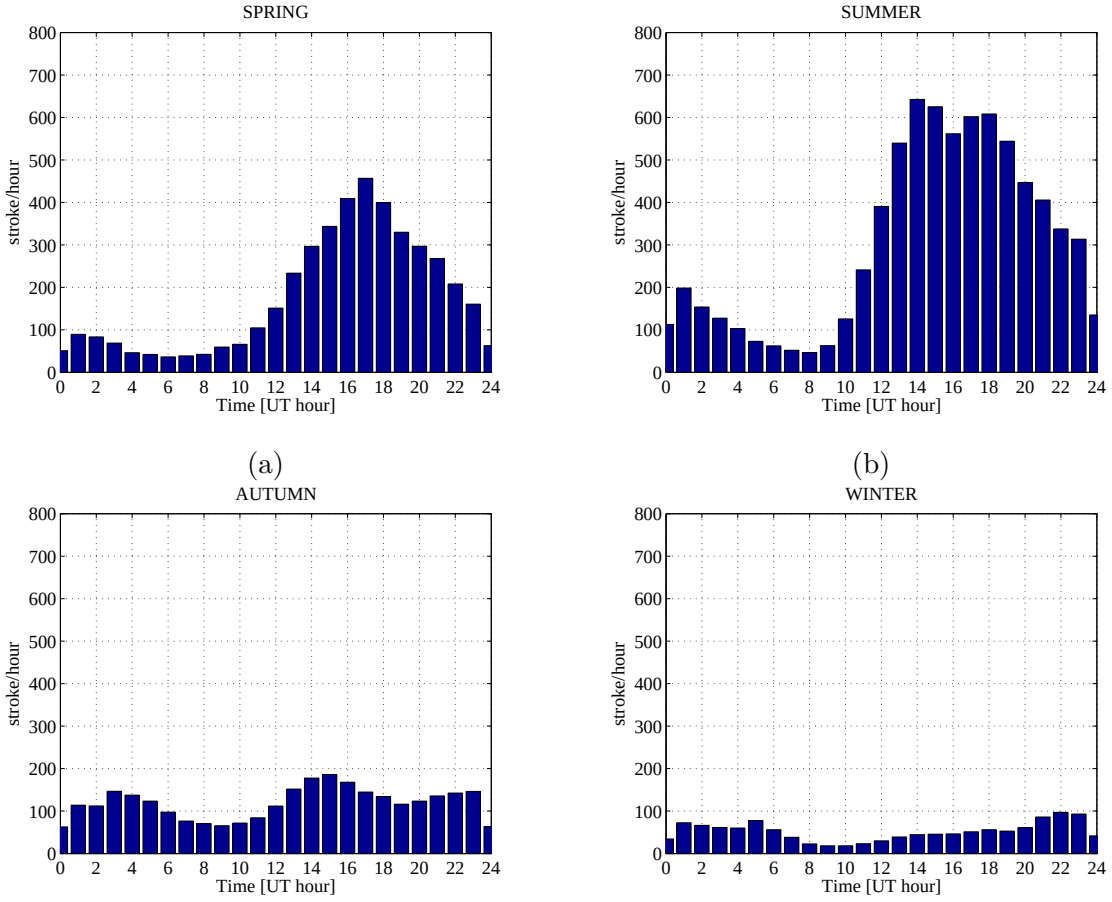

FIGURE 5.4: Diurnal variation of lightning as a function of season in 2012; (a) Spring, (b) Summer, (c) Autumn and (d) Winter.

In Figure 5.4 the diurnal variation in lightning activity in southern Africa is more evident during local Summer and Spring. This may be attributed to the fact that majority of lightning activity occurs over land where temperature varies considerably over time scales in the order of a day. On the contrary, no systematic diurnal variation is apparent during Autumn and Winter. This may be attributed to the fact that a significant amount of

lightning event occurs over the ocean where temperature is more stable due to the larger heat capacity of the ocean. One might expect that the temperature gradient, and hence the rate of convection, above the ocean would be maximized during the early morning hours when the air temperature reaches a minimum. This, however, is not reflected in the diurnal variation of the lightning activity during Autumn and Winter as shown in Figure 5.4(c) and Figure 5.4(d).

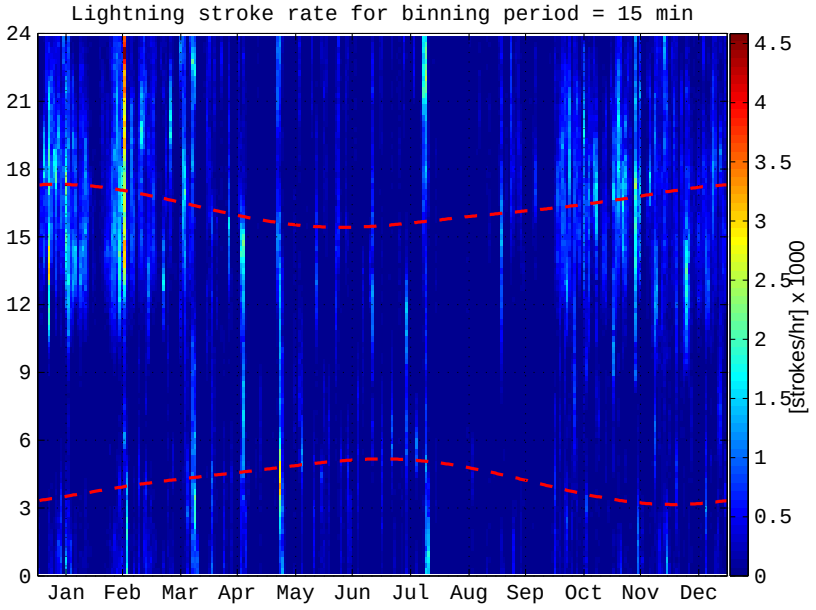

FIGURE 5.5: Seasonal and diurnal distribution of lightning activity over South Africa in 2012. The X-axis indicates months of the year and the Y-axis represent time in UT. The red dotted curves show the morning and evening Solar terminator.

The lightning data presented in Figure 5.5 also shows seasonal and diurnal dependence of lightning in terms of stroke rate. The x axis represents day number of the year and the y axis represents time of the day. The color bar indicates the intensity of the lightning activity. The seasonal dependence of lightning is apparent; the high rate (i.e., 30–40 strokes per minute) occurs between September and March but from April through August low stroke rate (i.e., 0–10 strokes per minute) of lightning occurs. Diurnal dependence of stroke rate is also evident; the high stroke rate (i.e., 30–40 strokes per minute) occurs between the hours of 12:00–22:00 UT. These results further confirm the seasonal and diurnal dependence of lightning activity and hence its potential influence on the generation of irregularities that appear as TIDs in the ionosphere.

5.3 TEC variability

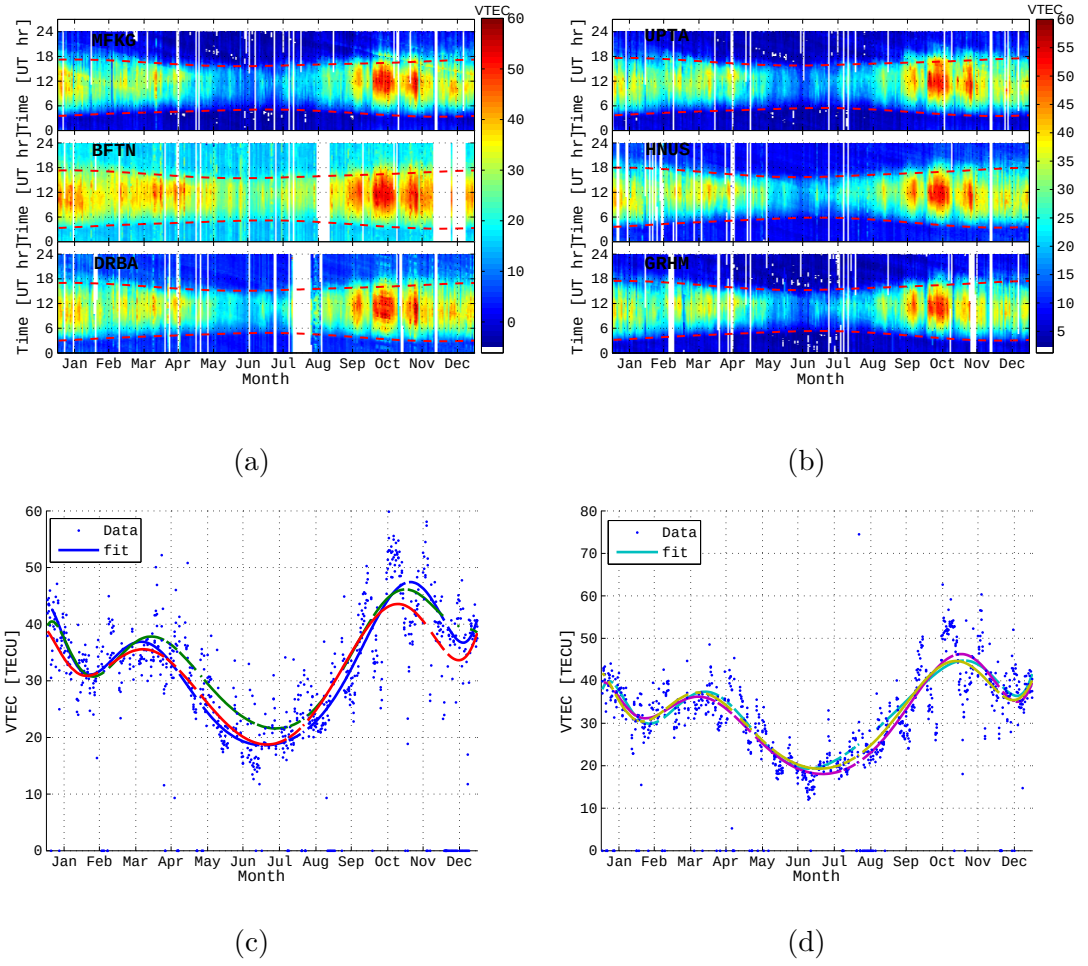

FIGURE 5.6: (a) and (b);TEC maps showing diurnal and seasonal variation of TEC over the six locations studied for the year 2012. The white spaces in the maps indicate absence of data. Th red dotted curves represent the times of the morning and evening terminators. (c) and (d); variation of daily maximum and a polynomial fit to the TEC data. The colors of the curves representing the GPS stations are similar to the colors in the legend of Figure 5.7.

The TEC over a specific region of the Earth does not remain constant throughout the year, month, day and even hour. Observations of the ionosphere at high time resolution reveal transient variations. The revolution of the Earth around the Sun gives rise to seasonal variations of TEC. These variations arise due to the relative position of the Sun with respect to a point on the atmosphere/Earth. This means that there will be varying radiation reaching the Earth's surface at different locations hence different ionization level at different seasons. The solar terminator is the line that separates the dayside from the nightside of the Earth. The location of the terminator depends on the

axial tilt of the Earth. Since the Earth is tilted by 23.5° away from the Sun's axis, the position of the terminator changes depending on the season.

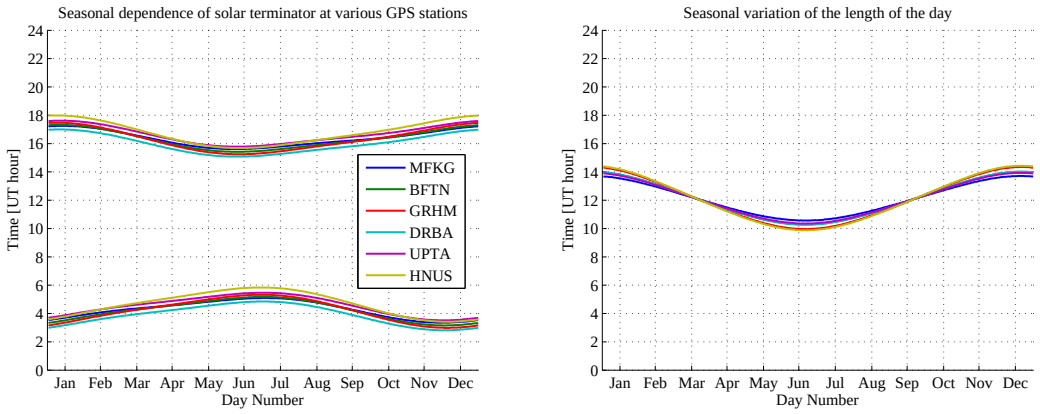

(a) (b)

FIGURE 5.7: Seasonal variation of (a) Solar terminator and (b) length of day over South Africa in the mid-latitude region. Data source: (http://aa.usno.navy.mil/data/docs/RS_OneYear.php)

Since the terminator represents the boundary between the day and night side of the Earth, the time difference between the morning and evening terminator can provide an estimate of the length of the day. Figure 5.7(a) shows that the solar terminator passes quickly over South Africa in the mid-latitude region during local Winter than during Summer and Spring. Figure 5.7(b) shows that the length of the day also varies with local season with the shortest days observed during Winter.

TEC maps were generated for the period of this study for all the six GPS receivers within South Africa. One important observation here is that the diurnal variation of TEC in different seasons is well defined by the morning and evening Solar terminator. During Summer and Spring seasons the morning terminator in most of the days occurs before 04:00 UT while the evening terminator occurs around 18:00 UT. Figure 5.6 shows the diurnal pattern of the TEC observed from the six GPS stations for the different months of 2012. This figure shows that TEC achieves a maxima and minima during the months of April and November respectively, throughout the study period. The seasonal pattern shows that ascending and descending phases of TEC occur during equinoxes (March and September) and solstices (June and December). The diurnal variability of TEC during these months is that it increases from about 5:00 UT in many months of the year (September through to March) except in Winter months and shows a peak at 12:00 UT

and decreases down up to about 18:00 UT. This pattern is a signature of the variability of solar radiation as indicated by the morning and evening terminator (i.e., dotted red curves in the figure in each of the panels) and zenith angle at mid-latitude region in the southern hemisphere. The fitted curves in Figure 5.6(c) and Figure 5.6(d) suggest that the ionosphere over South Africa does not vary from one station to another except at Bloemfontein where the VTEC seasonal variation differs from that of the other five stations by having higher diurnal VTEC values from March to August than the other regions.

5.4 Ionospheric irregularity occurrences and statistics

5.4.1 Diurnal and seasonal variation of IIE

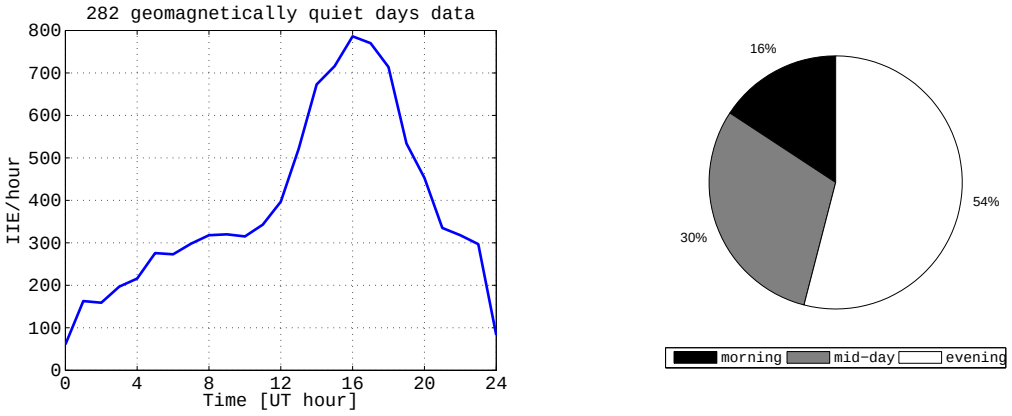

(a) (b)

FIGURE 5.8: (a) Diurnal variation of ionospheric irregularity occurrence (b) Diurnal variation of ionospheric irregularity occurrence over South Africa.

Figure 5.8 gives the diurnal distribution of hourly accumulated occurrence of IIE with elevation mask larger than 20° detected from GPS observation of 282 days in the study region at all GPS stations (January to December, 2012); the hourly accumulated occurrence of IIE is obtained from the GPS-TEC data and is defined as the total number of IIEs in each hour of the day. The IIE occurs in all hours of the day but dominate between 12:00 and 22:00 UT. The IIE occurrence gradually increases from 12:00 UT and reaches its peak in the time interval of 16:00–17:00 UT and then quickly reduces to a very low number before 00:00 UT. That is, the IIE with the elevation mask larger than 20° mainly occurs from about 12:00 UT to midnight during 2012.

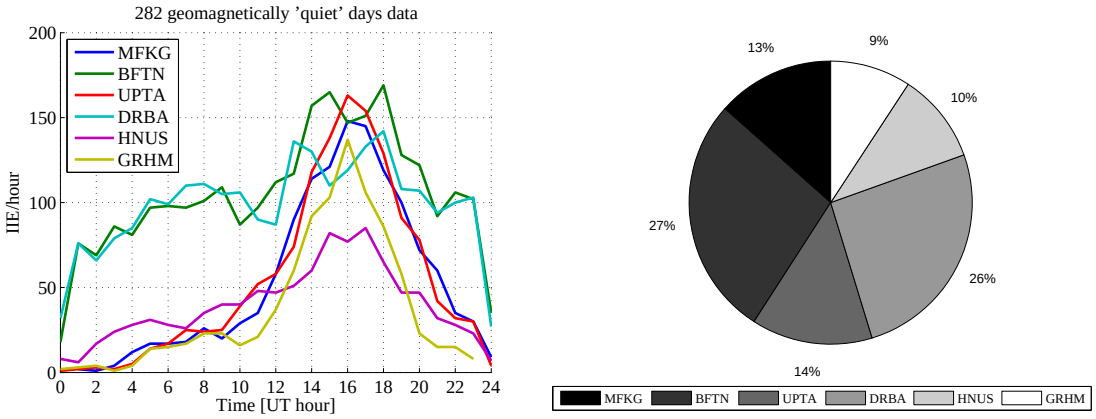

(a) (b)

FIGURE 5.9: Diurnal variation of IIE in various GPS station measurements on (a) geomagnetically 'quiet' days and (b) percentage contributions at each GPS station measurement.

In order to statistically reveal the diurnal dependence of IIE occurrence, the diurnal distribution of IIE occurrence detected from GPS observations during 2012 at the six GPS stations listed in Table 4.2 is also analyzed. Figure 5.9 gives the diurnal variation of daily averaged IIE occurrence accumulated in all valid observing days in 2012. The IIE occurrence is obtained by accumulating the IIE occurrence in every time interval in each observing day searched in the TEC data. Reflecting obstacles located in the vicinity of the receiving antenna can cause multipath effects, similar to scintillations associated with ionospheric irregularities [Romano et al., 2013]. The effect of multipath have been removed from this study by considering only TEC measurements observed by satellites above 20° elevation.

Also, two additional explanations about the IIE analysis should be given. Because of the obvious day to day variation of IIE occurrence shown in Figure 5.12, the daily average of the accumulated IIE occurrence over a year scale cannot reveal the detailed information about the daily diurnal variation of the ionospheric irregularity events. Even so, the result still can give some statistical features about the diurnal dependence of the IIE occurrence. On the other hand, the multisatellite configuration of the GPS constellation makes the difference of the available observation epochs over a regional area in the same time interval exhibits a small variation, which ensures the comparative analysis is reasonable.

From Figure 5.9(a) it can be seen that, although the IIE occurrence in the same time interval in different stations varies greatly, the diurnal distribution of IIE occurrence exhibits an obvious similarity. On the whole, the IIE occurs over South Africa predominantly in the evening times of the day. About 12:00 UT the IIE occurrence increases and usually reaches its peak between 14:00 and 18:00 UT as shown in Figure 5.9(a) and then gradually decreases until late evening.

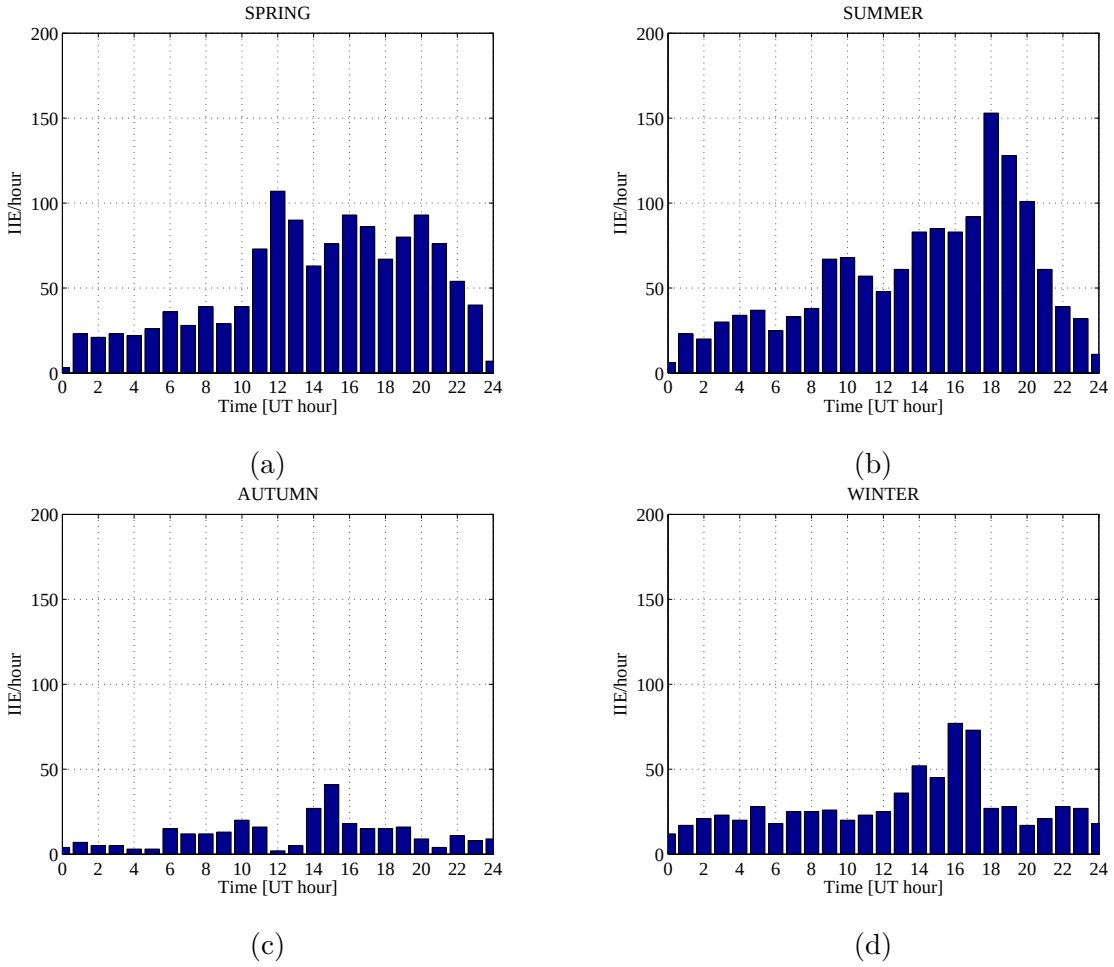

FIGURE 5.10: Variations of IIE as a function of season; (a) Spring, (b) Summer, (c) Autumn and (d) Winter.

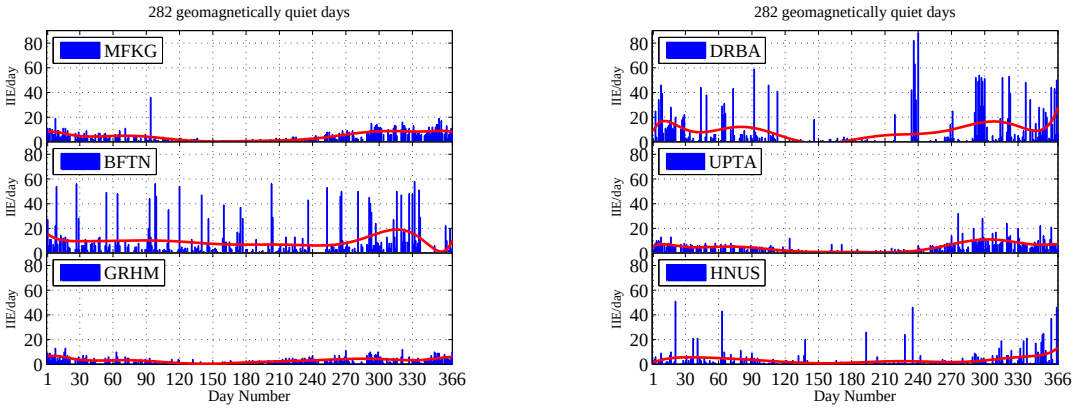

(a) (b)

FIGURE 5.11: Seasonal variation of IIE at the six GPS stations. The red curves in each plot is the polynomial fit to the data to show the seasonal trend.

Using the daily accumulated IIE occurrence from the TEC data with elevation larger than 20° measured from the GPS stations in Table 4.2, the seasonal dependence of IIE occurrence is investigated. The growth of ionospheric irregularities increases substantially during geomagnetic storms initiated by solar disturbances [Belehaki and Tsagouri, 2001; Buresova, 2005; Hunsucker and Hargreaves, 2002]. In order to remove any potential bias that may be caused by geomagnetic storms in our seasonal analysis of the IIE, only the IIE on geomagnetically quiet days (i.e., geomagnetic Kp index ≤ 4) is selected for the IIE seasonal distribution study.

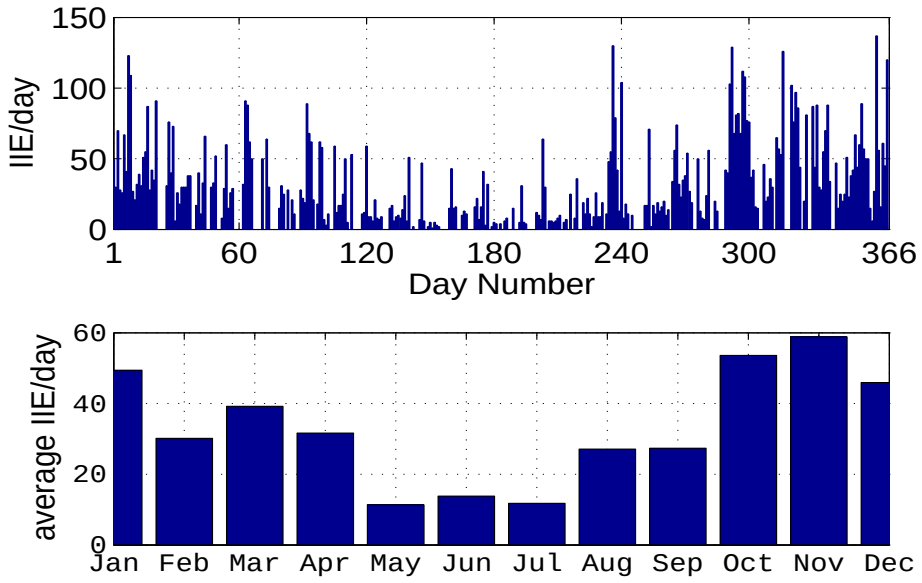

FIGURE 5.12: Day to day variation of IIE occurrence on geomagnetically inactive days over South Africa in 2012.

Figure 5.11 gives the seasonal dependence of the IIE occurrence accumulated from 00:00 to 23:00 UT every day detected from GPS data observed at the six GPS stations in 2012. The x axis is the day number (DN) of year , and the y axis is the total number of IIE that occurred from morning to evening hours every day. It can be seen in Figure 5.11 that the variation of IIE occurrences with DN is not quite clear even though there is some level of seasonal dependence at some stations; the IIE occurrence around the Spring months (i.e., September to November) is larger than that of the other months. During the Spring months, the feature of day to day variation of IIE occurrence is also obvious as shown in Figure 5.12. Furthermore, the IIE occurrence in the months of Spring is a little more frequent than that in the months Summer in this year.

5.5 Correlation between ionospheric irregularities and lightning

The diurnal and seasonal dependence of IIE occurrence revealed in the six GPS stations observation over South Africa during geomagnetically quiet days must have some relationship with the ionospheric environment of GPS signal propagation.

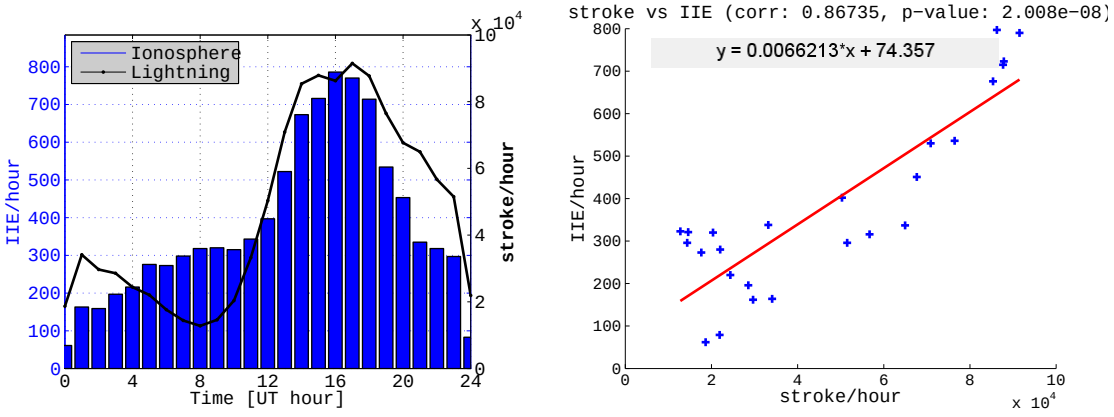

(a) (b)

FIGURE 5.13: (a):Annualized diurnal variation of lightning stroke rate in the study region compared with ionospheric event rate (bars). (b):correlation between ionospheric event and lightning stroke rates.

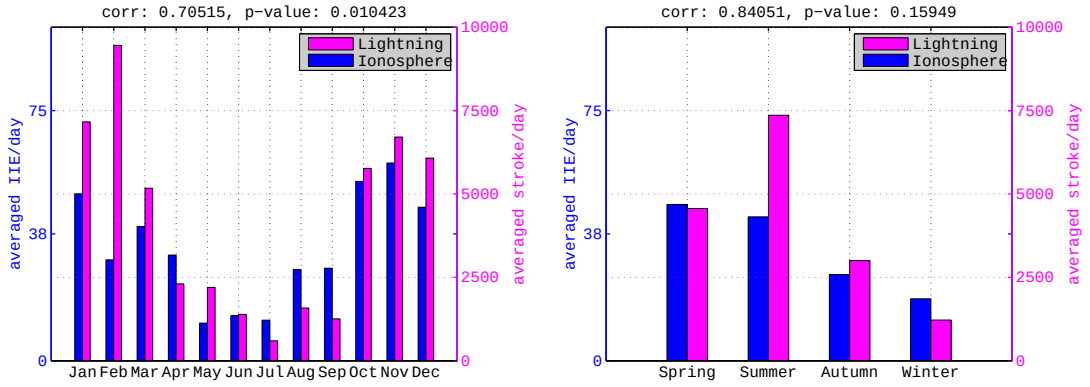

(a) (b)

FIGURE 5.14: Daily average count of lightning (magenta bars) and IIE (blue bars) for (a) months and (b) seasons

Figure 5.13(a) shows the annual diurnal dependence of both lightning stroke rate and IIE rate (i.e., ROTI above 0.8 TECU/min). The lightning stroke rate and IIE rate show similar trend with a peak around 16:00 UT. The scatter plots in Figure 5.13(b) shows the annual diurnal correlation between the lightning stroke rate and IIE rate. In Figure 5.13(b) the correlation between diurnal variations of IIE and stroke rate is found to be about 86%. Using the monthly average rate, we also investigated the seasonal correlation and results are presented in Figure 5.14. While the seasonal correlation between the monthly average IIE rate and average stroke rate is about 70%, the seasonal average IIE and average stroke rate correlation is found to be about 84%.

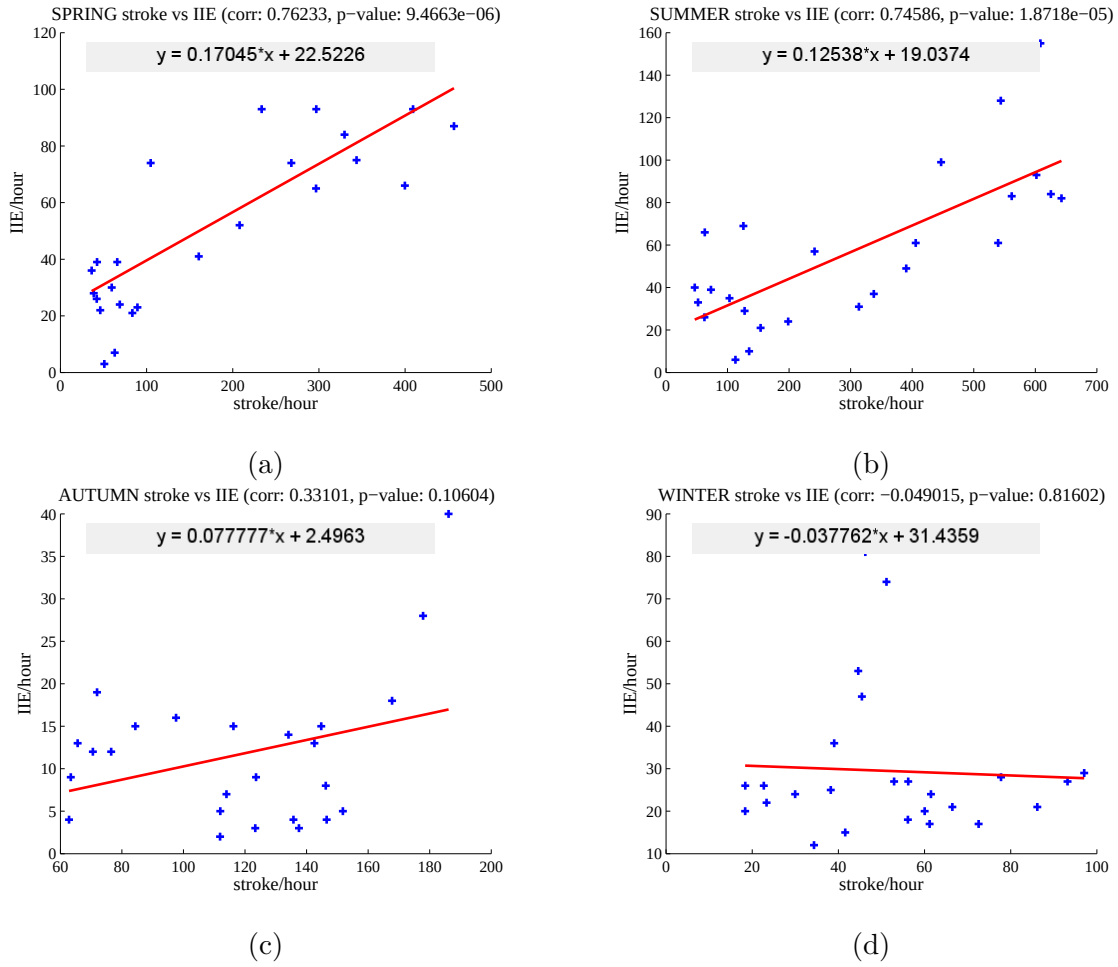

FIGURE 5.15: Diurnal correlation between lightning and IIE during: (a) Spring, (b) Summer (c) Autumn and (d) Winter

We have also investigated the diurnal correlation between IIE and lightning stroke within each season and the results are presented in Figure 5.15. Figure 5.15(a) and Figure 5.15(b) show strong positive correlations of about 76% and 75% between the lightning stroke and IIE during Spring and Summer respectively. However, Figure 5.15(d) shows a weak negative correlation during Winter.

The weak positive and negative correlation during Autumn and Winter respectively suggest that the source(s) of the ionospheric irregularities along the path of the GPS measurements has reduced significantly. These observations present lightning as a potential mechanism for causing IIEs. Figure 5.1 reveals that during Spring and Summer majority of lightning strokes occur over land whereas during Autumn and Winter relatively greater lightning activity is found over the ocean. Mechanisms involving electrical discharge (such as sprites) and infrasonic waves would enhance the ionosphere directly

above the thunderstorm while gravity waves launched by lightning [Chimonas, 1971] have a very small vertical component and would need to propagate several hundred kilometers horizontally before reaching ionospheric altitudes. This therefore suggests that the ionosphere over land where GPS measurements are taken could be disturbed considerably due to infiltration of lightning energy into the upper atmosphere during Spring and Summer and hence the increase in ionospheric irregularities occurrence.

The variation in solar heating through the year implies a seasonal variation in lightning activity. In the southern hemisphere a seasonal variation is more apparent, with a peak during Spring and Summer. While an average of about 7.4×10^3 strokes per day occur in the study region during Summer, this drops to about 1.2×10^3 per day in Winter. The seasonal daily average of lightning activity is dominated by the contribution in the month of February during Summer season with a daily average of about 9.5×10^3 per day. The IIE also maintained an average of about 50 per day during Spring which drops to about 20 per day during Winter. The seasonal daily average of ionospheric irregularity is dominated by the contribution in the month of November during Spring with a daily average contribution of about 135 per day.

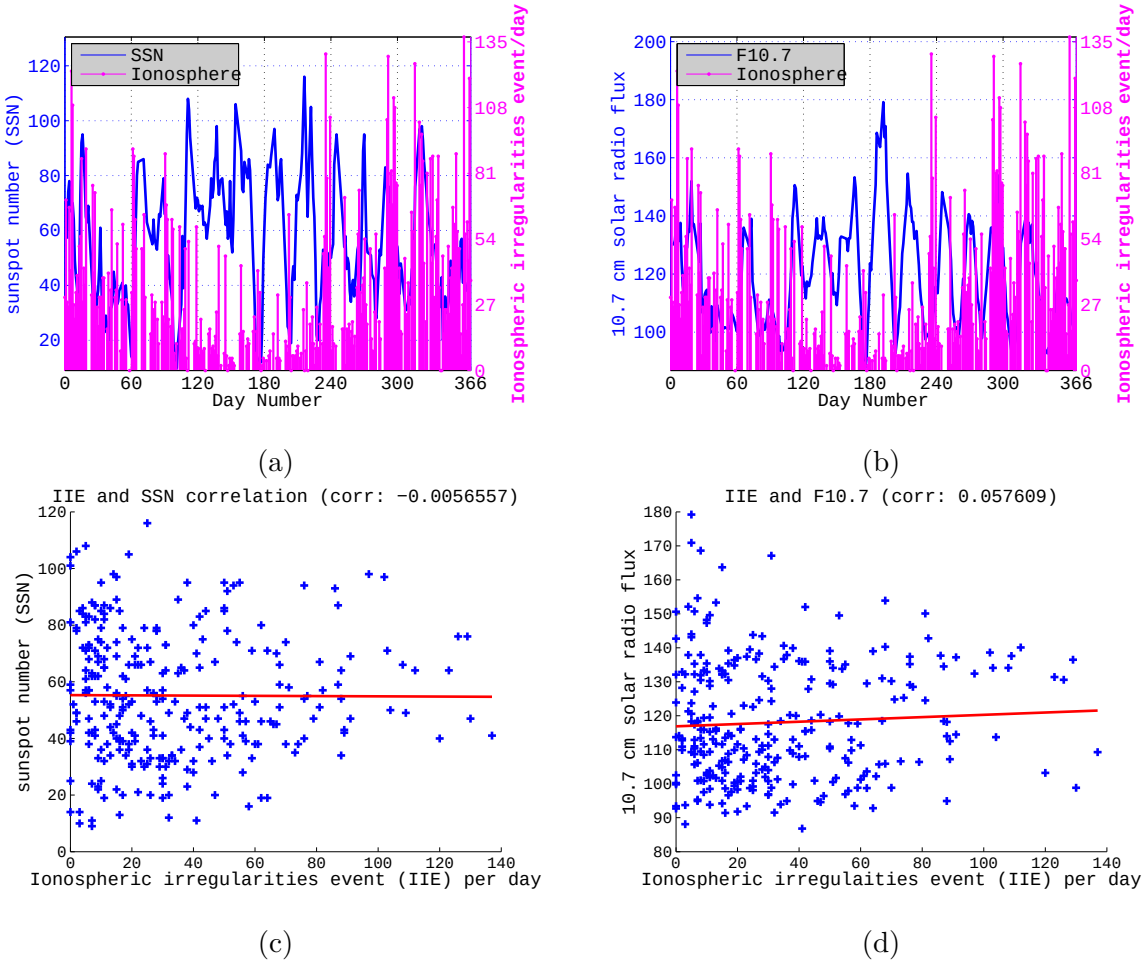

FIGURE 5.16: Correlation between (a) SSN and IIE, (b) F.10 and IIE. Scatter plot of (c) SSN and IIE and (d) F.10 and IIE

To understand the origin of the IIE, a further correlation study is conducted between the solar particle condition by looking at the radio flux (F10.7) and daily SSN (Rz) and IIE. The data used was supplied by and obtained from the NASA's SPDF-cdaweb . See (http://cdaweb.gsfc.nasa.gov/cdaweb/sp_phys/).

Sunspots themselves are merely a convenient proxy for Solar activity and hence can be used to investigate the influence of Solar activity on the occurrence of ionospheric irregularity events. However, the results of this investigation presented in Figure 5.16 (c) shows a weak negative correlation between sunspot and IIE over South Africa. Figure 5.16 (d) shows a weak positive correlation between 10.7 cm Solar radio flux and IIE over South Africa. These results therefore suggest that there is no Solar influence on the occurrence of ionospheric irregularities.

However, the statistical dependence is not sufficient to demonstrate the presence of a causal relationship (i.e., correlation does not imply causation). Correlations can indicate the potential existence of causal relations and there has to be a clear mechanism and an order of cause-then-effect, and the inverse: absence-of-cause then no effect to establish causality. This is done in the following sections.

5.6 Lightning intensity and TEC variability

After investigating the variability of IIE over the South African region, this study further analyzed some particular ionospheric disturbance events during geomagnetically quiet days to trace the origin and the nature of irregularities.

There is evidence [Johnson and Davis, 2006, and references therein] for multiple mechanisms by which lightning can enhance the ionospheric ionization. Some of the mechanisms proposed to explain the link between ionospheric irregularity and lightning event due to energy transfer from the troposphere include wave activity- both gravity and infrasonic [Chimonas, 1971; Shrrstha, 1971] through to electrical effects associated with observed optical signatures (electromagnetic pulses, electrical discharge or relativistic electrons) [e.g., Rodger et al., 2001; Sentman et al., 2003; Wilson, 1924].

On the basis of the ratio between the N_2^+ first negative emission and the time-integrated ionization production, Mende et al. [2005] estimate that the elves which are signatures of lightning produced an average electron density of 210 electrons cm^{-3} over a large (165 km diameter) circular area having an assumed 10 km altitude extent. Their observations indicate that thunderstorms and their associated lightning are a significant source of ionization in the low- to mid-latitude nighttime D region. Instabilities have also been shown to be generated in the ionosphere by lightning modulating the ambient electric field there [e.g., Woodman and Kudeki, 1984], and there is evidence that very-low-frequency waves launched by lightning can induce further lightning [Armstrong, 1987]. So it is not unexpected that lightning activity appearing in the troposphere should be linked to ionospheric irregularities.

For an assessment of lightning induced-GW influences on ionospheric irregularity event occurrences it is important to examine wave fluctuations in electron density immediately

preceding a lightning event so that possible influences from their continuing presence on instability growth can be evaluated.

Four events were carefully selected to cover; geomagnetically quiet days (i.e., 2012-02-11 and 2012-02-12) in which the lightning activity did not occur directly above the GPS stations and geomagnetically quiet days (2012-10-20 and 2012-11-16) in which the lightning activity occurs directly above the GPS stations. The lightning distributions for each of the days selected are presented in Figure 5.17.

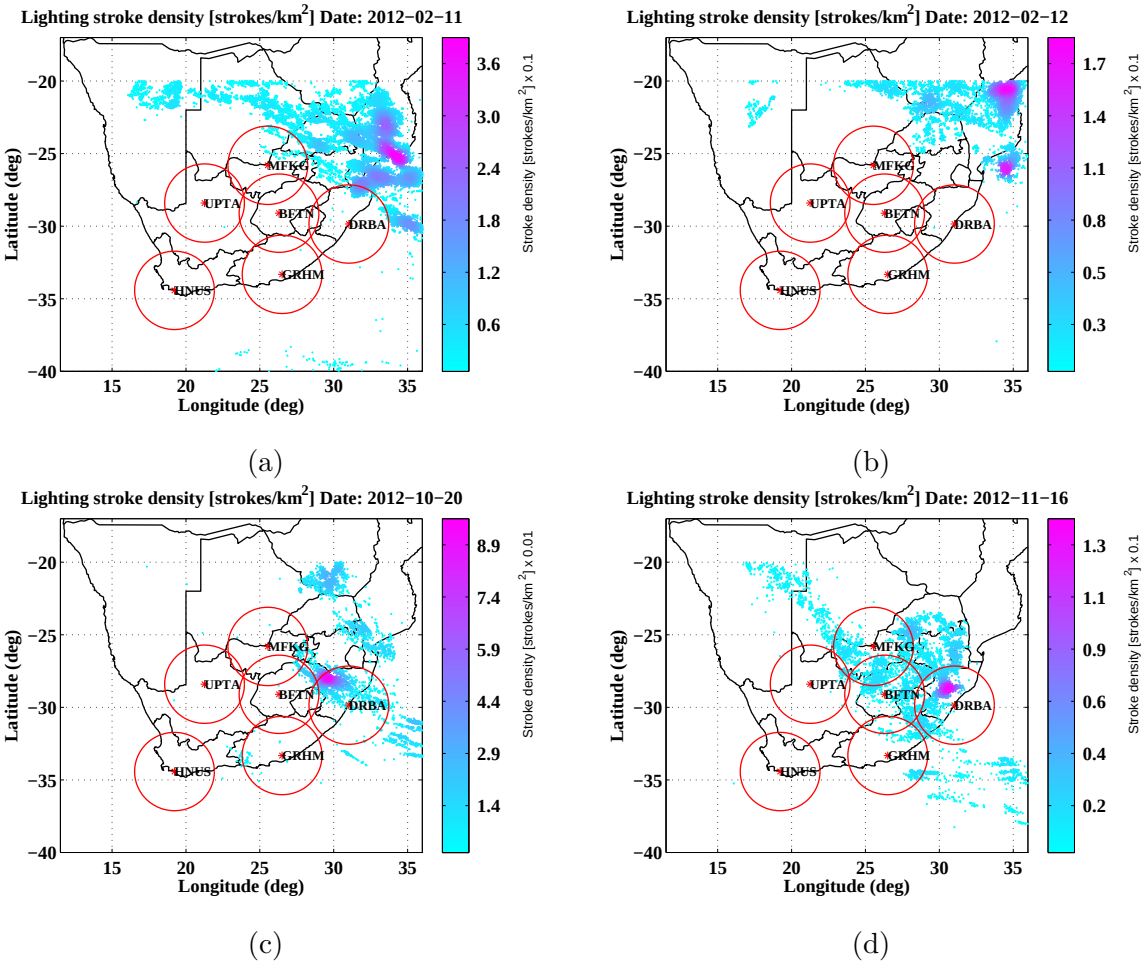

FIGURE 5.17: Lightning stroke density (i.e., stroke/km^2) for selected events. The color scale gives the intensity of the density as indicated on the colorbar scale.

Figure 5.17(a) shows that the lightning activity on 2012-02-11 has a maximum stroke density of about 0.36 stroke/km^2 with a maximum rate of about 5000 strokes per hour. A total of 38781 strokes was recorded on this day representing 3.3% of the total strokes recorded for the study period measured by WWLLN; the highest lightning stroke per day observed within the study region for all the 282 geomagnetically days in 2012. The

days 2012-02-12 and 2012-10-20 also observed significant lightning activity with stroke densities 0.17 stroke/km^2 and 0.13 stroke/km^2 respectively. On 2012-11-16 a maximum stroke density of about 0.081 stroke/km^2 was recorded the lowest of all the selected events.

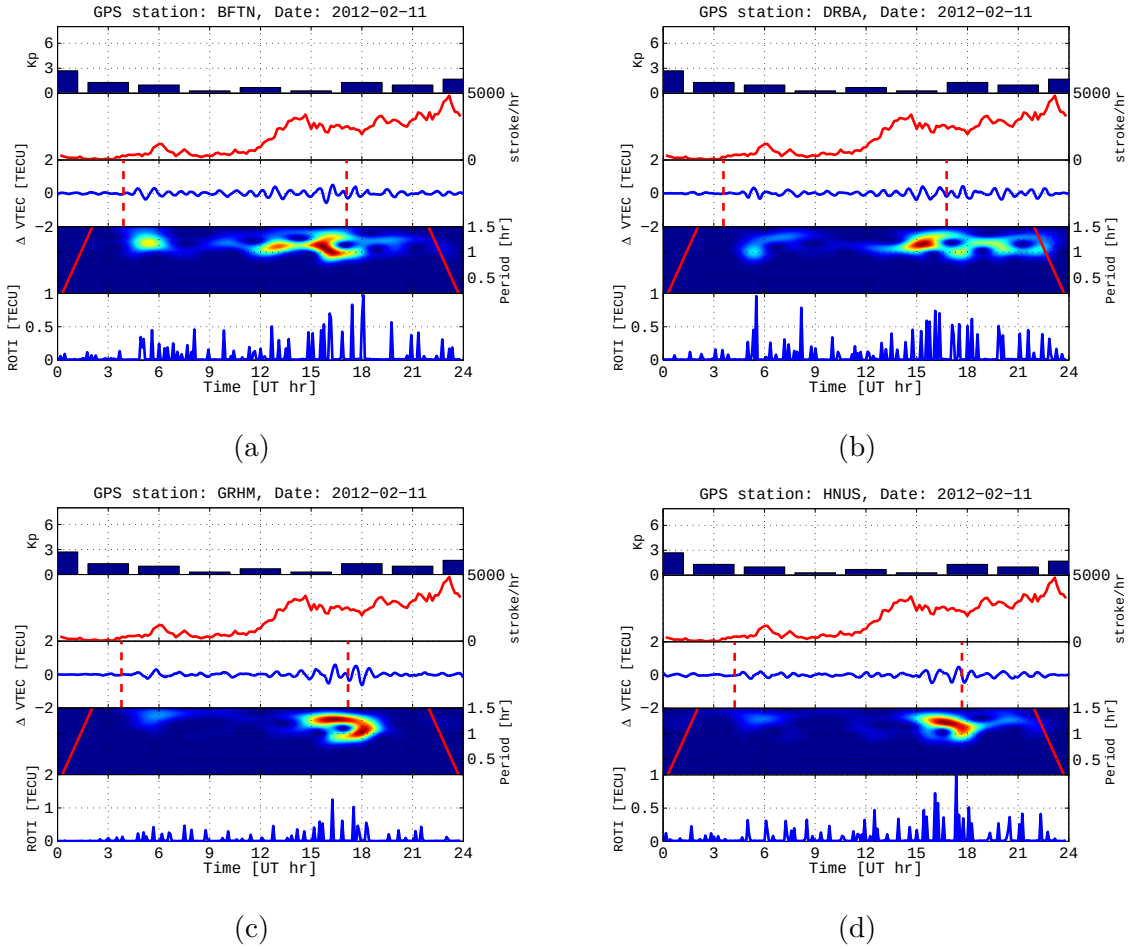

FIGURE 5.18: Diurnal dependence of lightning and lightning induced perturbations in the ionosphere over South Africa on geomagnetically quiet day (2012-02-11). In each plot from the top panel show: the geomagnetic condition (Kp), the lightning activity (stroke rate), the ionospheric disturbances (ΔVTEC), the dominant wave mode in the ionosphere (spectrograph) and ionospheric irregularity index (ROTI. The dotted vertical red lines in the ΔVTEC plot indicate the morning and evening terminator at each GPS station. The slanted red curves in the spectrograph represent cone of influence; that is any wave-like structure appearing before the line is considered dubious.

Considering the first example in Figure 5.18, the first panel of each figure suggests that the geomagnetic condition on February 11, 2012 can be characterized as quiet; the Kp index varied from 0.3 to 2.7 during the day. The lightning stroke density is obtained from the WWLLN measurement and presented in color scale (from light blue to violet) as shown in Figure 5.17(a). The color shows the intensity of strokes per square kilometer. It

is apparent that the lightning activity on this day was quite significant with a maximum stroke density of about 0.36 stroke/km^2. The second panel in Figure 5.18 shows that low level of lightning activity in terms of stroke rate was observed from morning to about 12:00 UT where it begun to increase substantially until mid-night. The results in the third panel in Figure 5.18 reveal that the ionosphere was not stable between the hours 03:00 and 23:00 UT. The disturbances is captured in the ionospheric measurements at all the selected stations. The instability is significant between 15:00 and 18:00 UT at all GPS stations.

However, Figure 5.17(a) shows that the lightning activity did not occur directly above the GPS receiver stations over South Africa and hence the possible link between the ionospheric irregularity and lightning on this day is limited to GWs. Gravity waves triggered by lightning events are expected to cause transient electron density variations transient by concentrating existing ionization in localized patches. Such waves have a small vertical component compared with their horizontal velocity and so would need to propagate for many hundreds of kilometers horizontally before reaching an ionospheric altitude [Davis and Johnson, 2005].

Although with some uncertainty of the initial value of TEC, GPS phase measurements can be made with a high degree of accuracy corresponding to the TEC error determination of at least 10^{14} m^{-2} when averaged on a 30 seconds time interval [Hofmann-Wellenhof et al., 1997]. This makes it possible to detect ionization irregularities and wave processes in the ionosphere over a wide range of amplitudes (up to 10^{-4}) of the diurnal TEC variation and periods (from 5 min up to about 24 hour).

Continuous wave transform (with Morlet as a mother wavelet) was carried out on TEC data. During the wavelet analysis, ΔVTEC which is computed by subtracting a modeled data (i.e., a third order fitted sgolayfilt with frame size of about 3 hours) values from actual VTEC data, was used. A third order sgolayfilt function is fitted to VTEC data to remove diurnal TEC pattern and reveal TEC perturbations. The Morlet wavelet was used because of its similarity in shape to geophysical parameter [Amabayo et al., 2014; Chane-Ming et al., 2000; Habarulema et al., 2013; Torrence and Compo, 1998]. This was primarily aimed at attempting to trace the source mechanisms behind the ionospheric disturbances observed. Wavelet analysis was performed on ΔVTEC to extract dominant wave modes in time series data.

Wave-like structures with period ranging from 40–90 min were observed in the ionosphere at all the GPS stations. The important observation here is that, with reference to the lightning source region in Figure 5.17(a), the BFTN and DRBA which are relatively closer to the lightning source observed wave-like structures in the ionosphere during morning (between 03:00 and 06:00) and evening (12:00 and 20:00 UT) hours. The two station HNUS and GRHM which are relatively further only observed wave-like structures in the ionosphere during evening (15:00 and 18:00 UT) hours. The lower panels in Figure 5.18 represent the ROTI. It is clear that the higher values of ROTI are well correlated with the wave-like structures in the ionosphere and their values maximized at points where the wave-like structures have well defined shapes.

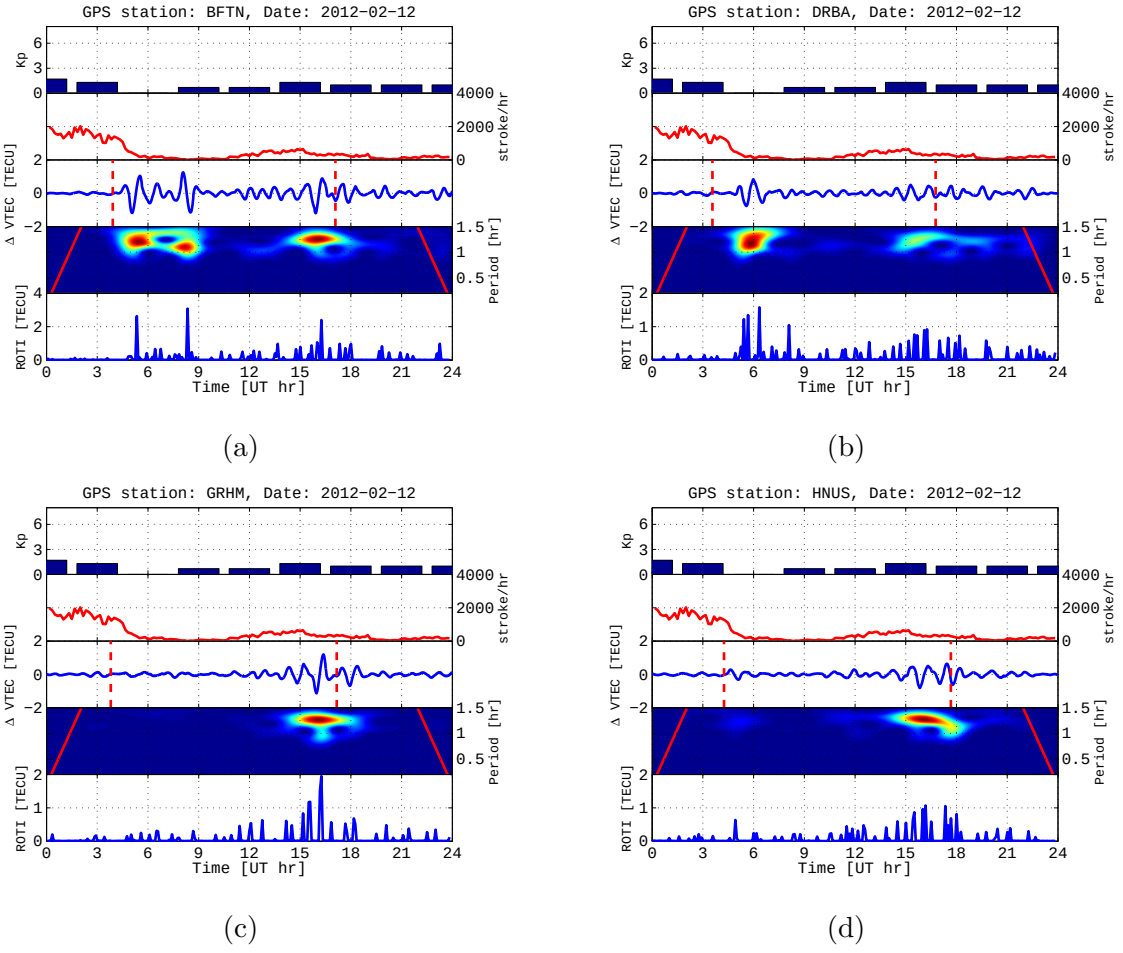

FIGURE 5.19: Diurnal dependence of lightning and lightning induced perturbations in the ionosphere over South Africa on 2012-02-12. Geomagnetic condition; maximum Kp = 1.7 and minimum Kp = 0.0.

Similarly to the first event, as shown in Figure 5.17(b) the lightning source region on February 12, 2012 is also far away from the GPS receiver stations where ionospheric

measurements are being conducted. However, on this day the lightning activity (i.e., stroke rate) is dominated during the morning between 00:00 and 06:00 UT with a maximum peak rate of about 2000 stroke/hr and decreased significantly afterward. A secondary peak rate is also observed at about 15:00 UT. The ionospheric measurement (i.e.,ΔVTEC) also reveals disturbances in the ionosphere at all the GPS stations. The important observation here is that the disturbances occurred in the morning between 04:00 and 09:00 UT at BFTN and DRBA and reappear in the evening between 12:00 and 21:00 UT at all the GPS stations. The Kp index also suggests that the day was geomagnetically quiet and hence suggests that the disturbances observed are not caused by a geomagnetic storm and its associated effects.

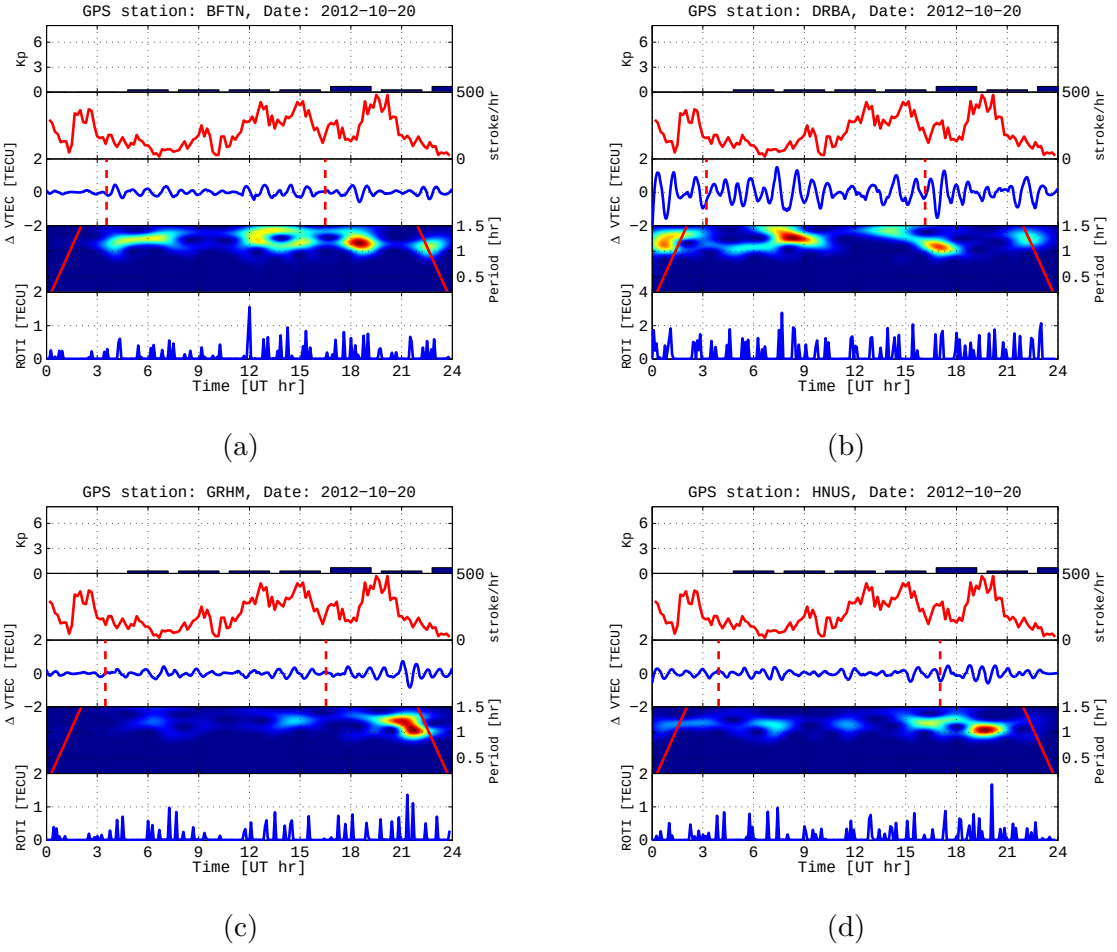

FIGURE 5.20: Diurnal dependence of lightning and lightning induced perturbations in the ionosphere over South Africa on 2012-10-20. The strong lightning source region is within 300 km radius of DRBA GPS receiver. This is to identify the spatial dependence of ionospheric irregularity on lightning. Geomagnetic condition; maximum Kp = 0.7 and minimum Kp = 0.0.

On October 20 2012, the lightning activity occurred over the GPS stations predominantly around Durban as shown in Figure 5.17(c). The the ΔVTEC, the spectrograph and the ROTI plots in Figure 5.20(b) show that the ionosphere is significantly disturbed at DRBA. The wave-like structures appeared at all times of the day and the high values of ROTI were also observed. Although the lightning activity is not intense compared to the previous events but the high level of the disturbances in the ionosphere over Durban could be attributed to the close proximity (i.e., within 300 km radius) of the strong lightning source region to the ionospheric measurement station and hence cause disturbances in the measuring path which is captured in the ΔVTEC and the spectrograph. Figure 5.17(c) shows that the regions around the other GPS stations did not experience lightning and hence the relatively low level of ionospheric disturbances.

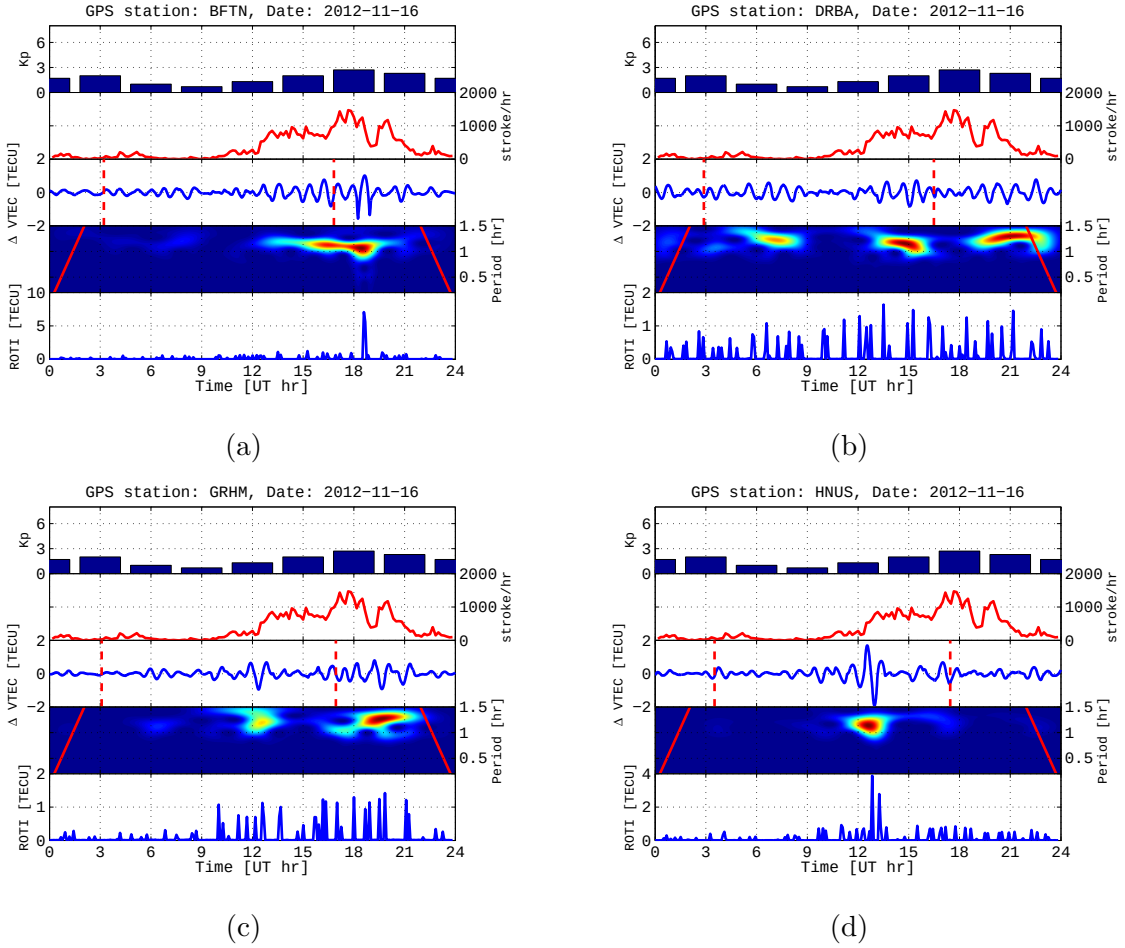

FIGURE 5.21: Diurnal dependence of lightning and lightning induced perturbations in the ionosphere over South Africa on 2012-11-16. The strong lightning source region is within 300 km radius of DRBA GPS receiver. This is to identify the spatial dependence of ionospheric irregularity on lightning. Geomagnetic condition; maximum Kp = 2.7 and minimum Kp = 0.7.

The second panel in Figure 5.21 shows that intense lightning activity occurred between 12:00 and 22:00 UT on this day. The day was geomagnetically quiet with maximum Kp of about 2.7. The dominant region of the lightning activity occurred around Durban as shown in Figure 5.17(d). The ionosphere over this region is significantly disturbed from morning to evening as indicated by the ΔVTEC plot in the Figure 5.21. This is consistent with the previous observation which also show that the ionospheric irregularities are dominant over the region in close proximity to the lightning source. Figure 5.21(c) and Figure 5.21(d) show that the disturbances in the ionosphere occurred during the time period of strong lightning activity.

5.7 Wave-like structures in the ionosphere

The Solar terminator is known to generate AGWs which cause MSTIDs. According to Hernández-Pajares et al. [2006] the local time dependency of TIDs seems to be confined by the Solar terminator. In this work, we study the relationship between the Solar terminator time and the appearance of MSTIDs to investigate the existence of a recurring pattern of ionospheric irregularities due to the day and night alternation.

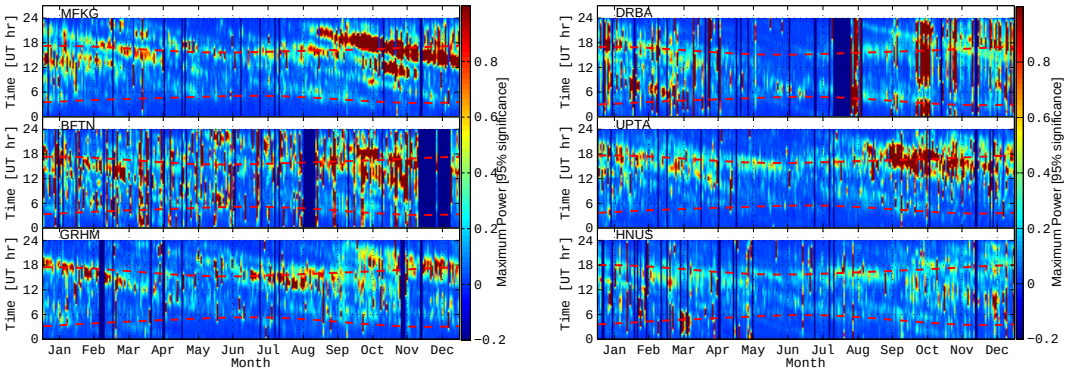

(a) (b)

FIGURE 5.22: Spectral power of the wave-like structure with 95% and above significant level in the filtered period ranges 15 – 60 min depicting both seasonal and diurnal distribution in the ionospheric data from the six GPS stations. The solid black lines represent the morning and evening Solar terminator.

A statistical ionospheric wave and lightning occurrences database was derived by scanning 282 geomagnetically "quiet" (Kp $\leq$ 4) days worth of mid-latitude TEC data collected from six GPS stations whose geographical locations are provided in Table 4.2 and

lightning data collected from WWLLN.

We compared statistically the level of ionospheric wave activity and Solar terminator on geomagnetically quiet days through out the year. Figure 5.23 summarizes diurnal and seasonal dependence of TIDs in the period range 15 min – 1 h. The results show that most of the wave-like structures in the ionospheric TEC appear frequently between September and March, but from April through August there is a low probability of having significant wave-like structures in the ionospheric TEC. The results also show that there is a diurnal variation of these waves in the ionosphere with the more-pronounced effect occurring between the hours of 12:00–22:00 UT. The strongest oscillations in the ionospheric TEC have periods of range 0.6 to 0.8 hours, typical periods for medium scale TIDs.

Figure 5.23 shows that the appearance of the wave-like structures in the ionosphere is not defined by the passage of the Solar terminator. Most of the wave-like structure predominantly occur in the ionosphere before the evening terminator and long hours after the morning terminator. Even though this result does not rule out the possible contribution of the Solar terminator but suggests that there are other mechanisms contributing significantly in the generation of TIDs mostly observed during geomagnetic inactive days over the southern Africa mid-latitude region.

Chapter 6

Discussion and Conclusion

The influence of lightning on electron concentration in the Southern Africa mid-latitude ionosphere was investigated by analyzing ionospheric irregularities and lightning strokes, based on GPS and WWLLN data sets. The lightning data is used as a proxy to identify periods of intense electrified clouds while the TEC data from GPS measurements is used to identify periods of ionospheric irregularities events. The GPS TEC and WWLLN data sets provided evidence that ionospheric irregularity and lightning frequently occur at the same time during almost all seasons over the southern African mid-latitude sector. The irregularity occurrence was characterized in terms of the level of Rate of Change of TEC (ROTI) for selected events. The dependence of irregularity occurrence on days, months and seasons was characterized statistically for the period of this study. Our analysis show strong correlation between occurrence of ionospheric irregularities and lightning activity within Southern Africa. This connection can be clearly seen where the diurnal variation in ionospheric irregularity occurrence appears to be essentially defined by the diurnal variation in the activity of the lightning in most of the seasons except in winter.

6.1 Discussion

The results of our investigation demonstrate that the presence of lightning is a likely cause of the generation of TIDs and ionospheric irregularities in the ionosphere capable of causing scintillation in the mid-latitude ionosphere over South Africa.

Considering the effect of ionospheric disturbance on radio wave propagation it can be concluded that the diurnal dependence of GPS signal scintillation during geomagnetically quiet days is correlated with the occurrence of ionospheric irregularities along the line of sight between the GPS satellite and the receiver.

Considering lightning as a potential source of ionospheric irregularities via wave activity-both gravity and infrasonic [Chimonas, 1971; Shrrstha, 1971] through to electrical effects associated with observed optical signatures (electromagnetic pulses, electrical discharge or relativistic electrons) [e.g., Rodger et al., 2001; Sentman et al., 2003; Wilson, 1924], one might expect that the ionosphere above the regions where lightning predominantly occurs would be disturbed considerably, and hence the rate of IIE would be maximized during the periods. Numerical simulations studies have suggested that density perturbations of the order of 5% or even less, attributed to gravity waves, can trigger instability growth in the ionosphere leading to vertical development of bubbles to the topside ionosphere under the typical dynamic state of the background ionosphere during the sunset period [Abdu et al., 2009]. Our study found that the variation of ΔVTEC during the events observed range from 0.5 to 2 TECU which suggest density perturbations of the order of 5% or even less at all levels of ROTI.

What we analyze here are examples of ionospheric irregularity development, and its day-to-day variability, under precursor conditions representative of competing influences from varying combinations of the driving forces from Solar terminator and lightning induced-GW features.

The Solar terminator is a time bound occurrence which occurs in the morning and in the evening, therefore any influence of this factor in the occurrence of ionospheric disturbance must also occur either shortly after sunrise or sunset. Our observations on events on four days as presented in Figure 5.18 and Figure 5.19, Figure 5.20, Figure 5.21 did not show any clear dependence of the ionospheric irregularity on the Solar terminator.

However, there is spatial and temporal correlation of the ionospheric irregularity with lightning activity as shown in Figure 5.20(b) and Figure 5.21(b). We found that both the ionospheric disturbances and lightning activity dominated around Durban. The period of the wave-like structures ranging between 40–90 minutes corresponds to the reported AGW range of periods [Hocke and Schlegel, 1996]. These wave-like structures

are observed during the same period as high ROTI events and so TIDs induced by lightning could be the causes of the ionospheric irregularity observed.

Thus from a comparison of the cause-effect sequences on these two days, and further considering the nearly identical behavior of the ΔVTEC on these two days, we conclude that the presence of GWs was a unique (and readily identifiable) factor that appears to have contributed to the development of ionospheric irregularities.

As mentioned in chapter 2, Christian et al. [2003] in their study found that lightning activity within South Africa is dominant around Bloemfontein, with an annual flash density rate of about 23.0 km^{-2} y^{-1}. It can be seen in Figure 5.9(a) that the daily summed IIE occurrence from morning to midnight in the BFTN GPS station is higher than in other stations with a maximum contribution of about 27% of the total IIE detected at the six GPS stations as seen in Figure 5.9(b). The geographic latitude and longitude of the BFTN station are 29.10°S and 26.30°E respectively, and its location is at close proximity to the region of intense lightning activity within South Africa during local Summer and Spring seasons as shown in Figure 5.1. This fact provides further evidences of connections between the tropospheric activity (i.e., thunderstorms and their associated lightning) and the ionospheric irregularities.

These connection therefore warrant our investigation of the seasonal and diurnal dependence of the ionospheric irregularities event over South Africa on lightning activity. Our results in Figure 5.8 suggests that ionospheric irregularities occurs almost at all times of the day but dominate in the late afternoon. This does not rule out the possible contribution of the RayleighTaylor instability and/or Solar terminator as influencing factors.

Lightning rates increase dramatically in Spring and Summer and decline significantly in Autumn and Winter. Any seasonal bias in the occurrence of lightning could therefore potentially introduce a bias in the number of ionospheric irregularities event throughout the time period of the study. This is indeed the case for the above analysis, more lightning events occurring in the Spring and Summer than in the Autumn and Winter months. One valid argument that can be proposed here is that the the lightning activity is dominant during Summer while the IIE is dominant during Spring and hence the larger values of TEC during Spring and lower values of TEC during Winter might be the cause of the seasonal variation of IIE (i.e., ROTI $\geq$ 0.8 TECU/min). This question

has been addressed by the strong positive correlation between lightning and IIE during Spring (i.e., ∼76%) and Summer (i.e.,∼75%) as well as the a weak negative correlation during Winter (i.e., ∼-6%).

The results of our investigations demonstrate that wave-like structures usually seen in the ionosphere are most likely generated by the lightning activity. As seen in Figure 5.18, Figure 5.19, Figure 5.20 and Figure 5.21, the ionospheric perturbation data (ΔVTEC) has been correlated with the lightning stroke rate data. It is observed that the largest oscillatory motion in the ionosphere data tends to localized in the region and time period where the lightning activity appearing in the troposphere intensify. This implies that the observed TIDs in the ionosphere with periods between 40 to 60 minutes are connected with internal waves belonging to the gravity part of AGW induced by the lightning.

According to Vadas and Liu [2009], thunderstorms and deep convection are an every day occurrence during the Spring, Summer and Autumn months in many parts of the world. Regardless of geomagnetic activity, this process therefore likely creates a nearly continuous supply of large-scale GWs in the thermosphere during these seasons. As seen in Figure 5.5 and Figure 5.23 the seasonal and diurnal variation of lightning is matched by the seasonal and diurnal variation of TIDs over the southern Africa mid-latitude region: effects are strongest between September and March, with the more-pronounced effect occurring between the hours of 12:00–22:00 UT, but from April through August there is low probability of having significant lightning induced-TID.

6.2 Conclusions

This study has reported comparative observational results of lightning-induced TIDs that occurred in 2012 over the southern Africa mid-latitude stations. We examine the occurrences of TIDs in some detail, focusing on probable mechanisms responsible for the observed TIDs over the regions. The mid-latitude TEC variation derived from data from six dual frequency GPS stations during geomagnetically quiet conditions has been correlated to lightning rates and distribution derived from WWLLN data.

The regions with most of the lightning activity (i.e., Bloemfontein) over South Africa is the same as the region with the highest ionospheric irregularity event occurrence. Both lightning and ionospheric irregularity events occur frequently during local Summer and

Spring. In particular, these results confirm the conclusion by Vadas and Liu [2009] that thunderstorms and deep convection are an every day occurrence during the Spring, Summer and fall months in many parts of the world and therefore likely creates a nearly continuous supply of large-scale GWs in the thermosphere during these seasons. The results concerning the seasonal and diurnal dependence of the ionospheric irregularities agree with theoretical indications [e.g., Hajkowicz, 1989; Hajkowicz and Dearden, 1988] of seasonal and diurnal dependence of the occurrence of scintillation in the mid-latitude regions.

The statistical database developed for this study can be used as a tool to develop a prediction model for the occurrence of TID and ionospheric scintillation over the South Africa. The observed correlation between ionospheric irregularities and regular and predictable lightning events may be beneficial to medium range forecasting of ionospheric disturbances. The results obtained here can contribute to the development of ionospheric irregularity physics and modeling transionosphere radio wave propagation over South Africa.

6.3 Future work

This study was limited to six selected dual frequency GPS receiver stations in South Africa. Future work should involve more GPS stations in South Africa and in other selected mid-latitude areas around the world since WWLLN has the capability to monitor lightning activity globally. An extension of this study should consider the correlation between ROTI and lightning activity over a whole solar cycle period. Other factors believed to cause daily variability, such as particle precipitation, vertical plasma drift, solar terminator, thermospheric winds and F2 layer height changes, should be followed up using a global instrumentation network. Lastly, the nature and size of the irregularities of tropospheric origin that can cause ionospheric scintillation should be examined and classified. The current research provides a background and enough motivation for developing a GISTM network for South Africa, and should form the basis upon which a scintillation model for this region is developed.

References

Abdu, M. (2001). Outstanding problems in the equatorial ionospherethermosphere electrodynamics relevant to spread F. *Journal of Atmospheric and Solar-Terrestrial Physics*, 63(9):869–884. Mesosphere-Thermosphere-Ionosphere Coupling and Energetics.

Abdu, M. A., Kherani, E. A., Batista, I. S., de Paula, E. R., Fritts, D. C., and Sobral, J. H. A. (2009). Gravity wave initiation of equatorial spread F/plasma bubble irregularities based on observational data from the SpreadFEx campaign. *Annales Geophysicae*, 27:2607–2622.

Akasofu, S.-I. (1983). Solar-wind disturbances and the solar wind-magnetosphere energy coupling function. *Space Science Reviews*, 34(2):173–183.

Allnutt, J. E. (1989). *Satellite-to-ground radiowave propagation: theory, practice and system impact at frequencies above 1GHz*. J. E. Allnutt P. Peregrinus on behalf of the Institution of Electrical Engineers London, U.K.

Amabayo, E. B. (2011). Multi-instrument observations of ionospheric irregularities over South Africa. Master's thesis, Rhodes University, South Africa.

Amabayo, E. B., Edward, J., Cilliers, P. J., and Habarulema, J. B. (2014). Climatology of ionospheric scintillations and TEC trend over the Ugandan region. *Advances in Space Research*, 53(5):734–743.

Antonova, V. P., Dungenbaeva, K. E., Zalizovskii, A. V., Inchin, A. S., Kryukov, S. V., Somsikov, V. M., and Yampolskii, Y. M. (2006). Difference between the Spectra of Acoustic GravityWaves in Daytime and Nighttime Hours due to Nonequilibrium Effects in the Atmosphere. *Geomagnetism Aeronomy*, 46(1):101–109.

Armstrong, W. C. (1987). Lightning triggered from the Earths magnetosphere as the source of synchronised whistlers. *Nature*, 327:405–408.

Banks, P. M., Schunk, R. W., and Raitt, W. J. (1976). The Topside Ionosphere: A Region of Dynamic Transition. *Annual Review of Earth and Planetary Sciences*, 4(1):381–440.

Barkhausen, H. (1930). Whistling Tones from the Earth. *Radio Engineers, Proceedings of the Institute of*, 18(7):1155–1159.

Barrington-Leigh, C. P. and Inan, U. S. (1999). Elves triggered by positive and negative lightning discharges. *Geophysical Research Letters*, 26(6):683–686.

Bartels, J., H. N. H. and Johnston, H. F. (1940). Geomagnetic three-hour-range indices for the years 1938 and 1939. *Terr. Magn. Atmos. Electr.*, 45(3):309–337.

Basu, S., Groves, K., Quinn, J., and Doherty, P. (1999). A comparison of TEC fluctuations and scintillations at Ascension Island. *Journal of Atmospheric and Solar-Terrestrial Physics*, 61:1219–1226.

Beer, T. (1978). On atmospheric wave generation by the terminator. *Planet. Space Sci.*, 26:185–189.

Belehaki, A. and Tsagouri, I. (2001). Study of the thermospheric-ionospheric response to intense geomagnetic storms at middle latitudes. *Physics and Chemistry of the Earth, Part C: Solar, Terrestrial & Planetary Science*, 26(5):353–357.

Bencze, P., Buresová, D., Lastovicka, J., and Märcz, F. (2004). Behaviour of the F1-region, and Es and spread-F phenomena at European middle latitudes, particularly under geomagnetic storm conditions. *Annals of Geophysics*, 47(2-3 Sup.):1131–1143.

Bilitza, D. (2003). International reference ionosphere 2000: Examples of improvements and new features. *Advances in Space Research*, 31(3):757–767.

Bilitza, D., McKinnel, L.-A., Reinisch, B., and Fuller-Rowell, T. (2011). International reference, ionosphere today and in the future. *J. Geod.*, 85:909–920, doi:10.1007/s00190–010–0427–x.

Boeck, W. L., Vaughan, O. H., Blakeslee, R. J., Vonnegut, B., Brook, M., and McKune, J. (1995). Observations of lightning in the stratosphere. *Journal of Geophysical Research: Atmospheres*, 100(D1):1465–1475.

Brunner, F. K. (1991). An improved model of the dual frequency ionospheric correction of GPS observations. *Manuscriptica geodetica*, 16:205–214.

Buresova, D. (2005). Effects of geomagnetic storms on the bottomside ionospheric F region. *Advances in Space Research*, 35:429–439.

Burke, C. and Jones, D. (1992). An experimental investigation of ELF attenuation rates in the Earth-ionosphere duct. *Journal of Atmospheric and Terrestrial Physics*, 54(34):243–250.

Chane-Ming, F., Molinaro, F., Leveau, J., Keckhut, P., and Hauchecorne, A. (2000). Analysis of gravity waves in the tropical middle atmosphere over La Reunion Island (21°S, 55°E) with lidar using wavelet techniques. *Annales Geophysicae*, 18:485–498.

Chimonas, G. (1971). Enhancement of sporadic E by horizontal transport within the layer. *Journal of Geophysical Research*, 76(19):4578–4586.

Christian, H. J., Blakeslee, R. J., Boccippio, D. J., Boeck, W. L., Buechler, D. E., Driscoll, K. T., Goodman, S. J., Hall, J. M., Koshak, W. J., Mach, D. M., and Stewart, M. F. (2003). Global frequency and distribution of lightning as observed from space by the optical transient detector. *Journal of Geophysical Research: Atmospheres*, 108(D1):ACL 4–1–ACL 4–15.

Collier, A. B., Hughes, A. R. W., Lichtenberger, J., and Steinbach, P. (2006). Seasonal and diurnal variation of lightning activity over southern africa and correlation with european whistler observations. *Annales Geophysicae*, 24(2):529–542.

Conker, R. S., El-Arini, M. B., and Hegarty, C. J. (2000). Modeling the effects of ionospheric scintillation on GPS/SBAS availability.

Cot, C. and Teitelbaum, H. (1980). Generated of the gravity waves by inhomogeneous heating of the atmosphere. *Journal of Atmospheric and Terrestrial Physics*, 42(9/10):877– 883.

Crombie, D. D. (1964). Periodic fading of VLF signals received over long paths during sunrise and sunset. *Journal of Research National Bureau of Standards, Radio Science*, 68D:2734.

Cummer, S. A. and Lyons, W. A. (2005). Implications of lightning charge moment changes for sprite initiation. *Journal of Geophysical Research: Space Physics*, 110(A4):10.1029/2004JA010812.

Curry M. J. and Murty R. C. (1974). Thunderstorm-Generated Gravity Waves. *Journal of the Atmospheric Sciences*, 31(5):1402–1408.

Danilov, A. D. and Lastovicka, J. (2001). Effects of geomagnetic storms on the ionosphere and atmosphere . *International Journal of Geomagnetism and Aeronomy*, 2(3):209–224.

Datta-Barua, S., Doherty, P. H., Delay, S. H., Dehel, T., and Klobuchar, J. A. Ionospheric scintillation effects on single and dual frequency GPS positioning. *Proceedings of* ION GPS/GNNS 2003, Portland, OR, pages 336–346.

Davies, K. (1990). *Ionospheric Radio*. IEE electromagnetic waves series. Peter Peregrinus London.

Davies, K. and Hartmann, G. K. (1997). Studying the ionosphere with the global positioning system. *Radio Science*, 32(4):1695–1703.

Davis, C. J. and Johnson, C. G. (2005). Lightning-induced intensification of the ionospheric sporadic E layer. *Nature*, 435(9):799–801.

Davis, C. J. and Lo, K.-H. (2008). An enhancement of the ionospheric sporadic-E layer in response to negative polarity cloud-to-ground lightning. *Geophysical Research Letters*, 35(5):doi:10.1029/2007GL031909.

Deng, B., Huang, J., Liu, W., Xu, J., and Huang, L. (2013). GPS scintillation and TEC depletion near the northern crest of equatorial anomaly over South China. *Adv. Space Res.*, 51:356–365.

Dierendonck, A. J. V., Klobuchar, J. A., and Hua, Q. (1993). Ionospheric scintillation monitoring using commercial single frequency C/A code receivers. Proceedings of ION GPS-93, Institute of Navigation, Salt Lake City, UT.

Dowden, R. L., Brundell, J. B., and Rodger, C. J. (2002). VLF lightning location by time of group arrival (TOGA) at multiple sites. *Journal of Atmospheric and Solar-Terrestrial Physics*, 64(7):817–830.

Du, J., Wilkinson, P., Thomas, R., and Cervera, M. (2000). "Determination of equatorial ionospheric scintillation S4 dual frequency GPS". URSI Commission G, Workshop, La Trobe University, Australia.

Dubey, S., Wahi, R., and Gwal, A. (2005). Effects of ionospheric scintillation on GPS receiver at equatorial anomaly region Bhopal. URSI XXVIIIth General Assembly,, New Delhi, India, 01238.

Dujanga, F., Baki, P., Olwendo, J., and Twinamasiko, B. (2013). Total electron content of the ionosphere at two stations in East Africa during the 24– 25 October 2011 geomagnetic storm. *Adv. Space Res.*, 51:712–721.

Eriksson, A. J. (1976). The measurement of lightning and thunderstorm parameters. Technical report, ELEK 103, CSIR special report, Pretoria, Republic of South Africa.

Forte, B. and Radicella, S. M. (2005). Comparison of ionospheric scintillation models with experimental data for satellite navigation applications. *Annals of Geophysics*, 48(3):505–514.

Fremouw, E. J., Secan, J. A., and Howe, B. M. (1992). Application of stochastic inverse theory to ionospheric tomography. *Radio Science*, 27(5):721732.

Fukunishi, H., Takahashi, Y., Kubota, M., Sakanoi, K., Inan, U. S., and Lyons, W. A. (1996). Elves: Lightning-induced transient luminous events in the lower ionosphere. *Geophysical Research Letters*, 23(16):2157–2160.

Füllekrug, M. and Constable, S. (2000). Global triangulation of intense lightning discharges. *Geophysical Research Letters*, 27(3):333–336.

Fuller-Rowell, T. J., Codrescu, M. V., Risbeth, H., Moffett, R. J., and Quegan, S. (1996). On the seasonal response of the thermosphere and ionosphere to geomagnetic storms . *Journal of Geophysical Research*, 101(A2):2343–2353.

Gosling, J. T., McComas, D. J., Phillips, J. L., and Bame, S. J. (1991). Geomagnetic activity associated with earth passage of interplanetary shock disturbances and coronal mass ejections. *J. Geophys. Res.*, 96(A5):7831–7839.

Habarulema, J. B., McKinnell, L.-A., Burešová, D., Zhang, Y., Seemala, G., Ngwira, C., Chum, J., and Opperman, B. (2013). A comparative study of TEC response for the

African equatorial and mid-latitudes during storm conditions. *Journal of Atmospheric and Solar-Terrestrial Physics*, 102:105–114.

Hajj, G. A., Wilson, B. D., Wang, C., Pi, X., and Rosen, I. G. Data assimilation of ground GPS total electron content into a physics-based ionospheric model by use of the Kalman filter. *Radio Science*, 39,:RS1S05, doi:10.1029/2002RS002859.

Hajkowicz, L. A. (1989). Simultaneous recordings of VHF scintillation occurrences over a wide range of southern latitudes. *Indian Journal of Radio and Space Physics*, 18:2–9.

Hajkowicz, L. A. and Dearden, D. J. (1988). Observations of random and quasi-periodic scintillations in southern mid-latitudes over a solar cycle. *Journal of Atmospheric and Terrestrial Physics*, 50(6):511–517.

Hajkowicz, L. A. and Minakoshi, H. (2003). Mid-latitude ionospheric scintillation anomaly in the Far East. *Annales of Geophysics*, 21(2):577–581.

Hayakawa, M., Ohta, K., and Baba, K. (1994). Wave characteristics of tweek atmospherics deduced from the direction-finding measurement and theoretical interpretation. *Journal of Geophysical Research: Atmospheres*, 99(D5):1073310743.

Helliwell, R. A. (1965). *Whistler and related ionospheric phenomena*. Stanford University Press, Stanford.

Hernández-Pajares, M., Juan, J. M., and Sanz, J. (2006). Medium-scale traveling ionospheric disturbances affecting GPS measurements: Spatial and temporal analysis. *Journal of Geophysical Research*, 111,:doi:10.1029/2005JA011474.

Hines, C. O. (1960). Internal atmospheric gravity waves at ionospheric heights. *Can. J. Phys.*, 38(8):1441–1481.

Hoang, T. L., Abdu, M., MacDougall, J., and Batista, I. S. (2010). Longitudinal differences in the equatorial spread F characteristics between Vietnam and Brazil. *Advances in Space Research*, 45(3):351–360.

Hocke, K. and Schlegel, K. (1996). A review of atmospheric gravity waves and travelling ionospheric disturbances: 1982-1995. *Annales Geophysicae*, 14(9):917–940.

Hofmann-Wellenhof, B., Lichtenegger, H., and Collins, J. (1997). *Global Positioning System: theory and practice*. Springer-Verlag.

Horner, F. and Clarke, C. (1955). Some waveforms of atmospherics and their use in the location of thunderstorms. *Journal of Atmospheric and Terrestrial Physics*, 7(0):1–13.

Huang, C. Y., Burke, W. J., Machuzak, J. S., Gentile, L. C., and Sultan, P. J. (2002). Equatorial plasma bubbles observed by DMSP satellites during a full solar cycle: Toward a global climatology. *Journal of Geophysical Research: Space Physics*, 107(A12):doi:10.1029/2002JA009452.

Hunsucker, R. and Hargreaves, J. (2002). *The High-Latitude Ionosphere and its Effects on Radio Propagation*. Cambridge Atmospheric and Space Science Series. Cambridge University Press.

Hunsucker, R. D. (1982). Atmospheric gravity waves generated in the high-latitude ionosphere: A review. *Reviews of Geophysics*, 20(2):293–315.

Immel, T. J., Mende, S. B., Hagan, M. E., Kintner, P. M., and England, S. (2009). Evidence of tropospheric effects on the ionosphere. *EOS*, 90(9):69–80.

Jacobson, A. R., Holzworth, R., Harlin, J., Dowden, R., and Lay, E. (2006). Performance assessment of the World Wide Lightning Location Network (WWLLN), using the Los Alamos Sferic Array (LASA) as Ground Truth. *Journal of Atmospheric and Oceanic Technology*, 23(8):1082–1092.

Jean, A. G., Taylor, W. L., and Wait, J. R. (1960). VLF phase characteristics deduced from atmospheric wave forms. *Journal of Geophysical Research*, 65(3):907–912.

Johnson, C. G. and Davis, C. J. (2006). The location of lightning affecting the ionospheric sporadic-E layer as evidence for multiple enhancement mechanisms. *Geophysical Research Letters*, 33(L07811):doi:10.1029/2005GL025294.

Joselyn, J. A. and McIntosh, P. S. (1981). Disappearing solar filaments: A useful predictor of geomagnetic activity. *Journal of Geophysical Research: Space Physics*, 86(A6):4555–4564.

Kazimirovsky, E., Herraiz, M., and De La Morena, B. A. (2003). Effects on the Ionosphere Due to Phenomena Occurring Below it. *Survey in Geophysics*, 24(2):139–184.

Kelley, M. C. (1997). In situ ionospheric observations of severe weather-related gravity waves and associated small-scale plasma structure. *Journal of Geophysical Research: Space Physics*, 102(A1):329–335.

Kelley, M. C. (2009). *The Earth's Ionosphere: Plasma Physics and Electrodynamics*, volume 96 of *International geophysics series*. Elsevier, second edition.

Kelley, M. C., Kotsikopoulos, D., Beach, T., Hysell, D., and Musman, S. (1996). Simultaneous Global Positioning System and radar observations of equatorial spread F at Kwajalein. *Journal of Geophysical Research: Space Physics*, 101(A2):2333–2341.

Kintner, P. M., Ledvina, B. M., and de Paula, E. R. (2007). GPS and ionospheric scintillations. *Space Weather*, 5(9):doi:10.1029/2006SW000260.

Klobuchar, J. A. (2001). Ionospheric effects on GPS. *Geoph. directorate, ionospheric effects division, Philips Lab. Massachusetts*.

Kumar, V., Parkinson, M., Dyson, P., and Burns, G. (2009). Thunderstorm-associated responses in the vertical motion of the mid-latitude F-region ionosphere. *Journal of Atmospheric and Solar-Terrestrial Physics*, 71(8–9):787–793.

Larkina, V. I., Nalivaiko, A. V., Gershenzon, N. I., and Gokhberg, M. B. (1983). The "Interkosmos–19" satellite observation of VLF radiation associated with seismic activity. *Geomagnetism and Aeronomy*, 23(5):842–846.

Lay, E. H., Holzworth, R. H., Rodger, C. J., Thomas, J. N., Pinto, O., and Dowden, R. L. (2004). WWLL global lightning detection system: Regional validation study in Brazil. *Geophysical Research Letters*, 31(3):doi:10.1029/2003GL018882.

Lay, E. H., Shao, X.-M., and Carrano, C. S. (2013). Variation in total electron content above large thunderstorms. *Geophysical Research Letters*, 40(10):1945–1949.

Liu, H., Lühr, H., and Watanabe, S. (2009). A solar terminator wave in thermospheric wind and density simultaneously observed by CHAMP. *Geophysical Research Letters*, 36:doi: 110.1029/2009GL038165.

Loewe, C. and Prölss, G. W. (1997). Classifcation and Mean Behavior of Magnetic Storm. *J. Geophys. Research*, 102(A7):14209–14213.

Lyon, J. G. (2000). The solar wind-magnetosphere-ionosphere system. *Science*, 288(5473):1987–1991.

Magono, C. (1980). Thunderstorms. *Elsevier Science, Amsterdam*.

Malan, D. J. (1963). *Physics of Lightening*. The English Universities Press, London.

McNamara, L. (1991). *The ionosphere: communications, surveillance, and direction finding*. Orbit, a foundation series. Krieger Pub. Co.

Mende, S. B., Frey, H. U., Hsu, R. R., Su, H. T., Chen, A. B., Lee, L. C., Sentman, D. D., Takahashi, Y., and Fukunishi, H. (2005). D region ionization by lightning-induced electromagnetic pulses. *Journal of Geophysical Research: Space Physics*, 110(A11):doi:10.1029/2005JA011064.

Moldwin, M. (2008). *An Introduction to Space Weather*. Cambridge University Press.

Ngwira, C. M., McKinnell, L. A., Cilliers, P. J., and Yizengawa, E. (2011). An investigation of ionospheric disturbances over South African during the magnetic storm on 15 May 2005. *Adv. in Space Res.*, 49(2012):327–335.

Oladipo, O. A. and Schüler, T. (2013). Equatorial ionospheric irregularities using GPS TEC derived index. *Journal of Atmospheric and Solar-Terrestrial Physics*, 92:78–82.

Oliver, W. L., Otsuka, Y., Sato, M., Takami, T., and Fukao, S. (1997). A climatology of F region gravity wave propagation over the middle and upper atmosphere radar. *Journal of Geophysical Research: Space Physics*, 102(A7):14499–14512.

Opperman, B. D. L. (2007). *Reconstruction ionospheric TEC over South Africa using signals from a regional GPS network*. PhD thesis, Rhodes University, South Africa.

Oron, S., Dujanga, F., and Ssenyonga, T. (2013). Ionospheric TEC variations during the ascending solar activity phase at an equatorial station, Uganda. *Indian J. Radio Space Phys.*, 42:7–17.

Pasko, V. P., Inan, U. S., Bell, T. F., and Taranenko, Y. N. (1997). Sprites produced by quasi-electrostatic heating and ionization in the lower ionosphere. *Journal of Geophysical Research: Space Physics*, 102(A3):4529–4561.

Pi, X., Mannucci, A. J., Lindqwister, U. J., and Ho, C. M. (1997). Monitoring of global ionospheric irregularities using the Worldwide GPS Network. *Geophysical Research Letters*, 24(18):2283–2286.

Pierce, E. (1977). Atmospherics and radio noise. *In: Lightning. Volume 1. London and New York, Academic Press*, 1:351–384.

Preston-Whyte, R. and Tyson, P. (1988). *The Atmosphere and Weather of Southern Africa*. Oxford University Press, South Africa.

Radicella, B. F. S. M. and Ezquer, R. (2002). A different approach to the analysis of GPS scintillation data. *Annals of Geophysics*, 45(3/4):551–561.

Rakov, V. and Uman, M. (2003). *Lightning: Physics and Effects*. Cambridge University Press.

Richmond, A. (1995). The ionospheric wind dynamo: effects of its coupling with different atmospheric regions. In Johnson, R. and Killeen, T., editors, *The Upper Mesosphere and Lower Thermosphere: A review of Experiment and Theory, Geophys.*, volume 87, pages 49–65. AGU, Washington D.C.

Rodger, C. J., Brundell, J. B., Dowden, R. L., and Thomson, N. R. (2004). Location accuracy of long distance VLF lightning location network. *Annales Geophysicae*, 22(3):747–758.

Rodger, C. J., Brundell, J. B., Holzworth, R. H., and Lay, E. H. (2009). Growing Detection Efficiency of the World Wide Lightning Location Network. In *American Institute of Physics Conference Series*, volume 1118 of *American Institute of Physics Conference Series*, pages 15–20.

Rodger, C. J., Cho, M., Clilverd, M. A., and Rycroft, M. J. (2001). Lower ionospheric modification by lightning-emp: Simulation of the night ionosphere over the united states. *Geophysical Research Letters*, 28(2):199–202.

Rodger, C. J., Werner, S., Brundell, J. B., Lay, E. H., Thomson, N. R., Holzworth, R. H., and Dowden, R. L. (2006). Detection efficiency of the vlf world-wide lightning location network (wwlln): initial case study. *Annales Geophysicae*, 24(12):3197–3214.

Rodger, C. J., J. B. B. and R. L. Dowden, . (2005). Location accuracy of vlf world wide lightning location (wwll) network: Post-algorithm upgrade. *Annales Geophysicae*, 23:277–290.

Romano, V., Spogli, L., Aquino, M., Dodson, A., Hancock, C., and Forte, B. (2013). GNSS station characterisation for ionospheric scintillation applications. *Advances in Space Research*, 52(7):1237–1246.

Schumann, U. and Huntrieser, H. (2007). The global lightning-induced nitrogen oxides source. *Atmospheric Chemistry and Physics*, 7(14):3823–3907.

Secan, J. A., Bussey, R. M., Fremouw, E. J., and Basu, S. (1997). High-latitude upgrade to the Wideband ionospheric scintillation model. *Radio Science*, 34(4):1567–1574.

Seemala, G. K. and Valladares, C. E. (2011). Statistics of total electron content depletions observed over the south american continent for the year 2008. *Radio Science*, 46(5):doi:10.1029/2011RS004722.

Sentman, D., Wescott, E., Picard, R., Winick, J., Stenbaek-Nielsen, H., Dewan, E., Moudry, D., Sabbas, F. S., Heavner, M., and Morrill, J. (2003). Simultaneous observations of mesospheric gravity waves and sprites generated by a midwestern thunderstorm. *Journal of Atmospheric and Solar-Terrestrial Physics*, 65(5):537–550.

Sentman, D. D., Wescott, E. M., Osborne, D. L., Hampton, D. L., and Heavner, M. J. (1995). Preliminary results from the Sprites 94 Aircraft Campaign: 1. red sprites. *Geophysical Research Letters*, 22(10):1205–1208.

Shrrstha, K. (1971). Sporadic-e and atmospheric pressure waves. *Journal of Atmospheric and Terrestrial Physics*, 33(2):205–211.

Somsikov, V. M. (1983). Solar terminator and dynamics of the atmosphere. 192.

Somsikov, V. M. (1987). A spherical model of wave generation in atmosphere by solar terminator. *J. Atmos. Terr. Phys*, 49(5):433–438.

Somsikov, V. M. and Ganguly, B. (1995). On the mechanism of formation of atmospheric inhomogeneties in the solar terminator region. *J. Atmos. Terr. Phys.*, 57:75–83.

Stolzenburg, M. and Marshall, T. C. (2008). Charge structure and dynamics in thunderstorms. In Leblanc, F., Aplin, K., Yair, Y., Harrison, R., Lebreton, J., and Blanc, M., editors, *Planetary Atmospheric Electricity*, volume 30 of *Space Sciences Series of ISSI*, pages 355–372. Springer New York.

Storey, L. R. O. (1953). An investigation of whistling atmospherics. *Philos. Trans. R. Soc. London. Ser. A*, 246:113–141.

Taranenko, Y. N., Inan, U. S., and Bell, T. F. (1993). Interaction with the lower ionosphere of electromagnetic pulses from lightning: Heating, attachment, and ionization. *Geophysical Research Letters*, 20(15):1539–1542.

Taylor, M. J., Bailey, M. A., Pautet, P. D., Cummer, S. A., Jaugey, N., Thomas, J. N., Solorzano, N. N., Sao Sabbas, F., Holzworth, R. H., Pinto, O., and Schuch, N. J. (2008). Rare measurements of a sprite with halo event driven by a negative lightning discharge over Argentina. *Geophysical Research Letters*, 35(14):10.1029/2008GL033984.

Taylor, W. L. (1960). VLF attenuation for east-west and west-east daytime propagation using atmospherics. *Journal of Geophysical Research*, 65(7):1933–1938.

Torrence, C. and Compo, G. (1998). A practical guide to wavelet analysis. *Bull. Am. Meteorol. Soc.*, 79:61–78.

Uman, M. A. (1984). *Lightning*. Dover Publications Inc., New York.

Uman, M. A. (1987). *The Lightning Discharge*, volume 39 of *International Geophysics Series* . Academic Press, Inc., Orlando, Florida 32887.

Vadas, S. L. and Fritts, D. C. (2004). Thermospheric responses to gravity waves arising from mesoscale convective complexes. *Journal of Atmospheric and Solar-Terrestrial Physics*, 66:781–804.

Vadas, S. L. and Liu, H.-l. (2009). Generation of large-scale gravity waves and neutral winds in the thermosphere from the dissipation of convectively generated gravity waves. *Journal of Geophysical Research: Space Physics*, 114(A10):doi:10.1029/2009JA014108.

Wanninger, L. (1993). Ionospheric monitoring using IGS data. *Proceedings of* the 1993 IGS Workshop, University of Berne, Berne, pages 351–360.

Warnant, R. and Pottiaux, E. (2000). The increase of the ionospheric activity as measured by GPS. *Earth, Planets and Space*, 52(11):1055–1060.

Wautelet, G., Aquino, M., Lejeune, S., Stankov, S., and Warnant, R. (2010). Understanding the occurrence of mid-latitude ionospheric irregularities by using GPS, ionosonde and geomagnetic measurements. In *P. Doherty, M. Hernandez-Pajares (Eds)*, Proc. International Beacon Satellite Symposium (IBSS), Barcelona, Spain.

Weidman, C. D. and Krider, E. P. (1986). The amplitude spectra of lightning radiation fields in the interval from 1 to 20 MHz. *Radio Science*, 21(6):964–970.

Wernik, A. W., Lucilla, A., and Materassi, M. (2004). Ionospheric irregularities, scintillation and its effects on systems. *Acta Geophysica Polonica*, 52(2):237–249.

Williams, E. R. and Heckman, S. J. (1993). The Local Diurnal Variation of Cloud Electrification and the Global Diurnal Variation of Negative Charge on the Earth. *J. Geophys. Res.*, 98:52215234.

Wilson, C. T. R. (1924). The electric field of a thundercloud and some of its effects. *Proceedings of the Physical Society of London*, 37(1):32D.

Woodman, R. F. and Kudeki, E. (1984). A causal relationship between lightning and explosive spread f. *Geophysical Research Letters*, 11(12):1165–1167.

Yamashita, M. (1978). Propagation of tweek atmospherics. *Journal of Atmospheric and Terrestrial Physics*, 40(2):151–156.

Yizengaw, E., Moldwin, M., Dyson, P., and Essex, E. (2007). Using tomography of GPS TEC to routinely determine ionospheric average electron density profiles. *Journal of Atmospheric and Solar-Terrestrial Physics*, 69(3):314–321.

Zhang, Y., Paxton, L. J., Morrison, D., Wolven, B., Kil, H., Meng, C.-I., Mende, S. B., and Immel, T. J. (2004). O/N2 changes during 14 October 2002 storms: IMAGE SI-13 and TIMED/GUVI observations. *Journal of Geophysical Research: Space Physics*, 109(A10):doi:10.1029/2004JA010441.